Hydraulic Performance of Shallow Foundations for the Support of Vertical-Wall Bridge Abutments

Course No: 2025-31-16
Credit: 6 PDH

Gilbert Gedeon, P.E.

Continuing Education and Development, Inc.

P: (877) 322-5800
info@cedengineering.com

This course was adapted from the Department of Transportation, Publication No. FHWA-HRT-17-013, "Hydraulic Performance of Shallow Foundations for the Support of Vertical-Wall Bridge Abutments", which is in the public domain.

SI* (MODERN METRIC) CONVERSION FACTORS

APPROXIMATE CONVERSIONS TO SI UNITS

Symbol	When You Know	Multiply By	To Find	Symbol
		LENGTH		
in	inches	25.4	millimeters	mm
ft	feet	0.305	meters	m
yd	yards	0.914	meters	m
mi	miles	1.61	kilometers	km
		AREA		
in^2	square inches	645.2	square millimeters	mm^2
ft^2	square feet	0.093	square meters	m^2
yd^2	square yard	0.836	square meters	m^2
ac	acres	0.405	hectares	ha
mi^2	square miles	2.59	square kilometers	km^2
		VOLUME		
fl oz	fluid ounces	29.57	milliliters	mL
gal	gallons	3.785	liters	L
ft^3	cubic feet	0.028	cubic meters	m^3
yd^3	cubic yards	0.765	cubic meters	m^3
		NOTE: volumes greater than 1000 L shall be shown in m^3		
		MASS		
oz	ounces	28.35	grams	g
lb	pounds	0.454	kilograms	kg
T	short tons (2000 lb)	0.907	megagrams (or "metric ton")	Mg (or "t")
		TEMPERATURE (exact degrees)		
°F	Fahrenheit	5 (F-32)/9 or (F-32)/1.8	Celsius	°C
		ILLUMINATION		
fc	foot-candles	10.76	lux	lx
fl	foot-Lamberts	3.426	$candela/m^2$	cd/m^2
		FORCE and PRESSURE or STRESS		
lbf	poundforce	4.45	newtons	N
lbf/in^2	poundforce per square inch	6.89	kilopascals	kPa

APPROXIMATE CONVERSIONS FROM SI UNITS

Symbol	When You Know	Multiply By	To Find	Symbol
		LENGTH		
mm	millimeters	0.039	inches	in
m	meters	3.28	feet	ft
m	meters	1.09	yards	yd
km	kilometers	0.621	miles	mi
		AREA		
mm^2	square millimeters	0.0016	square inches	in^2
m^2	square meters	10.764	square feet	ft^2
m^2	square meters	1.195	square yards	yd^2
ha	hectares	2.47	acres	ac
km^2	square kilometers	0.386	square miles	mi^2
		VOLUME		
mL	milliliters	0.034	fluid ounces	fl oz
L	liters	0.264	gallons	gal
m^3	cubic meters	35.314	cubic feet	ft^3
m^3	cubic meters	1.307	cubic yards	yd^3
		MASS		
g	grams	0.035	ounces	oz
kg	kilograms	2.202	pounds	lb
Mg (or "t")	megagrams (or "metric ton")	1.103	short tons (2000 lb)	T
		TEMPERATURE (exact degrees)		
°C	Celsius	1.8C+32	Fahrenheit	°F
		ILLUMINATION		
lx	lux	0.0929	foot-candles	fc
cd/m^2	$candela/m^2$	0.2919	foot-Lamberts	fl
		FORCE and PRESSURE or STRESS		
N	newtons	0.225	poundforce	lbf
kPa	kilopascals	0.145	poundforce per square inch	lbf/in^2

*SI is the symbol for the International System of Units. Appropriate rounding should be made to comply with Section 4 of ASTM E380.
(Revised March 2003)

TABLE OF CONTENTS

LIST OF ABBREVIATIONS AND SYMBOLS

Abbreviations

ADV	acoustic Doppler velocimeter
CFD	computational fluid dynamics
CTB	cable-tied block
DG	Design Guideline
FHWA	Federal Highway Administration
GRS	geosynthetic reinforced soil
HEC	Hydraulic Engineering Circular
IBS	Integrated Bridge System
LTD	long-term degradation
NCHRP	National Cooperative Highway Research Program
PIV	particle image velocimetry
RSF	reinforced soil foundation
TFHRC	Turner-Fairbank Highway Research Center
V:H	vertical-to-horizontal

Symbols

A_0	cross-sectional area of contracted section before contraction scour (ft^2 (m^2))
A_1	cross-sectional area of upstream section (ft^2 (m^2))
$\hat{A}_1$	cross-sectional area of upstream section for computational fluid dynamics experiments (ft^2 (m^2))
A_2	cross-sectional area of contracted section without riprap at equilibrium contraction scour (ft^2 (m^2))
A_{2R}	cross-sectional area of contracted section with riprap after contraction scour to a depth of y_c (ft^2 (m^2))
A_{2b}	cross-sectional area of contracted section before contraction scour (ft^2 (m^2))
α_1	energy correction factor for upstream section (dimensionless)
α_{2B}	energy correction factor for contracted section without riprap (dimensionless)
α_{2e}	energy correction factor for equivalent contracted section with riprap (dimensionless)
α_{2R}	energy correction factor for contracted section with riprap (dimensionless)
β_B	channel shape factor for model without riprap (dimensionless)
β_e	channel shape factor for equivalent model with riprap (dimensionless)
β_R	channel shape factor for model with riprap (dimensionless)
C_{cB}	contraction coefficient for model without riprap (dimensionless)
C_{ce}	contraction coefficient for equivalent model with riprap (dimensionless)
C_{cR}	contraction coefficient for model with riprap (dimensionless)
D_{50}	median noncohesive material size (bed material or riprap) (ft (m))
ΔZ	vertical adjustment for equivalent depth (ft (m))
ε	function related to ratio of roughness coefficient of riprap to that of erodible bed material (dimensionless)
Fr	Froude number (dimensionless)
$\widehat{Fr}$	Froude number for CFD experiments (dimensionless)

g	acceleration from gravity (ft/s^2 (m/s^2))
γ	unit weight of water (lbf/ft^3 (N/m^3))
h_B	head loss between upstream section and contracted section without riprap (ft (m))
h_e	head loss between upstream section and equivalent contracted section with riprap (ft (m))
h_R	head loss between upstream section and contracted section with riprap (ft (m))
K_r	coefficient equals to 0.89 for a spill-through abutment and 1.02 for vertical-wall abutment (dimensionless)
l_1	abutment length (ft (m))
l_2	abutment width (ft (m))
μ	viscosity (lbf·s/ft^2 (N·s/m^2))
n	composite Manning's roughness coefficient (dimensionless)
n_B	roughness coefficient for bed material (dimensionless)
n_R	roughness coefficient for riprap (dimensionless)
$\emptyset$	undefined function
P_d	downstream flow pressure (lbf/ft^2 (N/m^2))
P_u	upstream flow pressure (lbf/ft^2 (N/m^2))
Q	discharge (ft^3/s (m^3/s))
Re	Reynolds number (dimensionless)
ρ	water density (lb/ft^3 (kg/m^3))
R_h	hydraulic radius (ft (m))
S	energy slope in contracted section (ft/ft (m/m))
S_g	specific gravity of rock riprap (dimensionless)
τ_a	shear on front face of abutment (lbf/ft^2 (N/m^2 or Pa))
τ_{avg}	average bed shear stress for model with riprap (lbf/ft^2 (N/m^2 or Pa))
τ_B	average bed shear stress in middle portion of contracted section without riprap with scour at a depth of y_c (lbf/ft^2 (N/m^2 or Pa))
τ_c	critical shear stress on bed for model without riprap (lbf/ft^2 (N/m^2 or Pa))
τ_o	average bed shear stress in contracted section without riprap before scour (lbf/ft^2 (N/m^2 or Pa))
τ_R	average bed shear stress in contracted section between riprap aprons with scour at a depth of y_c (lbf/ft^2 (N/m^2 or Pa))
τ_{rip}	average bed shear stress on riprap (lbf/ft^2 (N/m^2 or Pa))
V_0	average velocity in contracted section before contraction scour (ft/s (m/s))
V_1	average velocity in upstream section (ft/s (m/s))
$\hat{V}_1$	average velocity in upstream section for CFD experiments (ft/s (m/s))
V_2	average velocity in contracted section without riprap at equilibrium contraction scour (ft/s (m/s))
V_{2b}	average velocity in contracted section before contraction scour (ft/s (m/s))
V_{2R}	average velocity in contracted section with riprap after contraction scour to a depth of the average equilibrium scour without riprap (y_c) (ft/s (m/s))
W_1	bottom width of upstream section (ft (m))
W_{1T}	top width of upstream section (ft (m))
$\bar{W}_1$	average width in upstream section (ft (m))
W_2	bottom width of contracted section (bridge opening width) (ft (m))
W_B	bottom width of bed material (ft (m))

W_R	riprap apron width (ft (m))
y_1	average flow depth in upstream section (ft (m))
y_{1M}	maximum flow depth in upstream section (ft (m))
$\hat{y}_1$	average flow depth in upstream section for CFD experiments (ft (m))
y_2	average flow depth in contracted section with riprap after contraction scour (ft (m))
y_{2M}	maximum flow depth in contracted section with riprap after contraction scour (ft (m))
y_{2R}	average flow depth in contracted section with riprap at equilibrium contraction scour (ft (m))
y_{2RM}	maximum flow depth in contracted section with riprap at equilibrium contraction scour (ft (m))
y_c	average equilibrium contraction scour depth without riprap (ft (m))
y_{cR}	maximum contraction scour depth with partial-width riprap scour countermeasures (ft (m))
y_e	equivalent flow depth in contracted section (ft (m))
y_0	average flow depth in contracted section before contraction scour (ft (m))
y_{0M}	maximum flow depth in contracted section before contraction scour (ft (m))
y_s	local scour depth (ft (m))
z_1	reference elevation for upstream section (ft (m))
z_2	reference elevation for downstream section (ft (m))

CHAPTER 1. BACKGROUND AND OBJECTIVES

Scour at the base of bridge abutments during floods is a common cause of bridge failure in the United States. Shallow abutment foundations located at or near the channel banks are considered more vulnerable than other foundations because they are closer to the streambed and can significantly constrict flood flows. These types of abutments are frequently implemented for single-span bridges, and scour countermeasures are often integrated into the design to avoid placing the foundation below local scour depth. About 80 percent of the more than 600,000 bridges over water in the U.S. national bridge inventory are single-span bridges 70 to 90 ft (21 to 28 m) in length.[1] Therefore, to protect small single-span bridge abutments built on shallow foundations from scour damage, methods for countermeasure design are needed that consider the abutment foundation and scour countermeasures as an integrated component of the bridge.

Extensive research has been conducted to determine the depth and location of the scour hole that develops around a bridge abutment. Design equations and procedures for estimating contraction scour and local abutment scour are provided in Hydraulic Engineering Circular (HEC)-18, *Evaluating Scour at Bridges*.[2] In recent years, risk-based design has been recommended in HEC-18. A risk-based design considers the need to provide safe and reliable waterway crossings while also taking into account the economic consequences and probability of failure.

One strategy that has emerged from this risk-based approach is the use of riprap to protect abutments, particularly for small bridges. At the time of this report, using riprap to protect abutments was the current design approach for vertical-wall abutments built on spread footings. The approach was to place the top of the foundation or footing below the depth of the sum of contraction scour and long-term degradation (LTD) referenced to the thalweg of the main channel and to provide rock riprap to protect the abutment from local scour. HEC-23, *Bridge Scour and Stream Instability Countermeasures*, provides guidelines for designing abutment scour countermeasures.[3]

New bridge construction techniques also increased the need for guidance for design and construction of vertical-wall abutments on shallow foundations. The Federal Highway Administration (FHWA) has promoted the use of geosynthetic reinforced soil-integrated bridge systems (GRS-IBS) founded on reinforced soil foundations (RSFs). While the study described in this report was not exclusively focused on this bridge type, an important goal was to specify appropriate application of riprap aprons for these systems and their abutment foundations.

Contraction scour occurs when a channel is narrowed by a bridge opening where the abutments constrain the flow, as shown in part A of figure 1. The flow accelerates in the contraction, increasing the bed shear stress and causing removal of bed materials. The flow depth in the contraction increases until equilibrium conditions are reached. The clear-water contraction scour equation recommended in HEC-18 is based on a development suggested by Laursen that assumes the flow transitions from uniform flow in the upstream approach section to a different uniform flow condition in the contracted section.[2,4] In Laursen's analysis, the contraction scour depth (y_c) is a function of the design discharge (Q) through the bridge opening, the pre-scour depth in the opening (y_0), the median bed material size (D_{50}), and the width of the bridge opening (W_2). The contraction scour and LTD of the channel are assumed to lower the streambed across

the entire channel. The local abutment scour, y_s, occurs at the abutment because of the turbulence caused in the flow by the abutment.

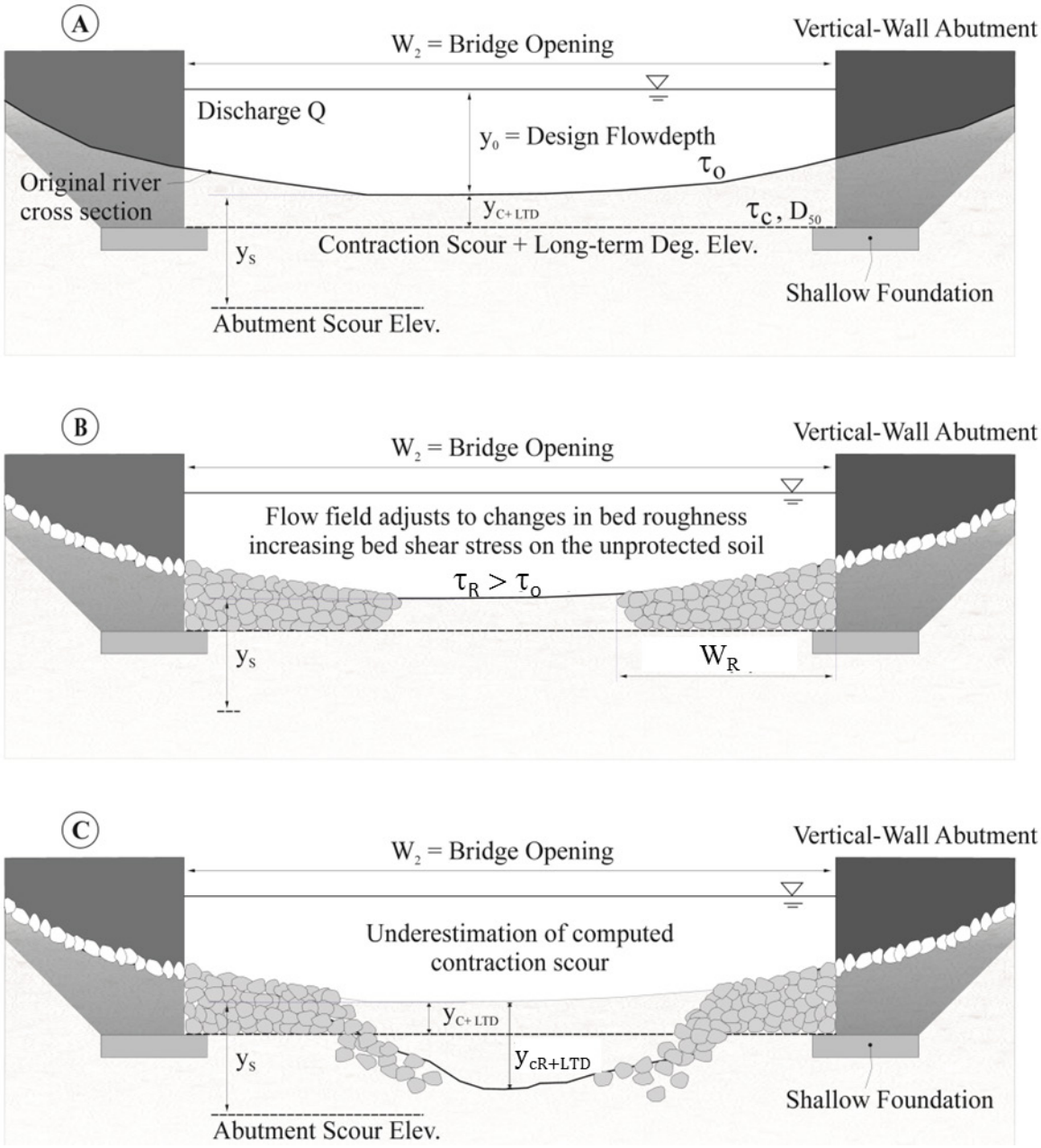

τ_o = Average bed shear stress in contracted section without riprap before scour.
τ_c = Critical shear stress on bed for model without riprap.
τ_R = Average bed shear stress in contracted section between riprap aprons with scour at a depth of y_c.
W_R =Riprap apron width.
y_{cR} = maximum contraction scour depth with partial-width riprap scour countermeasures.
Deg. = Degradation.
Elev. = Elevation.

Figure 1. Drawings. Effect of an abutment riprap apron on contraction scour.

A countermeasure against abutment scour is to place a riprap apron around the abutment to a width of W_R, as shown in part B of figure 1. HEC-23 provides guidelines for minimum apron thickness and extent to protect the abutment foundation from the induced local scouring vortices.(3)

However, the introduction of this heterogeneous roughness (riprap versus native bed materials) in the bridge opening alters the flow, initially manifesting as strong secondary currents originating from the transition in surface roughness. An experimental investigation by Petersen et al. demonstrated how the generated flow turbulence laterally diffused from the rough section over the riprap apron into the smoother bed sediment section.(5)

As shown in part C of figure 1, the adjustment of the flow to the change in bed roughness leads to an increased bed shear stress, τ_R, on the unprotected natural bed material, leading to a deeper contraction scour depth, y_{cR}, than would have occurred without the riprap protection. This increased depth can cause instability of the riprap apron and may ultimately cause riprap movement beginning at the apron edges.

The research study described in this report was designed to provide a more complete picture of the flow field and local bed shear stresses on heterogeneous bed roughness in the bridge opening. A series of physical and numerical simulations were conducted to achieve two main objectives: (1) quantify the change in shear stress adjacent to riprap aprons and (2) provide updated design guidance for riprap protection at vertical-wall abutments on shallow foundations in narrow contractions.

In addition to this introductory chapter, chapter 2 of this report summarizes the annotated literature search for this study. Chapter 3 describes the development of a conceptual model for the increased shear in the middle of the contracted channel (bridge) section. Chapters 4 and 5 describe the setup and results of the physical and numerical modeling, respectively. Based on the conceptual model and the results of the physical and numerical modeling, design guidance for riprap aprons for vertical-wall abutments with shallow foundations is provided in chapter 6. Chapter 7 briefly summarizes this research and presents recommendations for future research. Appendix A is an annotated review of the literature. Appendices B and C present the equilibrium scour maps from the physical experiments conducted in this study and the computational fluid dynamics (CFD) sheer stress and velocity distribution maps, respectively. Appendix D presents proposed guidance on the hydraulic requirements for shallow abutment foundations developed based on this research.

This Page Is Left Blank intentionally.

CHAPTER 2. LITERATURE REVIEW

A literature review was conducted to support and guide the design of this research study. It was found that research on the performance of riprap and other materials as countermeasures for protecting bridge abutments from scour had been studied for more than four decades.

Several researchers focused specifically on riprap aprons to protect abutments. (See references 6–11.) Others investigated alternative countermeasures such as cable-tied blocks (CTBs) and geobags. (See references 12–15.) These works were summarized and integrated into the National Cooperative Highway Research Program (NCHRP) study, *Countermeasures to Protect Bridge Abutments from Scour*.[16]

Subsequently, research was conducted on riprap and CTB applications.[17,18] Melville et al. investigated riprap sizing applications for abutment aprons and compared them with the available equations.[19]

More recently, others performed laboratory investigations of riprap apron failure mechanisms—in particular, edge scour.[5] Jesson et al. used physical and numerical modeling to estimate bed shear stresses.[20]

Appendix A contains the annotated literature review that is the result of the literature search.

This Page Is Left Blank intentionally.

CHAPTER 3. CONCEPTUAL MODEL FOR FLUSH RIPRAP APRONS

One hypothesis for this research effort was that the use of riprap aprons installed flush with the bed in some bridge openings might increase the depth of contraction scour within the opening between the riprap aprons. In this chapter, a conceptual model illustrating the basis for this hypothesis is developed.

INCREASED STRESS FROM THE RIPRAP APRON

Figure 2 shows a simplified plan view of a river channel with bridge abutments encroaching into the channel. Riprap aprons are also shown as a protection against abutment scour. The hypothesis was that the presence of these aprons for abutment scour had the potential to increase contraction scour in the area of the channel in the unprotected gap between the aprons. The relevant hydraulic parameters are also shown in the figure, including the upstream velocity (V_1,), velocity in the abutment opening (V_2), riverbed bottom width upstream (W_1), the bridge opening (W_2), the flow depth upstream (y_1), abutment length (l_1), and abutment width (l_2).

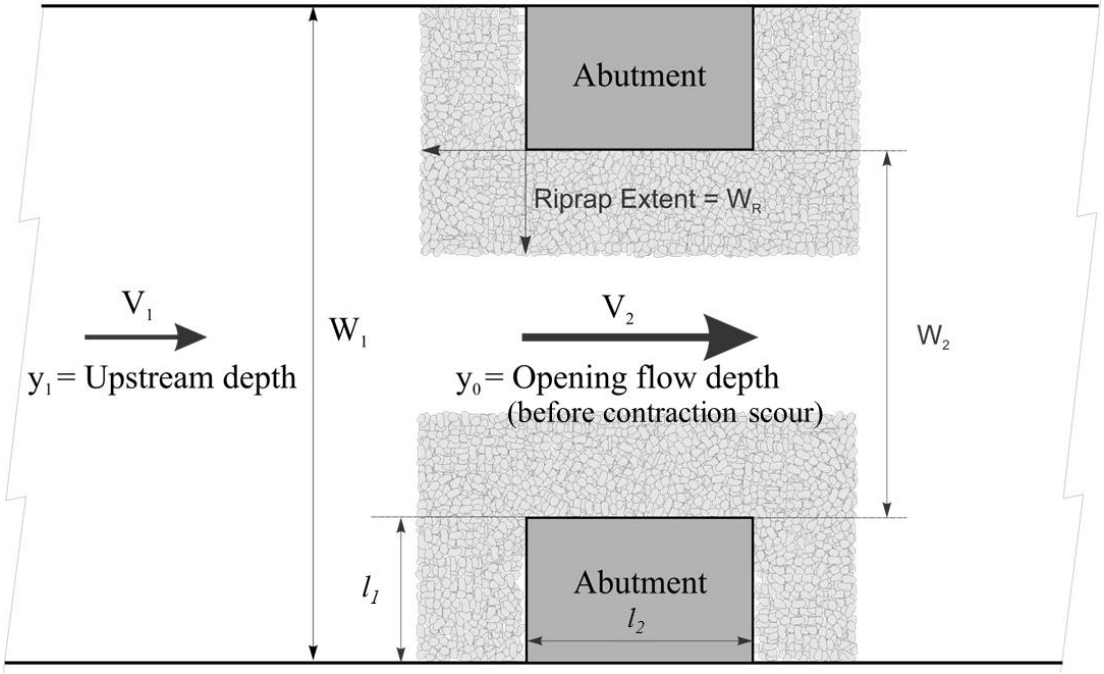

W_R = Riprap apron width.

Figure 2. Sketch. Plan view of a bridge contraction with riprap apron.

Figure 3 shows a schematic of a simple bridge opening (contraction) without a riprap apron. As previously defined, W_1 is the bottom width of the upstream (approach) channel, and W_2 is the bottom width of the contracted (bridge) opening. The average contraction scour in the bridge opening is y_c.

This study focused on vertical-wall abutments, as shown in figure 3. These abutments take many forms, including GRS abutments placed on RSFs. This type of abutment and foundation is considered a non-rigid foundation. According to design guidance in HEC-23, the top of the

abutment foundation should be located at the lower extent of the estimated contraction scour and LTD.[3] LTD was negligible in the physical modeling because equilibrium conditions were used.

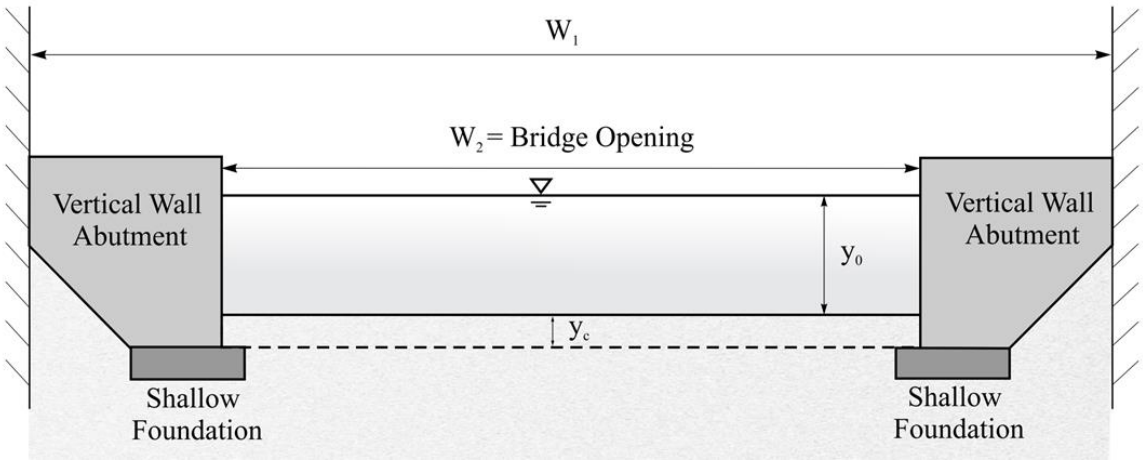

Figure 3. Sketch. Cross section of pre-scour condition for case without riprap.

Figure 4 shows the contracted bridge opening with the riprap apron to protect the abutment foundation from abutment scour as specified in HEC-23. [3] The apron width, W_R, is extended from the abutment face a distance equal to twice the pre-scour flow depth in the opening, y_0. The recommended apron thickness, according to HEC-23, is $1.5 \times D_{50}$ or D_{100} (the maximum rock size), whichever is greater. It is shown in the figure from the pre-scour bed elevation to the top of the foundation.[23]

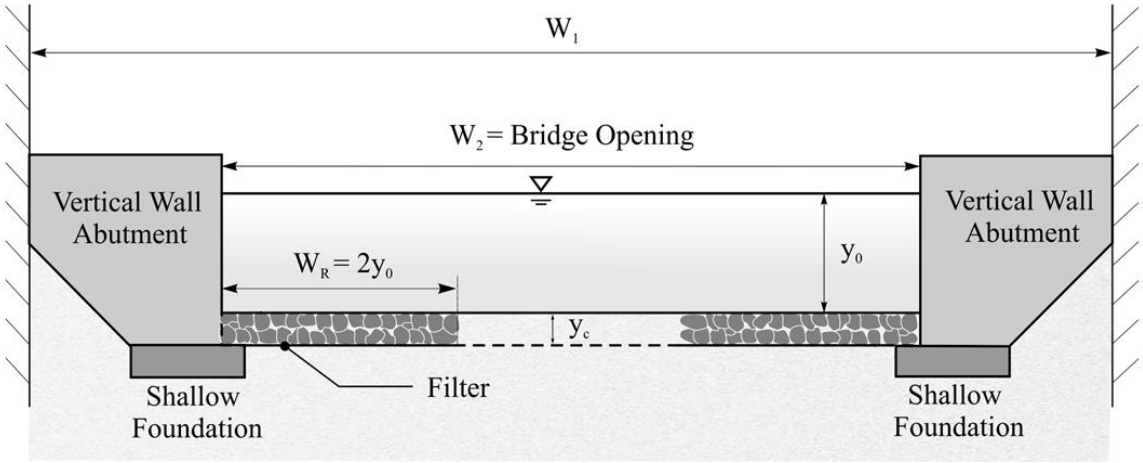

Figure 4. Sketch. Cross section of pre-scour condition for case with riprap.

When the contraction scour for the situation shown in figure 3 occurred, a shear stress remained on the bed material. If this was the equilibrium contraction scour depth, the shear stress would equal the critical shear stress for the bed material. To generalize, that shear stress on the bed without riprap aprons was referred to in this study as τ_B. Similarly, when the same contraction scour shown in figure 4 occurred but with riprap aprons present, that shear stress was defined in this study as τ_R. Although both shear stresses were considered at the same depth ($y_0 + y_c$), the

hypothesis of this study was that the presence of the riprap caused τ_R to exceed τ_B so that further contraction scour would occur for the case with riprap.

Numerical CFD modeling, which is discussed in chapter 5, supported this hypothesis. Figure 5 shows the bed shear stress distribution for a case without riprap after contraction scour occurred. In the region of interest, the value of τ_B was approximately 0.023 lbf/ft^2 (1.1 Pa). Figure 6 displays the bed shear stress distribution at the same level of scour for the same contraction geometry, but with riprap aprons. In the same region of interest, the shear stress was higher, such that τ_R was approximately 0.031 lbf/ft^2 (1.5 Pa). The difference between the two values depended on the specific circumstances of the contraction and riprap characteristics. The shear ratio τ_R/τ_B was used as an index to evaluate the influence induced by a riprap installation.

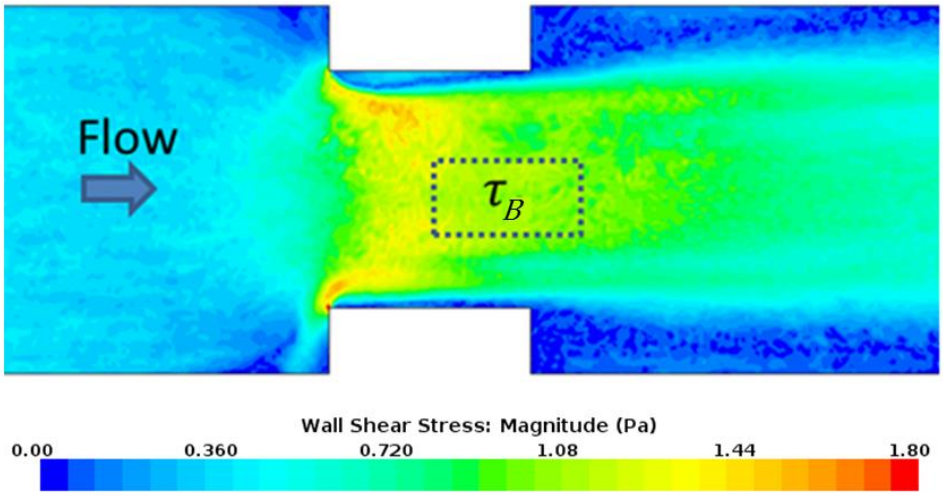

1 lbf/ft^2 = 47.88 Pa.

Figure 5. Graphic. Numerically modeled shear stress distribution for case without riprap.

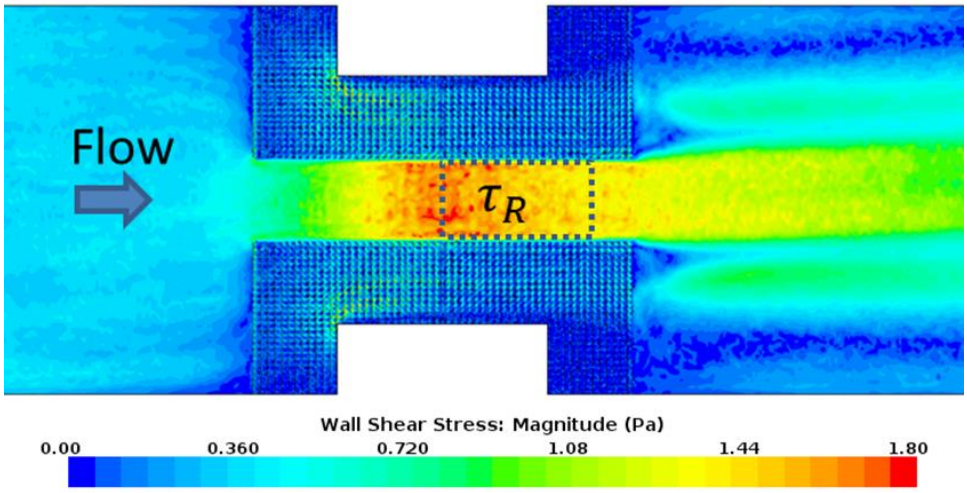

1 lbf/ft^2 = 47.88 Pa.

Figure 6. Graphic. Numerically modeled shear stress distribution for case with riprap.

DIMENSIONAL ANALYSIS

A dimensional analysis was used to better understand the relationship between the ratio of shear with and without riprap abutment protection to potential independent variables. The general equations for the case without riprap and with riprap are shown in figure 7 and figure 8, respectively.

$$f_1(V_1, V_2, \rho, g, l_1, l_2, \tau_B, \mu, W_1, W_2, y_1, y_2) = 0$$

Figure 7. Equation. Relevant variables for case without riprap.

$$f_2(V_1, V_2, \rho, g, l_1, l_2, D_{50}, \tau_R, \mu, W_1, W_2, y_1, y_2) = 0$$

Figure 8. Equation. Relevant variables for case with riprap.

Where:

ρ = Water density (lb/ft^3 (kg/m^3)).
g = Acceleration resulting from gravity (ft/s^2 (m/s^2)).
μ = Viscosity (lbf·s/ft^2 (N s/m^2)).

These equations can be expressed as ratios, normalizing using the upstream hydraulic variables and water density, as shown in figure 9 and figure 10.

$$f_1\left(\frac{V_2}{V_1}, \frac{gy_1}{V_1^2}, \frac{l_1}{y_1}, \frac{l_2}{y_1}, \frac{\tau_B}{V_1^2\rho y_1}, \frac{\mu}{V_1\rho y_1}, \frac{W_1}{y_1}, \frac{W_2}{y_1}, \frac{y_2}{y_1}\right) = 0$$

Figure 9. Equation. Normalized variables for case without riprap.

$$f_2\left(\frac{V_2}{V_1}, \frac{gy_1}{V_1^2}, \frac{l_1}{y_1}, \frac{l_2}{y_1}, \frac{D_{50}}{y_1}, \frac{\tau_R}{V_1^2\rho y_1}, \frac{\mu}{V_1\rho y_1}, \frac{W_1}{y_1}, \frac{W_2}{y_1}, \frac{y_2}{y_1}\right) = 0$$

Figure 10. Equation. Normalized variables for case with riprap.

These relations can be reduced further by recognizing the following:

- $V_2 = F_1(V_1, W_1, W_2, y_1, y_2)$ from continuity.
- $D_{50} = F_2(V_2, y_1, g)$ or $\frac{K_r}{(S_g - 1)}\left(\frac{V_2^2}{gy_1}\right)^{0.33}$ as described by HEC-23 Design Guideline (DG) 18, where S_g is the specific gravity of rock riprap (dimensionless) and K_r is an abutment coefficient (dimensionless).(2)
- $W_1 = W_2 + 2l_1$ as described in figure 2.
- Abutment width, l_2, is a constant.
- $y_2 = F_3(D_{50}, y_0)$ or $y_0 + 2D_{50}$, assuming the riprap apron thickness is twice the riprap D_{50}.

With these observations, the cases without and with riprap are summarized in figure 11 and figure 12, respectively.

$$f_1\left(\frac{gy_1}{V_1^2}, \frac{l_1}{y_1}, \frac{\tau_B}{V_1^2\rho y_1}, \frac{\mu}{V_1\rho y_1}, \frac{W_2}{y_1}\right) = 0$$

Figure 11. Equation. Reduced function for case without riprap.

$$f_2\left(\frac{gy_1}{V_1^2}, \frac{l_1}{y_1}, \frac{\tau_R}{V_1^2\rho y_1}, \frac{\mu}{V_1\rho y_1}, \frac{W_2}{y_1}\right) = 0$$

Figure 12. Equation. Reduced function for case with riprap.

Conversion of these equations to a formulation expressing the shear is shown in figure 13 and figure 14 for the cases without and with riprap, respectively.

$$\frac{\tau_B}{V_1^2\rho y_1} = f_1\left(Fr, Re, \frac{l_1}{y_1}, \frac{W_2}{y_1}\right)$$

Figure 13. Equation. Shear function for case without riprap.

$$\frac{\tau_R}{V_1^2\rho y_1} = f_2\left(Fr, Re, \frac{l_1}{y_1}, \frac{W_2}{y_1}\right)$$

Figure 14. Equation. Shear function for case with riprap.

Where:

Fr = Froude number (dimensionless).
Re = Reynolds number (dimensionless).

Then, the ratio of shear stress with riprap to the case without riprap can be written as shown in figure 15.

$$\frac{\tau_R}{\tau_B} = f_3\left(Fr, Re, \frac{l_1}{y_1}, \frac{W_2}{y_1}\right)$$

Figure 15. Equation. Shear ratio of case with riprap to case without riprap.

The *Reynolds number* (*Re*) is defined as the ratio of inertial forces to viscous forces and consequently quantifies the relative importance of these two types of forces. For this application, *Re* was not important because the bed shear primarily depended on the local velocity gradient on the bed.

Further, if a constant abutment length was assumed, the term with l_1 was not needed. Dropping the terms with *Re* and l_1 yielded the formulation shown in figure 16.

$$\frac{\tau_R}{\tau_B} = \emptyset\left(Fr, \frac{W_2}{y_1}\right)$$

Figure 16. Equation. Final shear ratio of case with riprap to case without riprap.

Where:

ϕ = Undefined function.

DERIVATION OF THE FUNCTIONAL FORM

The specific functional formulation expressing the ratio of τ_R/τ_B was derived from the continuity, energy, and momentum equations comparing the situations with and without riprap aprons.

Natural Bed Materials: No Riprap

Figure 17 provides a conceptual definition sketch of the approach (upstream) section and contracted (bridge opening) section for the case where there is no riprap. To simplify the numerical modeling with CFD, an alternative definition sketch was used, as shown in figure 18. The change from the conceptual definition was to alter the upstream section so that the bottom elevation was increased by the estimated contraction scour depth, y_c.

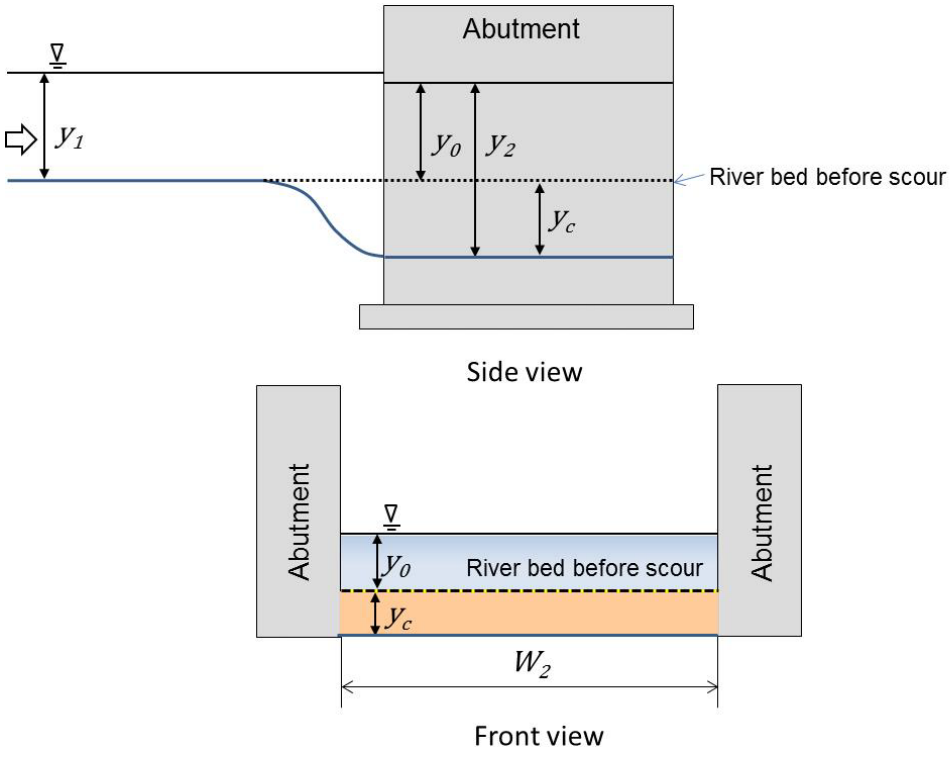

Figure 17. Sketch. Conceptual schematic for case without riprap.

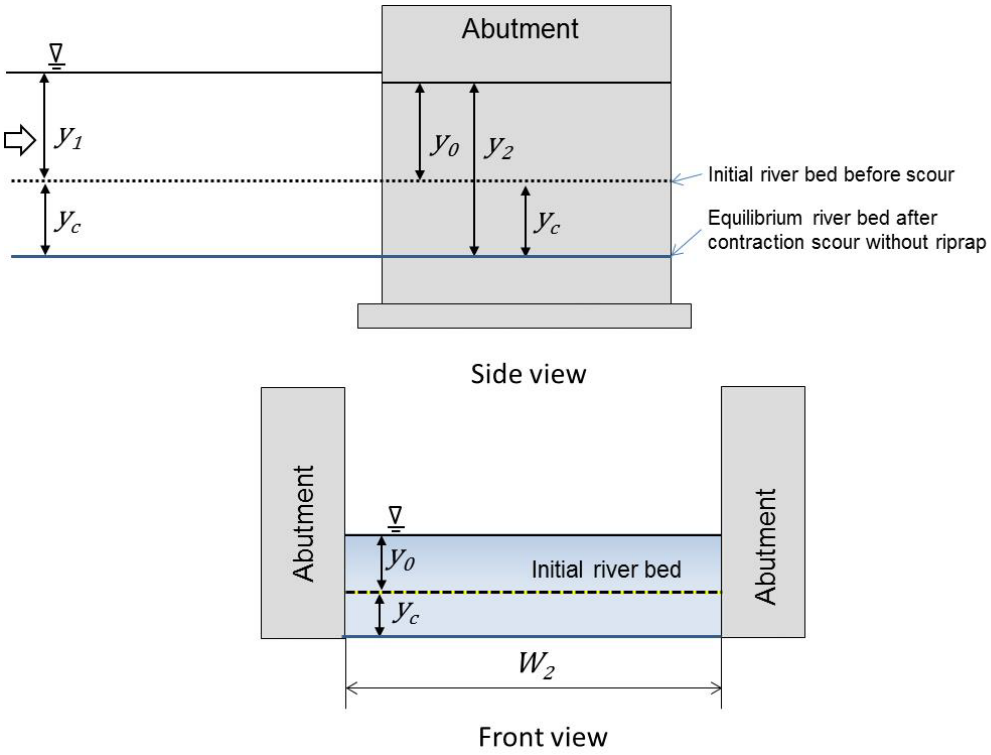

Figure 18. Sketch. CFD schematic for case without riprap.

The flow condition in the opening without riprap at equilibrium contraction scour is shown in figure 19. For this case, the bottom roughness for the natural bed material is n_B and the average shear stress on the bed is τ_B.

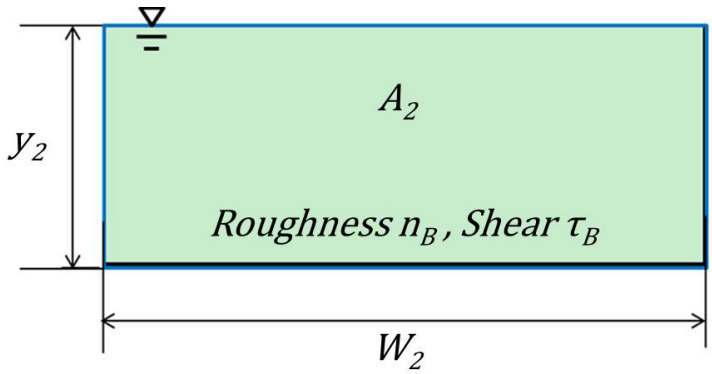

Figure 19. Schematic. Cross section in the opening for the case without riprap.

Figure 20 displays a schematic consistent with the CFD analysis for use with the continuity and energy equations. The variable $\hat{y}_1$ is equal to $y_1 + y_c$, as shown in figure 18.

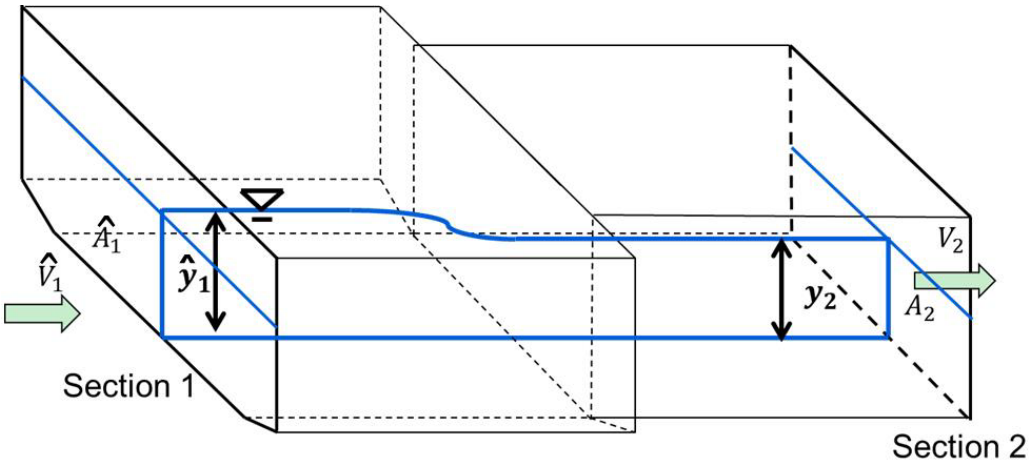

$\hat{V}_1$ = Average velocity in upstream section for CFD experiments.
$\hat{A}_1$= Cross-sectional area of upstream section for CFD experiments.
$\hat{y}_1$ = Average flow depth in upstream section for CFD experiments.
y_2 = Average flow depth in contracted section with riprap after contraction scour.
A_2 = Cross-sectional area of contracted section without riprap at equilibrium contraction scour.

Figure 20. Schematic. Continuity and energy control volume for case without riprap.

For the case without riprap, the continuity equation is summarized in figure 21, and the energy equation is summarized in figure 22.

$$\hat{V}_1 \hat{A}_1 = V_2 A_2$$

Figure 21. Equation. Continuity equation for case without riprap.

$$z_1 + \hat{y}_1 + \alpha_1 \frac{\hat{V}_1^2}{2g} = z_2 + y_2 + \alpha_{2B} \frac{V_2^2}{2g} + h_B$$

Figure 22. Equation. Energy equation for case without riprap.

Where:

z_1 = Reference elevation for upstream section (ft (m)).
z_2 = Reference elevation for downstream section (ft (m)).
α_1 = Energy correction factor for upstream section (dimensionless).
α_{2B} = Energy correction factor for contracted section without riprap (dimensionless).
h_B = Head loss between upstream section and contracted section without riprap (ft (m)).

The energy correction factors were approximately equal to 1.00 to 1.01 for gradually varied flow. The head loss between to the two sections without riprap, h_B, is defined as the contraction coefficient without riprap, C_{cB}, times the velocity head in the contracted section. Therefore, the equation in figure 22 was modified to the equation in figure 23 assuming that the two reference elevations were approximately equal (mild slope) and substituting for V_2 from the continuity equation.

$$y_2 = \hat{y}_1 + \frac{\hat{V}_1^2}{2g} - (1 + C_{cB})\frac{V_2^2}{2g} = \hat{y}_1 + \frac{\hat{V}_1^2}{2g}\left[1 - (1 + C_{cB})\frac{\hat{A}_1^2}{A_2^2}\right]$$

Figure 23. Equation. Modified energy equation for case without riprap.

Where:

C_{cB} = Contraction coefficient for model without riprap (dimensionless).

The quantity in brackets is defined in figure 24 as the channel shape factor for the case without riprap.

$$\beta_B = 0.5\left[1 - (1 + C_{cB})\frac{\hat{A}_1^2}{A_2^2}\right]$$

Figure 24. Equation. Channel shape factor for case without riprap.

Where:

β_B = Channel shape factor for model without riprap (dimensionless).

Substituting the channel shape factor yielded the equation in figure 25.

$$\frac{y_2}{\hat{y}_1} = 1 + \beta_B \widehat{Fr}_1^2$$

Figure 25. Equation. Flow depth ratio for case without riprap.

Where:

$\widehat{Fr}_1$ = Froude number for CFD experiments, which is defined as $\hat{V}_1/\sqrt{g\hat{y}_1}$ (dimensionless).

An equation for shear stress was also required, as shown in figure 26.

$$\tau_B = \gamma y_2 S$$

Figure 26. Equation. Average bed shear stress for case without riprap.

Where:

S = Energy slope (ft/ft (m/m)).
γ = Unit weight of water (lbf/ft^3 (N/m^3)).

Using Manning's equation, as shown in figure 27, and assuming relatively smooth walls so that the hydraulic radius can be approximated as area divided by width (A/W) yielded the equation given in figure 28.

$$Q = \frac{1}{n_B} A_2 R_h^{\frac{2}{3}} S^{\frac{1}{2}}$$

Figure 27. Equation. Manning's equation for case without riprap.

Where:

n_B = Roughness coefficient for bed material (dimensionless).
R_h = Hydraulic radius (ft (m)).

$$\tau_B = \gamma \left(\frac{W_2^{\frac{1}{7}}}{A_2} \right)^{\frac{7}{3}} (Q n_B)^2$$

Figure 28. Equation. Bed shear for case without riprap.

Riprap Apron

The same application of the continuity, energy, and momentum equations was applied to the case with riprap. Figure 29 provides a conceptual definition sketch of the approach (upstream) section and contracted section for the case where there was riprap. The flow depth at equilibrium scour, y_{2R}, is shown as greater than the flow depth at equilibrium without the riprap, y_2. As for the case without riprap, to simplify the numerical modeling with CFD, an alternative definition sketch was used, as shown in figure 30. The change from the conceptual definition was to alter the upstream section so that the bottom elevation was increased by the estimated contraction scour, y_c.

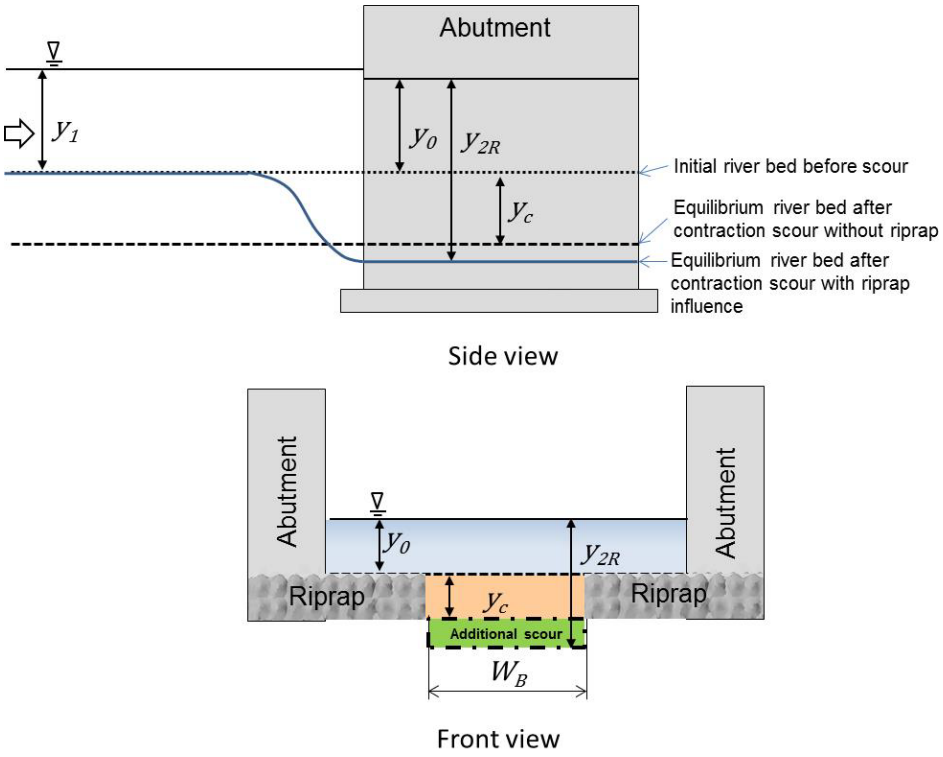

W_B = Bottom width of bed material.

Figure 29. Sketch. Conceptual schematic for case with riprap.

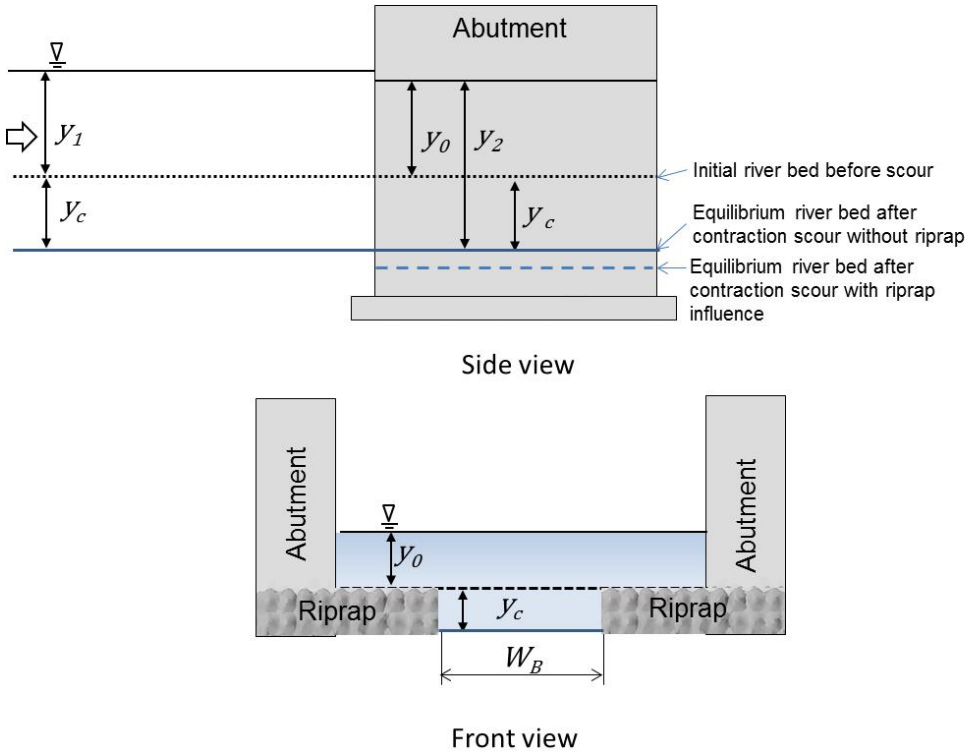

Figure 30. Sketch. CFD schematic for case with riprap.

The flow condition in the opening with riprap at the estimated contraction scour without riprap ($y_2 = y_0 + y_c$) is shown in figure 31. For this case, the bottom roughness for the natural bed material was n_B, and the bottom roughness for the riprap was n_R.

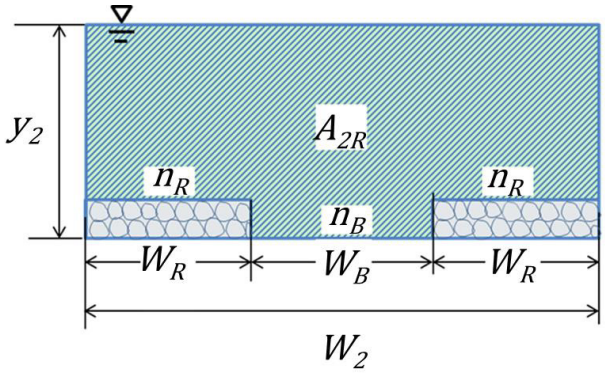

A_{2R} = Cross-sectional area of contracted section with riprap after contraction scour to a depth of y_c.

Figure 31. Schematic. Cross section in the opening for case with riprap.

Figure 32 displays a schematic consistent with the CFD analysis for use with the continuity and energy equations. The variable $\hat{y}_1$ was equal to $y_1 + y_c$, as shown in figure 30.

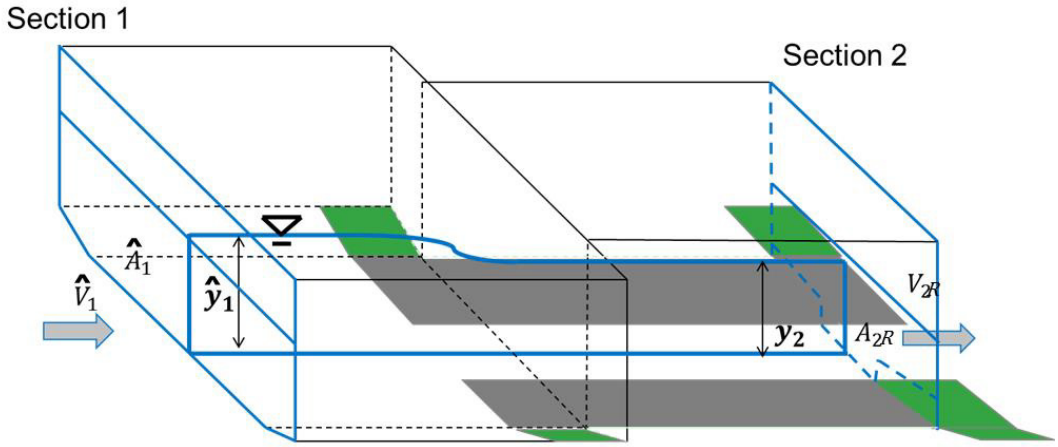

Figure 32. Schematic. Continuity and energy control volume for case with riprap.

For the case with riprap, the continuity equation is summarized in figure 33, and the energy equation is summarized in figure 34.

$$\hat{V}_1 \hat{A}_1 = V_{2R} A_{2R}$$

Figure 33. Equation. Continuity equation for case with riprap.

$$z_1 + \hat{y}_1 + \alpha_1 \frac{\hat{V}_1^2}{2g} = z_2 + y_2 + \alpha_{2R} \frac{V_{2R}^2}{2g} + h_R$$

Figure 34. Equation. Energy equation for case with riprap.

Where:

V_{2R} = Average velocity in contracted section with riprap after contraction scour to a depth of y_c (ft/s (m/s))
α_{2R} = Energy correction factor for contracted section with riprap (dimensionless).
h_R = Head loss between upstream section and contracted section with riprap (ft (m)).

The energy correction factors were approximately equal to 1.00 to 1.01 for gradually varied flow. The head loss between to the two sections, h_R, was defined as the contraction coefficient for the model without riprap, C_{cR}, times velocity head in the contracted section. The equation in figure 34 was modified to the equation in figure 35 assuming that the two reference elevations were approximately equal (mild slope) and substituting for V_2 from the continuity equation.

$$y_2 = \hat{y}_1 + \frac{\hat{V}_1^2}{2g} - (1 + C_{cR})\frac{V_{2R}^2}{2g} = \hat{y}_1 + \frac{\hat{V}_1^2}{2g}\left[1 - (1 + C_{cR})\frac{\hat{A}_1^2}{A_{2R}^2}\right]$$

Figure 35. Equation. Modified energy equation for case with riprap.

To develop a relation for shear stress at the bed after contraction scour had reached a depth of y_2, two assumptions were made. First, it was assumed that flow in the contraction could be characterized as gradually varied flow. From this, it followed that the flow acceleration was approximated as 0, and the difference between the upstream pressure and the downstream pressure, $P_u - P_d$, was also approximately 0. Second, it was assumed that the front faces of abutment were smooth. From this, the shear on the front face of abutment, τ_a, was approximately 0. These quantities are shown on the control volume schematic in figure 36.

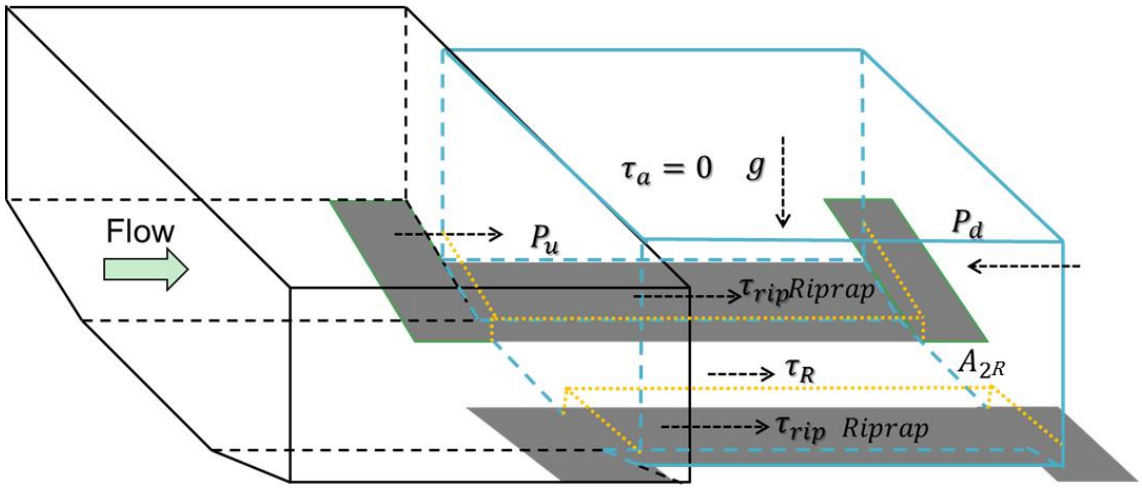

τ_{rip} = Average bed shear stress on riprap.

Figure 36. Schematic. Momentum control volume for case with riprap.

The average bed shear for the case with riprap in the contraction is shown in figure 37.

$$\tau_R(W_2 - 2W_R)l_2 + \tau_{rip}\,2W_R l_2 = \gamma A_{2R} l_2 S$$

Figure 37. Equation. Bed shear stress for case with riprap.

The average bed shear in the opening is expressed in figure 38.

$$\tau_{avg} = \frac{\left[\tau_R(W_2 - 2W_R) + \tau_{rip}\,2W_R\right]}{W_2}$$

Figure 38. Equation. Average bed shear stress for case with riprap.

By substituting the equation in figure 38 into the equation in figure 37, an expression for the energy slope was derived, as shown in the equation in figure 39.

$$S = \frac{\tau_{avg} W_2}{\gamma A_{2R}}$$

Figure 39. Equation. Energy slope for case with riprap.

Manning's formula in the open channel with composite roughness, *n,* is written as shown in figure 40.

$$Q = \frac{1}{n} A_{2R} R_h^{\frac{2}{3}} S^{\frac{1}{2}}$$

Figure 40. Equation. Manning's equation for case with riprap.

Assuming relatively smooth abutment walls and neglecting the vertical sides of the riprap, the hydraulic radius could be approximated as A_{2R}/W_2. Substituting the equation in figure 39 into the equation in figure 40 yields the expression shown in figure 41 for average bottom shear stress.

$$\tau_{avg} = \gamma \left(\frac{W_2^{\frac{1}{7}}}{A_{2R}} \right)^{\frac{7}{3}} (Qn)^2$$

Figure 41. Equation. Bed shear for case with riprap.

The composite Manning's roughness coefficient, *n*, can be calculated using the composite roughness formula shown in figure 42.[21,22]

$$n = \left(\frac{2W_R n_R^{1.5} + W_B n_B^{1.5}}{W_2} \right)^{2/3}$$

Figure 42. Equation. Composite *n*.

Composite *n* for the bed and riprap materials was calculated using Strickler's equation, which relates roughness coefficient to the size of bed material.[23] Following the HEC-23 design guidance, the apron width, W_R, was specified as $2y_0$. Expressing the natural bed width in terms of W_2 led to the representation of composite *n* in figure 43.[3]

$$n = \left(\frac{4y_0 n_R^{1.5} + (W_2 - 4y_0) n_B^{1.5}}{W_2} \right)^{2/3}$$

Figure 43. Equation. Composite *n* in terms of depth and width.

Equivalent Depth for the Riprap Apron

The section in figure 31 for the riprap case was simplified to the equivalent rectangular cross section shown in figure 44. The equivalent depth, y_e, plus the vertical adjustment, ΔZ, was equal to y_2. The bed had a composite roughness, n, and an average bed shear stress of τ_{avg}. The cross-sectional area was the same as it was for the previous riprap case.

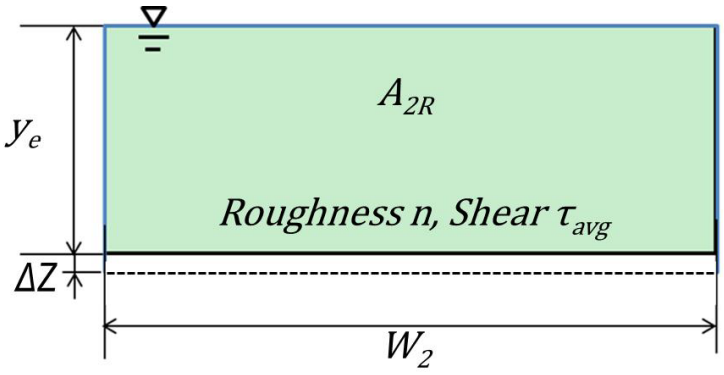

Figure 44. Schematic. Equivalent opening cross section with uniform roughness and shear.

Figure 45 illustrates the control volume for the equivalent depth case with riprap. The energy equation for this case is shown in figure 46.

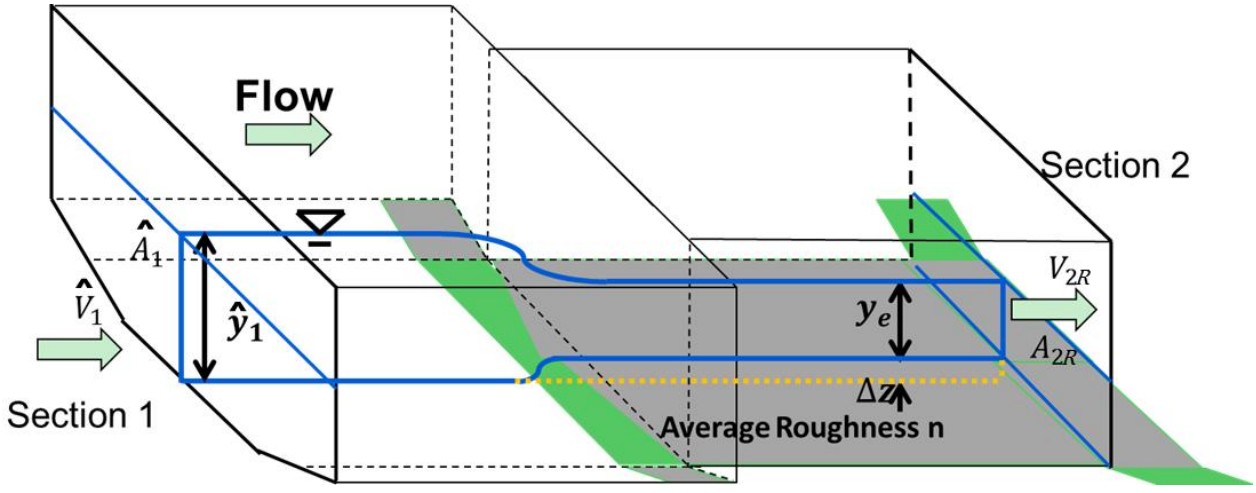

Figure 45. Schematic. Control volume for equivalent depth with riprap.

$$z_1 + \hat{y}_1 + \alpha_1 \frac{\hat{V}_1^2}{2g} = z_2 + y_2 + \alpha_{2R} \frac{V_{2R}^2}{2g} + h_R = z_2 + y_e + \alpha_{2e} \frac{V_{2R}^2}{2g} + h_e + \Delta Z$$

Figure 46. Equation. Energy equation for equivalent depth case with riprap.

Assuming a mild slope where z_1 was approximately equal to z_2 and taking the energy correction factors α_{2R} and α_{2e} as equal to 1.0 led to the equation shown in figure 47.

$$y_e = \hat{y}_1 + \frac{\hat{V}_1^2}{2g} - (1 + C_{ce})\frac{V_{2R}^2}{2g} - \Delta Z = \hat{y}_1 + \frac{\hat{V}_1^2}{2g}\left[1 - (1 + C_{ce})\frac{\hat{A}_1^2}{A_{2R}^2}\right] - \Delta Z$$

Figure 47. Equation. Modified energy equation for equivalent depth case with riprap.

Where:

C_{ce} = Contraction coefficient for equivalent model with riprap (dimensionless).

Defining the channel shape factor, β_e, as shown in figure 48, and rewriting the equation in figure 47 in terms of a depth ratio led to the equation in figure 49.

$$\beta_e = 0.5\left[1 - (1 + C_{ce})\frac{\hat{A}_1^2}{A_{2R}^2}\right]$$

Figure 48. Equation. Channel shape factor for equivalent depth case with riprap.

$$\frac{y_e}{\hat{y}_1} = 1 + \beta_e \widehat{Fr}_1^2 - \frac{\Delta Z}{\hat{y}_1}$$

Figure 49. Equation. Depth ratio for equivalent depth case with riprap.

Where:

B_e = Channel shape factor for equivalent model with riprap (dimensionless).

Shear Stress Ratio

The ratio of bed shear for the case with riprap (figure 41) to the one without riprap (figure 28) is shown in figure 50.

$$\frac{\tau_{avg}}{\tau_B} = \left(\frac{A_2}{A_{2R}}\right)^{\frac{7}{3}}\left(\frac{n}{n_B}\right)^2$$

Figure 50. Equation. Shear stress ratio.

Using the expression for composite *n* in figure 43, the ratio of roughness values is shown in the equation in figure 51.

$$\frac{n}{n_B} = \left[\frac{4y_0 n_R^{1.5} + (W_2 - 4y_0)n_B^{1.5}}{W_2}\right]^{2/3}\frac{1}{n_B} = \left[\frac{4n_R^{1.5} + \left(\frac{W_2}{y_0} - 4\right)n_B^{1.5}}{\frac{W_2}{y_0}}\right]^{\frac{2}{3}}\frac{1}{n_B}$$

Figure 51. Equation. Manning's roughness ratio.

The area ratio in figure 50 can be expressed in terms of depth. Because A_2 was equal to W_2 times y_2 (figure 19), and A_{2R} was equal to W_2 times y_e (figure 44), the area ratio is represented as shown in figure 52.

$$\frac{A_2}{A_{2R}} = \frac{y_2}{y_e}$$

Figure 52. Equation. Area ratio.

Substituting the roughness ratio in figure 51 and the area ratio in figure 52 into the equation in figure 50 led to the shear stress ratio in figure 53.

$$\frac{\tau_{avg}}{\tau_B} = \left(\frac{y_2}{y_e}\right)^{\frac{7}{3}} \left(\left[\frac{4n_R^{1.5} + \left(\frac{W_2}{y_0} - 4\right) n_B^{1.5}}{\frac{W_2}{y_0}} \right]^{\frac{2}{3}} \frac{1}{n_B} \right)^2$$

Figure 53. Equation. Shear stress ratio with substitutions.

Further substitution for y_2 (figure 25) and y_e (figure 49) led to the equation in figure 54.

$$\frac{\tau_{avg}}{\tau_B} = \left[\frac{4\left(\frac{n_R}{n_B}\right)^{1.5} + \left(\frac{w_2}{y_0} - 4\right)}{\frac{w_2}{y_0}} \right]^{\frac{4}{3}} \left(\frac{1 + \beta_B \widehat{FR}_1^2}{1 + \beta_e \widehat{FR}_1^2 - \frac{\Delta Z}{\hat{y}_1}} \right)^{\frac{7}{3}}$$

Figure 54. Equation. Shear stress ratio with average shear stress.

Where:

$\widehat{Fr}_1$ = Froude number for CFD experiments, which is defined as $\hat{V}_1/\sqrt{g\hat{y}_1}$ (dimensionless).

On the left side of the equation, τ_{avg} was replaced with τ_R, and on the right side, the exponent of $^4/_3$ was replaced by a new parameter, ε, as shown in figure 55. A relation for estimating ε was explored by evaluating the CFD analytical results.

$$\frac{\tau_R}{\tau_B} = \left[\frac{4\left(\frac{n_R}{n_B}\right)^{1.5} + \left(\frac{w_2}{y_0} - 4\right)}{\frac{w_2}{y_0}} \right]^{\varepsilon} \left(\frac{1 + \beta_B \widehat{Fr}_1^2}{1 + \beta_e \widehat{Fr}_1^2 - \frac{\Delta Z}{\hat{y}_1}} \right)^{\frac{7}{3}}$$

Figure 55. Equation. Shear stress ratio with τ_R.

Where:

ε = Function related to ratio of roughness of riprap to that of erodible bed material (dimensionless).

As is apparent from the equation in figure 55, the ratio of the shear stress in the middle of the channel with and without the riprap aprons varied with several factors. The relative size of the riprap relative to the bed material was expressed in the ratio of the Manning's roughness values, n_R/n_B. The flow dimensions in the contraction were expressed in the ratio of the contraction width to the flow depth before scour. A high value of this ratio could be considered a wide channel, and a low value might be called a narrow channel. In addition, the degree of contraction, including energy losses, was included in the term in the equation that included the channel shape factors. The extent of contraction would also influence the size of riprap required for abutment protection. This shear ratio was investigated with the CFD modeling described in chapter 5.

CHAPTER 4. PHYSICAL MODELING

This chapter describes the experimental equipment, program, and findings for several abutment riprap layouts installed according to HEC-23 as well as common practice of riprap installations in the field.[3] A second set of experimental results is described, where the performance of a proposed buried riprap installation focused on potential edge failure of the riprap and impact on the predicted contraction scour equation under clear-water conditions. *Edge failure* is defined as scour (movement) of the riprap stones at the edges of a riprap apron.[16] The experiments were conducted at the J. Sterling Jones Hydraulics Research Laboratory located in McLean, VA.

EXPERIMENTAL EQUIPMENT

The physical experiments were conducted using a tilting flume with a model test section, as described in the following sections.

Tilting Flume

A 6-ft (1.8-m)-wide, 1.8-ft (0.55 m)-deep, and 70-ft (21.3-m)-long tilting flume with transparent glass side walls and water recirculation was used to conduct the experiments. An illustration of the flume is presented in figure 56.

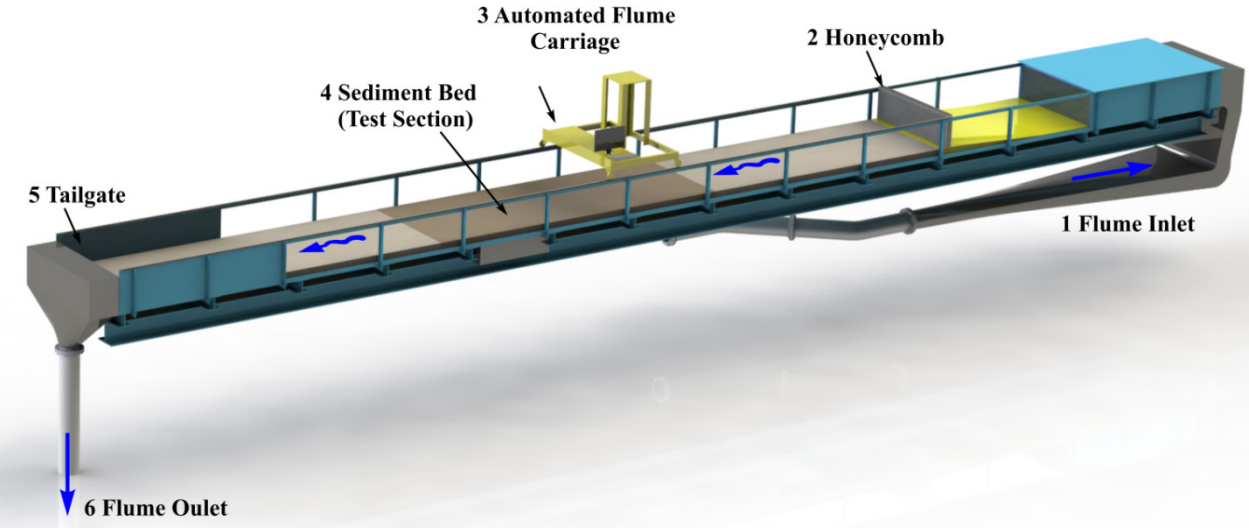

Figure 56. Illustration. FHWA tilting flume.

The structure's skeleton was composed of U-shaped lateral steel frames supported on box-sectioned longitudinal girders. A walkway was provided on one side of the structure. Water was supplied to the flume by a circulation system with a ground sump of 7,400 ft^3 (210 m^3) and a pump with a maximum capacity of 10.6 ft^3/s (0.30 m^3/s). The discharge was measured by an electromagnetic flowmeter installed before the flow was introduced to an upstream head box equipped with a screen and filter. Rapid development of the fully turbulent boundary layer was achieved through an upstream ramp followed by a honeycomb mesh as a flow straightener and an upstream transition zone composed of a layer of coarse sediments carefully placed on the flume

bed to provide excess friction. The flow depth was regulated through a computer-operated downstream adjustable tail gate.

Test Section

A 0.5-ft (0.15-m)-thick layer of uniform bed material (D_{50} = 0.039 inches (1 mm)) was evenly spread along the full length of the test section that was 17.4 ft (5.3 m) long by 6 ft (1.8 m) wide and started after the transition zone. The surface of the sand bed was level with the fixed flume floor prior to any scouring. A sediment bed recess where the vertical-wall abutment models were installed was sufficiently deep to model local scour to a depth of 1.3 ft (0.40 m). Figure 57 shows the test section looking in the upstream direction.

As was common practice for clear-water scour experiments, there was no compaction of the bed material after leveling the sand bed in the test section. The requirement for clear-water scour was that bed transport or scour was not evident in the upstream approach section.

Figure 57. Photo. Vertical-wall abutment models installed in the test section.

In addition to a manually moving carriage, the flume was instrumented with an automated three-axis positioning system shown in figure 58, with traversing capability for the entire length, width, and height of the flume at a resolution of 0.039 inches (1 mm). This carriage could position probes at any location within the test section to make point measurements for flow velocities using an acoustic Doppler velocimeter (ADV) and measurements of bed surface bathymetry using a laser distance sensor.

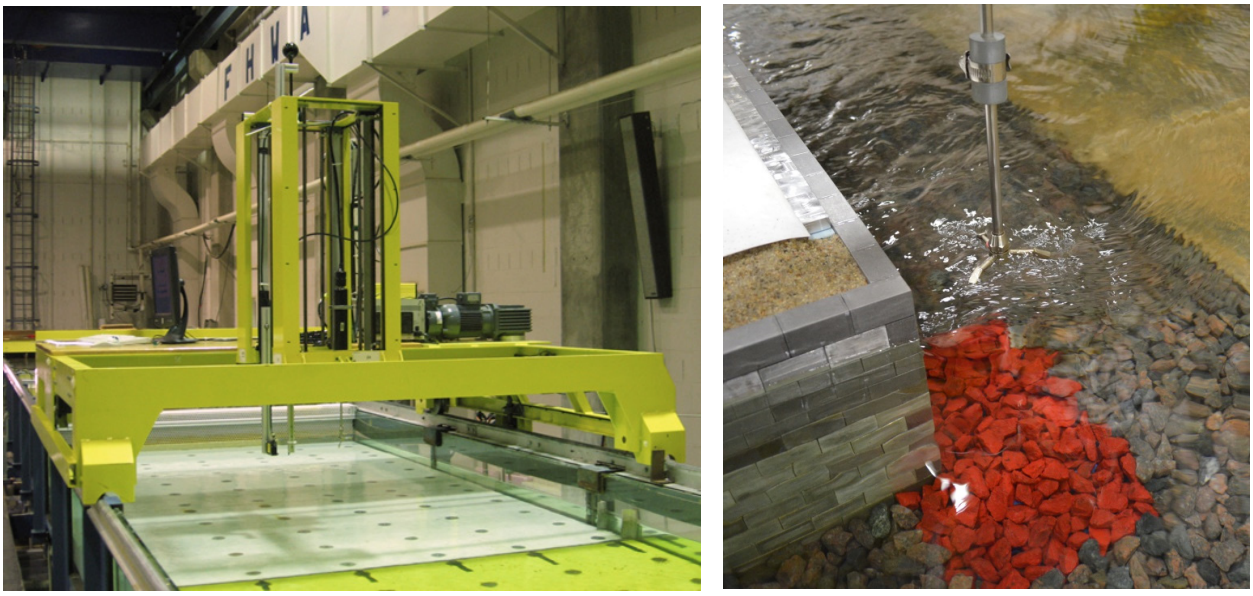

Figure 58. Photos. Automated flume carriage (left) and ADV probe (right).

MODEL LAYOUT AND EXPERIMENTAL PROCEDURE

The laboratory experiments were designed to study the effect of several riprap installations on the contraction scour depth for a small-scale model of a single-span bridge opening. Figure 59 shows a cross-section view of the layout with principal dimensions and relevant hydraulic parameters. Two vertical-wall model abutments built on shallow foundations with the same length were placed in the sediment bed recess. The approach channel width (W_1) was 6 ft (1.8 m), and the contracted (bridge opening) width (W_2) was allowed to vary. The varied contracted width permitted investigation of alternative contraction ratios (W_2/W_1). The abutment width (parallel to the flow direction) of 2.0 ft (0.61 m) was scaled down to represent a road width for two lanes plus shoulders, based on U.S. standards. Froude similarity was applied to set the approach flow (depth and velocity) conditions. All of the physical experiments were performed with a uniform sediment bed (D_{50} = 0.039 inches (1 mm)) under clear-water scour conditions.

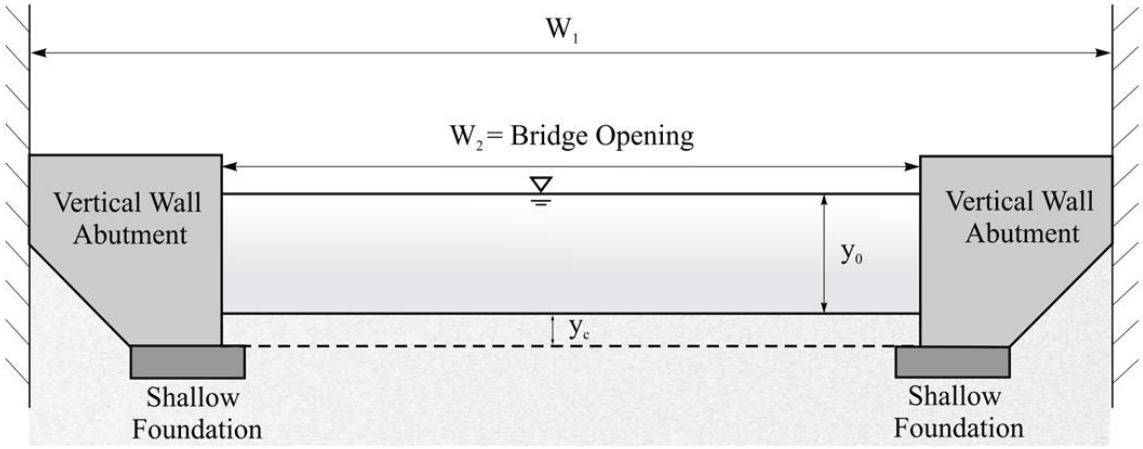

Figure 59. Sketch. Cross-section view of bridge opening for physical experiments.

Based on the design procedure in HEC-23, the base of the abutment (top of foundation) was set at or below the estimated contraction scour plus the LTD.[3] For these experiments, LTD was not considered. For this investigation, Laursen's clear-water contraction scour equation from HEC-18 was used to estimate the predicted contraction scour.[2] Using the contraction ratio (W_2/W_1) and the approach flow conditions, the clear-water contraction scour was computed, and the top of the shallow foundations were placed at the limit of estimated contraction scour, as shown in figure 59.

Several riprap installations for abutment scour from HEC-23 DGs 14 and 18 as well as variations observed in the field were tested.[3] Tests with riprap covering the entire bed were also conducted to explore improved installation practices. In all cases, the test riprap layout was placed on a geotextile filter. The median diameter of the riprap rock was sized for the flow conditions in the bridge opening using the recommendations in HEC-23. All riprap tests had a running time of 24 h to achieve equilibrium conditions during the test. Using the laser distance sensor, a digital bed bathymetry map was obtained to measure the scour depth with the riprap (y_{cR}). These scour depths were compared with the computed contraction scour depths for a condition without riprap.

To ensure that the riprap size determined from the HEC-23 guidance (DGs 14 and 18) would not be susceptible to shear failure, a preliminary series of experiments on a fixed bed were conducted.[3] These experiments confirmed that the riprap size chosen would not fail by shear alone. This would simplify interpretation of failure mechanisms for the experiments with an erodible bed.

EXPERIMENTAL MATRIX AND OBSERVATIONS

Overall, 11 erodible bed experiments were run and are summarized in table 1. Runs 1–5 represented riprap layouts that corresponded to HEC-23 guidelines or variations that had been observed in the field.[3] Runs 6, 8, 9, and 11 were variations of a full-width installation where riprap was extended across the entire contracted channel. Runs 7 and 10 did not have riprap and were provided for comparison. Detailed equilibrium scour maps for all runs are provided in appendix B.

Table 1 summarizes the riprap size used, the contraction ratio, and the approach flow characteristics. The flow depth in the contracted section before erosion (y_0) is also provided. Finally, the table summarizes the estimated contraction scour depth from the HEC-18 equation (y_c) and the measured maximum contraction scour depth with the riprap (y_{cR}).[2] The model scale for length and velocity for the physical experiments was based on a prototype-to-model ratio of 10.

The contraction ratios, W_2/W_1, chosen for the experiments were intended to represent a range within the bounds of a very severe contraction (small contraction ratio) and no contraction (contraction ratio equal to 1). The selected contraction ratios were intended to be conservative for what was likely to occur in the field, which were dependent on stream width.

Table 1. Abutment riprap experimental results.

Run	Riprap Layout	D_{50} (inches)	W_2/W_1	V_1 (ft/s)	y_1 (ft)	y_0 (ft)	W_2/y_0	W_2/y_1	Est. y_C (ft)	y_{cR} (ft)
1	HEC-23 DG 14[3]	0.91	0.64	0.98	0.623	0.623	6.2	6.2	0.20	0.46
2	HEC-23 DG 18[3]	1.46	0.64	0.98	0.623	0.623	6.2	6.2	0.20	0.52
3	Sloped field installation	1.46	0.64	0.98	0.623	0.623	6.2	6.2	0.20	0.56
4	Sloped with $W_R = y_0$	1.46	0.64	0.98	0.623	0.623	6.2	6.2	0.20	0.52
5	Flush with $W_R = y_0$	1.46	0.64	0.98	0.623	0.623	6.2	6.2	0.20	0.46
6	Buried full-width level	1.46	0.64	0.98	0.623	0.623	6.2	6.2	0.20	0.20
7	No riprap	N/A	0.25	0.46	0.541	0.476	3.1	2.7	0.36	0.62*
8	Buried full-width level	1.77	0.25	0.46	0.541	0.476	3.1	2.7	0.36	0.36
9	Buried full-width sloped	1.77	0.25	0.46	0.541	0.476	3.1	2.7	0.36	0.36
10	No riprap (30° skew)	N/A	0.25	0.46	0.541	0.476	3.1	2.7	0.36	0.66*
11	Buried full-width (30° skew)	1.77	0.25	0.46	0.541	0.476	3.1	2.7	0.36	0.36

*Measured depths represent total (abutment and contraction) scour.
Est. = Estimated.
N/A = Not applicable.
1 inch = 25.4 mm.
1 ft/s = 0.305 m/s.
1 ft = 0.305 m.

HEC-23 DGs and Field Installations

The runs for riprap aprons based on HEC-23 guidelines and related field installations (runs 1–5) were all conducted with the same riprap size (except for run 1), contraction ratio, and approach flow conditions.[3] The only change was the riprap layout. For these runs, the HEC-18 estimated contraction scour depth was 0.20 ft (0.061 m).[2] The measured maximum contraction scour depth for these runs ranged from 0.46 to 0.56 ft (0.14 to 0.17 m). However, for these five runs, the estimated contraction scour should not be directly compared with the measured maximum scour because these conditions without riprap were not tested as a reference point.

Figure 60 illustrates the riprap apron layout according to HEC-23 DG 14 for bridge abutments (run 1).[3] The bottom of the apron is located on top of the foundation at an elevation corresponding to the estimated contraction scour depth. It extends out from the abutment a distance of twice the pre-scour flow depth in the contracted section. Photographs of run 1 before and after scour are shown in figure 61. Because the geometric form of the GRS and Plexiglass™

abutments were identical, there was no difference in test results between the two sides. The GRS side was used to provide a more realistic representation of the field installation, while the Plexiglass™ side was used for observational instrumentation.

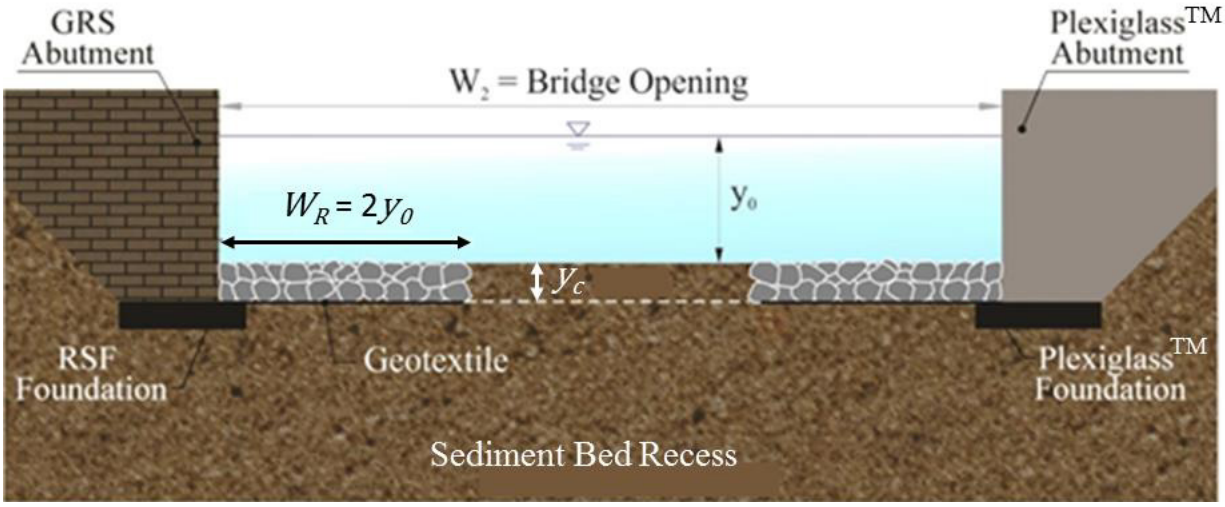

Figure 60. Sketch. Run 1 cross section—HEC-23 DG 14.

Figure 61. Photos. Comparison of run 1 as-built riprap installation (left) and at equilibrium scour (right).

Initial edge failure of the rock occurred near the abutment width centerline. The deepest scour was measured downstream of the abutment width centerline. This result suggested that the apron extent of twice the pre-scour flow depth was sufficient to protect the erodible bed from local vortices and large turbulent structures that developed at the upstream abutment corners, confirming the efficacy of the design guideline for abutment (local) scour. At the same time, the large apron (compared with the opening width) appeared to change the discharge distribution in the contracted section, leading to higher bed shear stresses and, potentially, deeper contraction scour than would have occurred for an unprotected channel bed.

Figure 62 illustrates the riprap apron layout according to HEC-23 DG 18 for bottomless culverts (run 2).[(2)] The bottom of the apron is located on top of the foundation at an elevation corresponding to the estimated contraction scour depth and reaches below the estimated

contraction scour depth beyond the foundation. It extends out from the abutment and slopes down to a toe at a 1:3 vertical-to-horizontal (V:H) slope. Figure 63 compares the run 2 before and after scour.

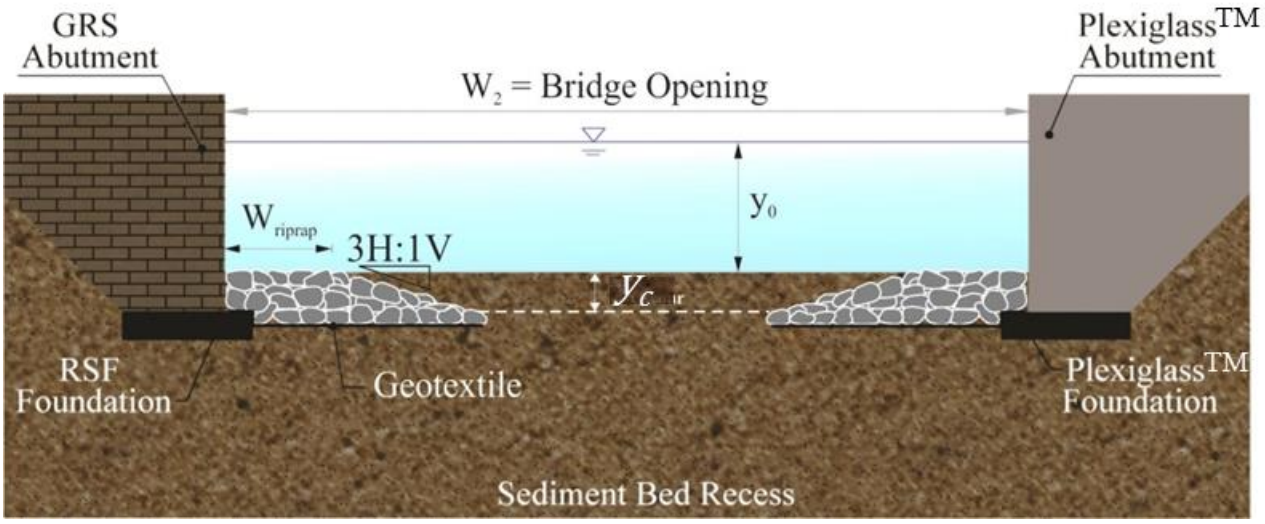

Figure 62. Sketch. Run 2 cross section—HEC-23 DG 18.

Figure 63. Photos. Comparison of run 2 as-built riprap installation (left) and at equilibrium scour (right).

This apron configuration for run 2 was more difficult to prepare than for run 1 because it was difficult to compact the bed material that covered the toe of the riprap. (Geotechnical engineers at the Turner Fairbank Highway Research Center (TFHRC) have noted problems with compaction of the bed materials on top of the sloped riprap for field applications.) In addition, the riprap volume required was almost twice the amount as that for DG 14 layout. Initially, bed material on top of the riprap was easily eroded owing to the horseshoe vortex at the upstream edge of the abutments. Subsequently, an edge failure similar to that observed for run 1 was also observed for run 2.

Figure 64 illustrates a sloped riprap apron layout loosely based on HEC-23 DG 18 for bottomless culverts (run 3).[2] In this installation, the effect on the streambed was reduced by decreasing the

apron extent. This was compensated for by piling the riprap higher so that when scour occurred, the reserves of rock could tumble into the scour hole thereby armoring the hole. Photographs of run 3 before and after scour are shown in figure 65.

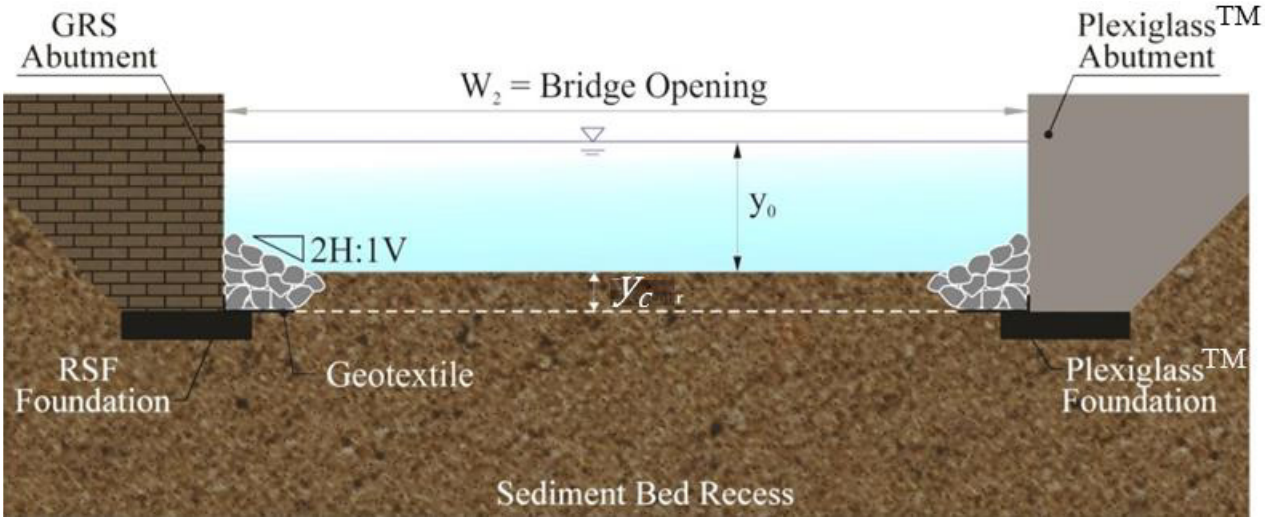

Figure 64. Sketch. Run 3 cross section—sloped field installation.

Figure 65. Photos. Comparison of run 3 as-built riprap installation (left) and at equilibrium scour (right).

In run 3, the scour hole at the upstream edge of the riprap developed quickly and before any erosion across the bridge opening was visible. The edge failure was followed by a translational slide (or modified slump) of the riprap once the geotextile filter at the bottom was undermined. The downslope movement of rock resulted from a loss of foundation support at the toe induced by the edge failure. As is seen in the figure, large amounts of riprap material fell into the scour hole.

Figure 66 illustrates a sloped riprap apron (run 4) that expanded on the configuration in run 3 by extending the riprap apron to a distance equal to the pre-scour water depth. As with run 3, a reserve of riprap was piled above the bed elevation so that when scour occurred, the reserves of rock could tumble into the scour hole thereby armoring the hole. Photographs of the run 4 before and after scour are shown in figure 67.

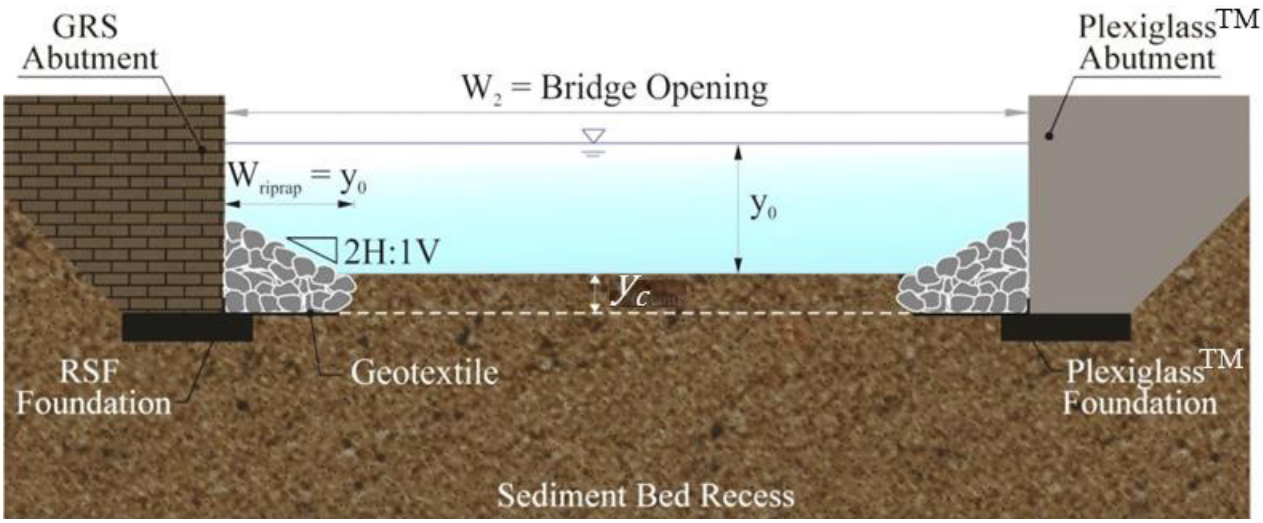

Figure 66. Sketch. Run 4 cross section—sloped.

Figure 67. Photos. Comparison of run 4 as-built riprap installation (left) and at equilibrium scour (right).

For run 4, scour started at the upstream edge of the riprap with substantial erosion across the bridge opening. An edge failure was followed by a translational slide (or modified slump) of the riprap once the geotextile filter at the bottom was undermined. The downslope movement of rock resulted from a loss of foundation support at the toe induced by edge failure. The effect of side slope geometry appeared to increase the erosion intensity on the bed material. After equilibrium was reached, the remaining horizontal apron width was measured along the periphery of the abutment. The average remaining width at the front face was 60 percent of the installed apron width (i.e., about 40 percent of the original apron was undermined).

Figure 68 illustrates a level riprap apron that follows HEC-23 DG 14 except that the apron width extends only to a distance equal to the pre-scour water depth rather than twice the pre-scour water depth (run 5).[3] Photographs of the run 5 before and after scour are shown in figure 69.

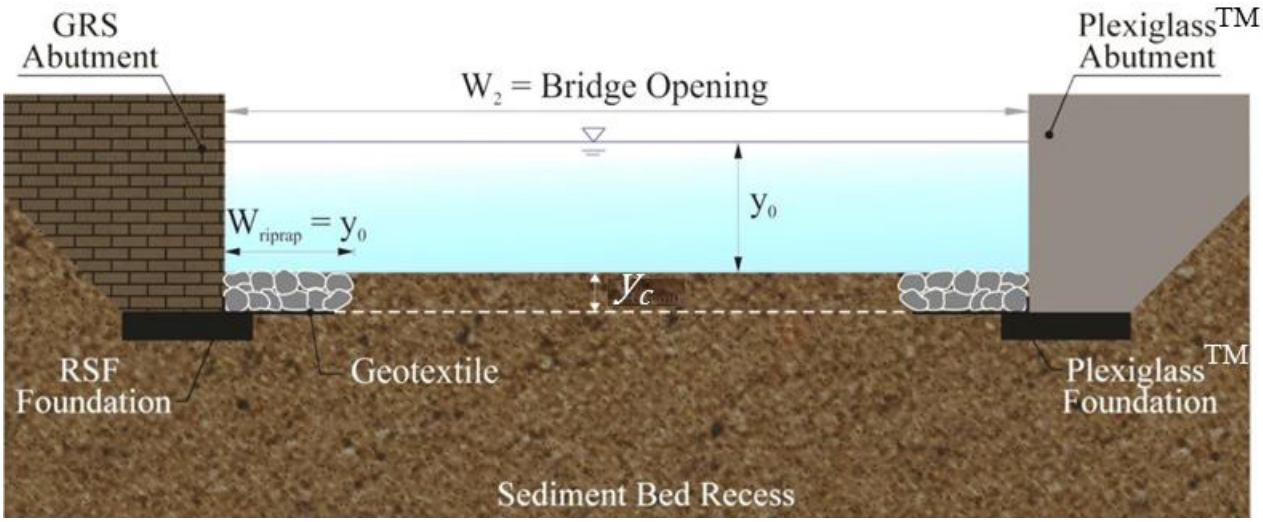

Figure 68. Sketch. Run 5 cross section—flush.

Figure 69. Photos. Comparison of run 5 as-built riprap installation (left) and at equilibrium scour (right).

In run 5, the scour hole at the upstream edge of the riprap developed quickly before contraction scour began. An edge failure then occurred, resulting in riprap falling into the scour hole. The remaining apron was measured along the periphery of the abutment. The remaining apron width at the front face was 70 percent of the original width, that is, 30 percent of the original apron was undermined.

All five of the initial set of runs resulted in edge failures with loss of riprap into the contraction scour hole. Runs 1 and 5 were based on HEC-23 DG 14 and differed only in apron extent.[3] Even with the differing extents, the measured maximum scour for these two runs was the same at 0.46 ft (0.14 m). This was less than the measured scour depth for the three sloped riprap installations (runs 2–4).

In general, the edge failure observed in runs 1–5 did not result in a threatening situation for the model abutments or abutment foundations during the test period. However, edge failure could lead to shear failure or could be combined with winnowing failure or failure resulting from bed-form movement.[16]

Because these riprap aprons are considered a structural component of shallow foundation designs, they must maintain their integrity throughout the design life of the bridge. Therefore, while edge failure in a 24-h steady-state hydrologic event might not result in abutment failure in the laboratory, edge failure may result in more threatening consequences in the field because of the hydrologic, geomorphic, debris, and sediment transport variability experienced.

Buried Full-Width Installations

A proposed variation on HEC-23 DG 14 for narrow openings was evaluated in a second set of runs.[3] The major differences between the original HEC-23 DG 14 and the proposed variation were that the apron extent fully spanned the contracted section and was buried to potentially address environmental and aesthetic concerns. However, installation would require initial disturbance of the entire channel cross section at the bridge. Runs 8, 9, and 11 were all conducted with the same riprap size, contraction ratio, and approach flow conditions; however, these conditions were not the same as those for the first set of runs (1–5). Riprap rock size for runs 8, 9, and 11 was computed using HEC-23 DG 14. In each case, the apron was extended upstream and downstream of the abutment a distance equal to 1.5 times the pre-scour flow depth in the contracted section. For these runs, the HEC-18 estimated contraction scour depth was 0.36 ft (0.11 m).[2] The measured maximum contraction scour depth for these runs was also 0.36 ft (0.11 m), because once the scour depth reached this elevation, further scour was prevented by the riprap apron.

Run 6 was conducted with the same set of hydraulic conditions as runs 1–5. Runs 7 and 10 did not include riprap and provide a reference for comparing measured scour depths.

Figure 70 illustrates a full-width buried apron (run 6). The top of the apron is located flush with the top of the foundation at an elevation corresponding to the estimated contraction scour depth. It extends the full width of the contracted opening. The apron extends upstream of the abutment a distance of $1.5y_0$. It was speculated that for flows lower than the scouring flows, sediment might replenish the bed. Photographs of run 6 before and after scour are shown in figure 71.

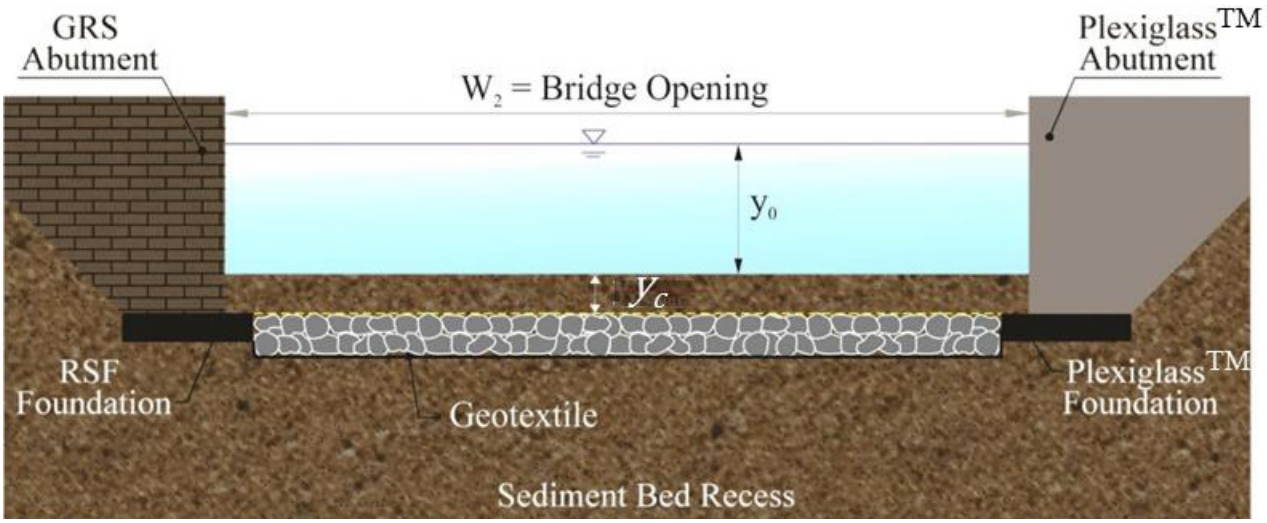

Figure 70. Sketch. Run 6 cross section—buried full-width level.

Figure 71. Photos. Comparison of run 6 as-built riprap installation (left) and at equilibrium scour (right).

As shown in figure 71, there was no edge failure at the upstream or downstream edges; the apron remained intact. Local scour naturally formed at the abutment toe upstream corner. This erosion process occurred rapidly until the riprap apron surface became exposed. The scour hole expanded toward the centerline of the bridge opening.

Figure 72 also illustrates a full-width buried apron (run 8) as was shown for run 6. In run 8, the contraction was more severe, and the approach flow conditions were changed from run 6. Photographs of run 8 before and after scour are shown in figure 73.

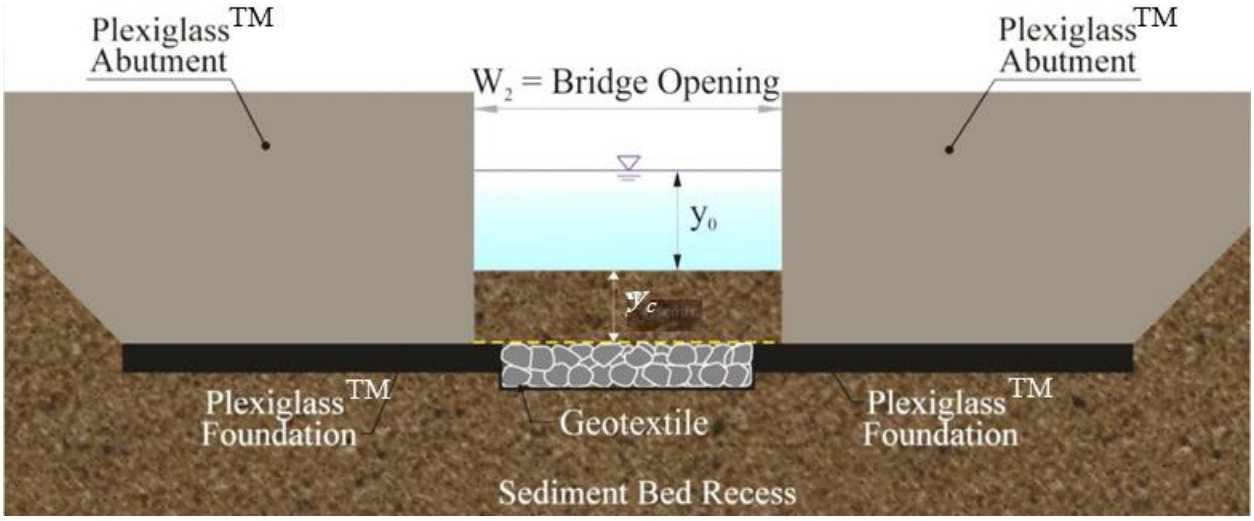

Figure 72. Sketch. Run 8 cross section—buried full-width level.

Figure 73. Photos. Comparison of run 8 as-built riprap installation (left) and at equilibrium scour (right).

In run 8, local scour formed at the abutment toe upstream corner. This erosion process occurred rapidly until the riprap apron surface became exposed. The riprap apron halted the scouring process, and no edge failure occurred. The scour hole expanded toward the centerline of the bridge opening.

Figure 74 illustrates a sloped full-width buried apron that was tested in run 9. The concept of the sloped configuration was to facilitate a transition from the channel to the channel bank upstream and downstream of the contraction. Photographs of the run 9 before and after scour are shown in figure 75.

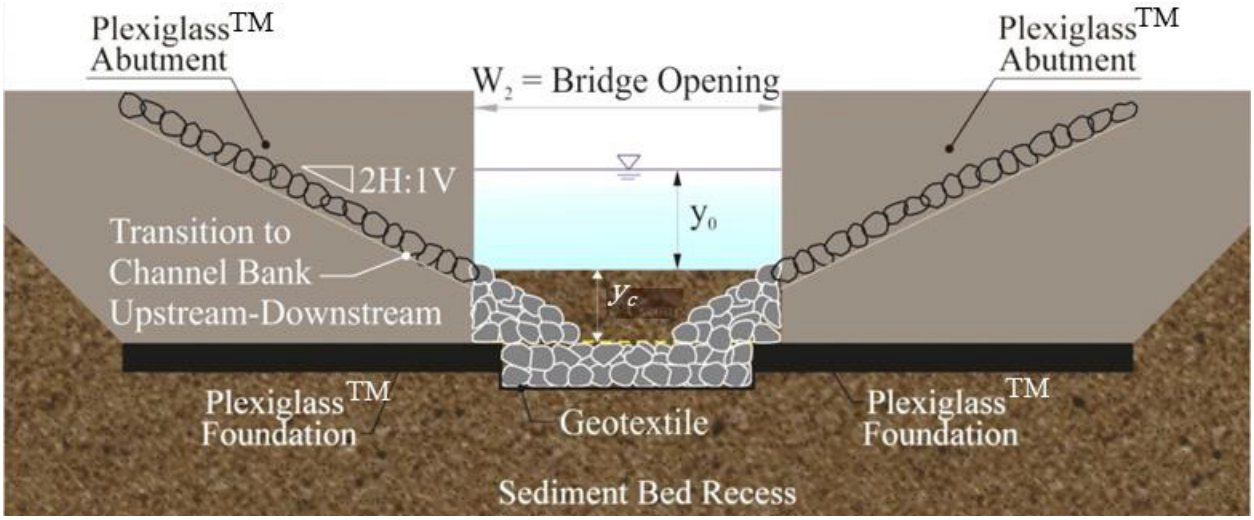

Figure 74. Sketch. Run 9 cross section—buried full-width sloped.

Figure 75. Photos. Comparison of run 9 as-built riprap installation (left) and at equilibrium scour (right).

During run 9, local scour formed at the upstream corner of the abutment toe. The erosion process occurred rapidly until the riprap apron surface became exposed and halted further erosion. No edge failure was observed. The scour hole expanded toward the centerline of the bridge opening.

Figure 76 illustrates a full-width buried apron for an opening on a 30-degree skew that was tested in run 11. The apron configuration and opening width was the same as that used for run 8. Photographs of run 11 before and after scour are shown in figure 77.

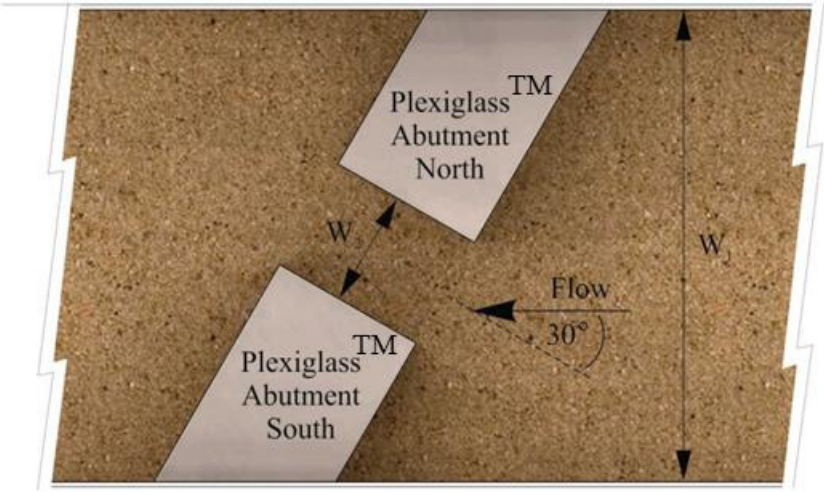

Figure 76. Sketch. Run 11 plan view—buried full-width 30-degree skew.

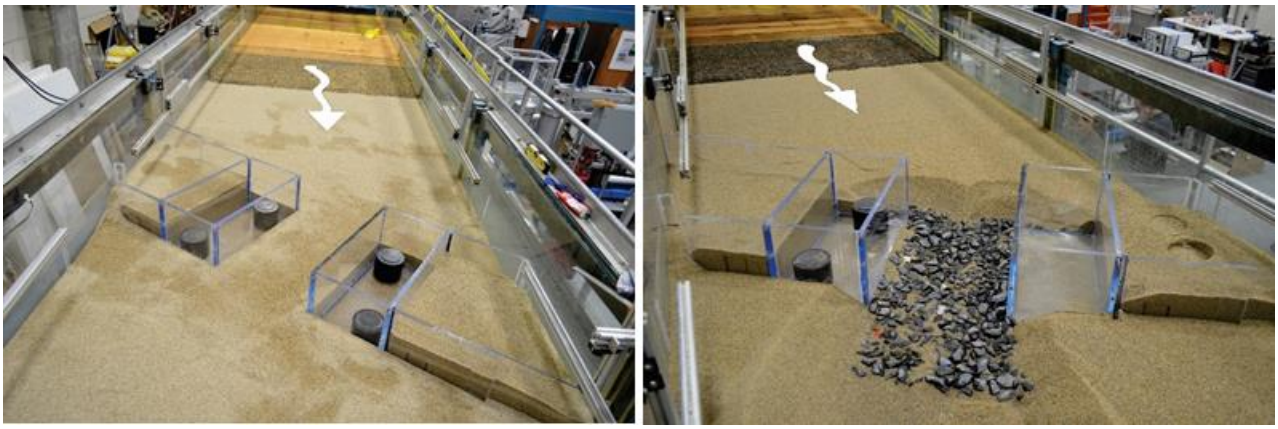

Figure 77. Photos. Comparison of run 11 as-built riprap installation (left) and at equilibrium scour (right).

As with the other runs in this set, local scour formed at the upstream corner of the abutment toe. This erosion process occurred rapidly until the riprap apron surface became exposed and halted further scour. No edge failure occurred. The scour hole expanded toward the centerline of the bridge opening.

DISCUSSION

The physical experiments were designed to validate the hypothesis of increased shear stress with riprap aprons and to provide observations regarding riprap apron failure modes. The physical experiments also provided a basis for designing the numerical modeling experiments conducted using CFD. The CFD experiments are discussed in chapter 5.

Regardless of the type of riprap installation, the riprap aprons in runs 1–5 experienced an edge failure as contraction scour occurred in the area of the contracted section not protected by riprap. For each of these cases, the maximum scour with the riprap, y_{cR}, exceeded the estimated average contraction scour without riprap, y_c (see table 1). However, the former value was a maximum

value and the latter was intended to be a cross-section average; therefore, they were not directly comparable. In addition, there was no run with these abutment and hydraulic characteristics without riprap to use as a benchmark.

Run 6 tested the same hydraulic characteristics as runs 1–5 but employed a buried full-width riprap protection layer. Abutment and contraction scour in this case went down to the riprap layer but was stopped by the riprap. If the riprap was adequately sized and properly installed, these results indicate the effectiveness of the full-width protection strategy in both arresting the abutment scour and the added contraction scour resulting from the presence of the riprap.

Variations of buried full-width protection at a more severe contraction ratio were tested in runs 8, 9, and 11. Whether sloped or level, the riprap stopped the contraction scour at the top of the riprap layer, and riprap failure was not observed. The appropriate approach to designing a full-width apron likely depends on the configuration of the channel and the need to transition to sloping channel banks up and downstream of the abutment. (It was noted that some field installations that nominally followed HEC-23 DG 18 included mounded riprap layers, not recognizing that the shape of the installation was intended to conform to the channel banks rather than mounding for its own sake.[3])

Finally, the two cases without riprap aprons, runs 7 and 10, experienced the greatest scour depths. While these scour depths were nearly double the estimated contraction scour for these conditions, the measured value was a point value and the estimated scour was a cross-section average. Also for these cases, the maximum measured scour represented the local abutment scour, which would be significantly greater than the estimated contraction scour depth. For this abutment geometry, amplification of contraction scour could be a factor of 1.75 based on the NCHRP abutment scour method.[2]

Overall, these experiments showed that for the contractions tested, partial-width aprons placed flush with the original streambed surface were prone to failure because of contraction scour in the gap between the aprons. The experiments further demonstrated that, if properly designed, full-width riprap aprons buried so that the top of the apron was located at the estimated contraction scour depth could be effective at protecting against both abutment and contraction scour.

CHAPTER 5. NUMERICAL MODELING

CFD modeling was conducted to supplement the physical experiments by expanding the range of bridge opening widths and contraction ratios to validate and further develop the conceptual model described in chapter 3. The CFD experiments were used for comparative purposes to evaluate the relative effects of alternative riprap apron designs, particularly partial-width buried installations, to support development of design guidelines. CFD and physical modeling results were not compared. With respect to the conceptual model described in chapter 3, one objective of the CFD modeling was to determine a function for the parameter ε given in the equation in figure 55.

MODEL CONFIGURATION

Numerical models were developed with and without riprap aprons to obtain the bed shear stresses τ_R and τ_B, respectively. The following four general sets of models were developed and analyzed:

- Flush installations of riprap at a model scale.
- Flush installations of riprap at a prototype scale.
- Buried installations of riprap at a prototype scale.
- Alternative abutment setbacks at a prototype scale.

For the flush installations at both the model and prototype scales, the riprap was modeled as recommended in HEC-23 DG 14.[3] The riprap apron extended into the channel at a distance from the abutment of $2y_0$ (not to exceed 25 ft (7.6 m)) and upstream and downstream at a distance from the abutment of $2y_0$ (not less than 25 ft (7.6 m)). The channels were trapezoidal with 1:2 (V:H) side slopes, as shown for with and without riprap conditions in figure 78.

An additional set of models were prepared for the buried installation. The same channel geometry and riprap installation were used for these runs except the apron was located so that the top of the riprap layer was located at the contraction scour depth. That is, the apron was buried below the original bed elevation by the estimated contraction depth. The CFD runs were performed assuming this bed material had been eroded away and the riprap apron was exposed. The geometry for these models is shown in figure 79.

The alternative channel shape models differed from one another by the setback of the abutment face to the bottom of the trapezoidal channel, as shown in figure 80. The top geometry was used for the buried installation comparisons. The other two represented a short extension in the setback and a long extension in the setback. The setbacks were 0.98, 2.53, and 3.97 ft (0.30, 0.77, and 1.21 m), respectively.

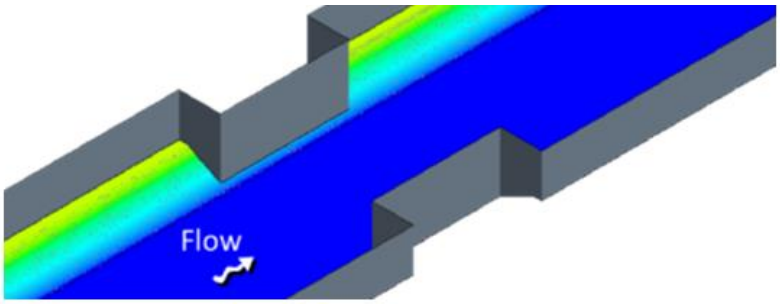

Model without riprap

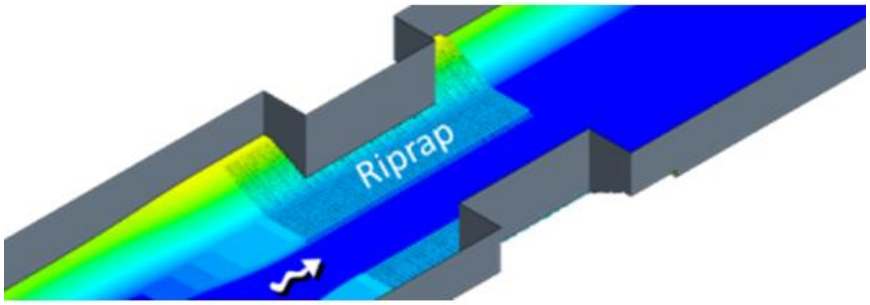

Model with riprap

Figure 78. Schematics. Comparison of CFD models for flush installation.

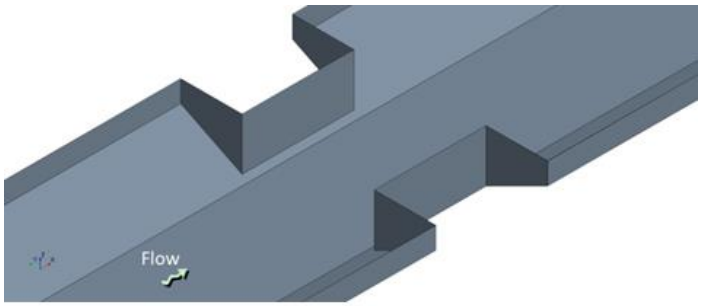

Model without riprap

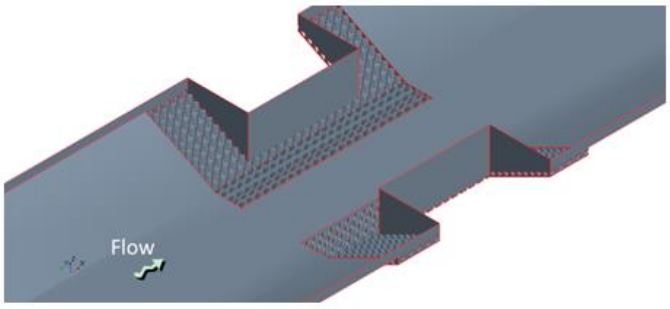

Model with riprap

Figure 79. Schematics. Comparison of CFD models for buried installation.

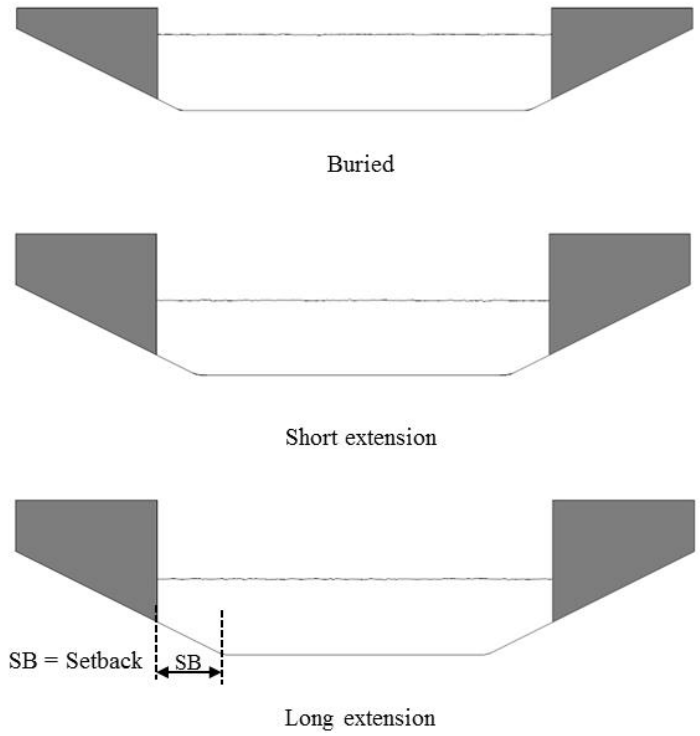

Figure 80. Schematics. Comparison of channel setback alternatives.

CFD TEST MATRIX

To study the interaction between bed shear stress and riprap for bridge openings of different widths and the effects of flush versus buried installations, a series of bridge opening models with a range of W_2 and riprap sizes were built in CFD simulation and are summarized in table 2.

Table 2. CFD test matrix for riprap comparisons.

	Model Scale			Prototype Scale			
W_2/y_0	Flush Group #1	Flush Group #2	Flush Group #3	Flush Group #4	Flush Group #5	Flush Group #6	Buried Group #7
6.2	Case 1	Case 6	Case 11	Case 16	Case 21	Case 26	Case 31
8	Case 2	Case 7	Case 12	Case 17	Case 22	Case 27	Case 32
10	Case 3	Case 8	Case 13	Case 18	Case 23	Case 28	Case 33
12	Case 4	Case 9	Case 14	Case 19	Case 24	Case 29	Case 34
16	Case 5	Case 10	Case 15	Case 20	Case 25	Case 30	Case 35
Riprap D_{50} (inches)	0.91	1.38	2.07	9.06	13.78	20.67	20.67

1 inch = 25.4 mm.

Each case consisted of two CFD models—one with and one without a riprap apron—so that the ratio of τ_R/τ_B could be estimated. A total of 35 cases (70 models) were established and divided into

several groups. The first three groups of numerical models were built at a model scale. Case 1 most closely resembled the physical tests performed at the TFHRC and discussed in chapter 4.

The subsequent groups were built in prototype scale with a length ratio of 10 (prototype to model). The prototype tests were conducted to demonstrate that CFD modeling effectively represents both model and prototype scales.

The first six groups used a flush installation of the riprap apron, while the last group used a buried installation. Each group consisted of five cases for bridge openings with W_2/y_0 ranging from 6.2 to 16. Constants within each group were the riprap size D_{50} and velocity in the opening V_2. The riprap size is determined by the sizing equation in HEC-23 (DG 14), as shown in figure 81.[3]

$$\frac{D_{50}}{y_0} = \frac{K}{(S_g - 1)} Fr_0^2$$

Figure 81. Equation. HEC-23 (DG 14) riprap sizing.

Where:

K = Coefficient (0.89 for a spill-through abutment and 1.02 for vertical-wall abutment) (dimensionless).

An additional series of CFD models were developed and run to investigate the effects of alternative channel setbacks and are summarized in table 3. All of these cases were at prototype scale and only included the natural bed material; no riprap aprons were evaluated.

Table 3. CFD test matrix for alternative setbacks.

W_2/y_0	Short Extension Slope	Long Extension Slope
8	Case 36	Case 40
10	Case 37	Case 41
12	Case 38	Case 42
16	Case 39	Case 43

NUMERICAL MODELING RESULTS

Bed shear stress distributions and cross-section velocity distributions of the central cross sections for each of the CFD models were determined. The results are discussed for the flush installation of riprap, the buried installation of riprap, and the alternative channel setback cases.

Flush Installation

Table 4 summarizes the defining parameters for each case, including the geometry, riprap size, bed material size, and hydraulics for the flush and buried installation riprap cases. Table 5 summarizes the shear stress and other results from the runs. The equivalent width was the cross-section area divided by the depth.

Table 4. CFD test parameters for riprap installations.

Group	Case	Riprap D_{50} (inches)	Bed D_{50} (inches)	W_1 (ft)	y_1 (ft)	A_1 (ft^2)	V_1 (ft/s)	W_2 (ft)	y_0 (ft)	y_2 (ft)	V_2 (ft/s)
Flush Group #1	1	0.91	0.04	6.57	0.77	3.9	1.24	3.87	0.62	0.77	1.61
	2	0.91	0.04	7.68	0.77	4.8	1.30	4.99	0.62	0.77	1.61
	3	0.91	0.04	8.93	0.77	5.7	1.35	6.23	0.62	0.77	1.61
	4	0.91	0.04	10.18	0.77	6.7	1.39	7.48	0.62	0.77	1.61
	5	0.91	0.04	12.67	0.77	8.6	1.44	9.97	0.62	0.77	1.61
Flush Group #2	6	1.38	0.04	6.88	0.85	4.4	1.34	3.87	0.62	0.85	1.80
	7	1.38	0.04	8.00	0.85	5.4	1.42	4.99	0.62	0.85	1.80
	8	1.38	0.04	9.25	0.85	6.4	1.48	6.23	0.62	0.85	1.79
	9	1.38	0.04	10.49	0.85	7.5	1.52	7.48	0.62	0.85	1.79
	10	1.38	0.04	12.99	0.85	9.6	1.58	9.97	0.62	0.85	1.79
Flush Group #3	11	2.07	0.04	7.34	0.97	5.2	1.38	3.87	0.62	0.97	1.94
	12	2.07	0.04	8.46	0.97	6.3	1.47	4.99	0.62	0.97	1.93
	13	2.07	0.04	9.70	0.97	7.5	1.55	6.23	0.62	0.97	1.94
	14	2.07	0.04	10.95	0.97	8.7	1.60	7.48	0.62	0.97	1.94
	15	2.07	0.04	13.44	0.97	11.1	1.67	9.97	0.62	0.97	1.93
Flush Group #4	16	9.06	0.16	65.68	7.74	388.7	3.17	38.71	6.23	7.74	4.14
	17	9.06	0.16	76.84	7.74	475.0	3.34	49.87	6.23	7.74	4.13
	18	9.06	0.16	89.30	7.74	571.6	3.47	62.34	6.23	7.74	4.13
	19	9.06	0.16	101.77	7.74	668.1	3.56	74.80	6.23	7.74	4.12
	20	9.06	0.16	126.71	7.74	861.2	3.68	99.74	6.23	7.74	4.11
Flush Group #5	21	13.78	0.16	68.83	8.53	441.6	3.12	38.71	6.23	8.53	4.20
	22	13.78	0.16	79.99	8.53	536.8	3.31	49.87	6.23	8.53	4.20
	23	13.78	0.16	92.45	8.53	643.1	3.46	62.34	6.23	8.53	4.19
	24	13.78	0.16	104.92	8.53	749.5	3.56	74.80	6.23	8.53	4.19
	25	13.78	0.16	129.86	8.53	962.2	3.70	99.74	6.23	8.53	4.19
Flush Group #6	26	20.67	0.16	73.43	9.68	523.3	3.04	38.71	6.23	9.68	4.27
	27	20.67	0.16	84.58	9.68	631.3	3.25	49.87	6.23	9.68	4.27
	28	20.67	0.16	97.05	9.68	751.9	3.41	62.34	6.23	9.68	4.27
	29	20.67	0.16	109.51	9.68	872.6	3.53	74.80	6.23	9.68	4.26
	30	20.67	0.16	134.45	9.68	1113.9	3.68	99.74	6.23	9.68	4.26
Buried Group #7	31	20.67	0.04	71.85	9.68	508.1	1.76	38.71	6.23	9.68	2.41
	32	20.67	0.04	82.94	9.68	615.4	1.88	49.87	6.23	9.68	2.41
	33	20.67	0.04	95.41	9.68	736.0	1.97	62.34	6.23	9.68	2.42
	34	20.67	0.04	107.87	9.68	856.7	2.03	74.80	6.23	9.68	2.42
	35	20.67	0.04	132.81	9.68	1098.0	2.12	99.74	6.23	9.68	2.42

1 inch = 25.4 mm.
1 ft = 0.305 m.
1 ft^2 = 0.093 m^2.
1 ft/s = 0.305 m/s.

Table 5. CFD test results for riprap installations.

Group	Case	Equivalent W_1 (ft)	W_2/y_0	Fr_1	τ_B (lbf/ft^2)	τ_R (lbf/ft^2)	τ_R/τ_B	n_B	n_R	n_R/n_B	W_2/W_1
Flush Group #1	1	5.02	6.2	0.25	0.0191	0.0243	1.27	0.013	0.022	1.69	0.77
	2	6.14	8.0	0.26	0.0186	0.0224	1.21	0.013	0.022	1.69	0.81
	3	7.38	10.0	0.27	0.0185	0.0210	1.14	0.013	0.022	1.69	0.84
	4	8.63	12.0	0.28	0.0189	0.0200	1.06	0.013	0.022	1.69	0.87
	5	11.12	16.0	0.29	0.0183	0.0189	1.03	0.013	0.022	1.69	0.90
Flush Group #2	6	5.18	6.2	0.25	0.0243	0.0367	1.51	0.013	0.023	1.81	0.75
	7	6.29	8.0	0.27	0.0224	0.0301	1.34	0.013	0.023	1.81	0.79
	8	7.54	10.0	0.28	0.0214	0.0259	1.21	0.013	0.023	1.81	0.83
	9	8.79	12.0	0.29	0.0206	0.0242	1.18	0.013	0.023	1.81	0.85
	10	11.28	16.0	0.30	0.0192	0.0217	1.13	0.013	0.023	1.81	0.88
Flush Group #3	11	5.41	6.2	0.25	0.0291	0.0698	2.40	0.013	0.025	1.94	0.72
	12	6.52	8.0	0.26	0.0293	0.0560	1.91	0.013	0.025	1.94	0.76
	13	7.77	10.0	0.28	0.0253	0.0352	1.39	0.013	0.025	1.94	0.80
	14	9.02	12.0	0.29	0.0238	0.0312	1.31	0.013	0.025	1.94	0.83
	15	11.51	16.0	0.30	0.0236	0.0267	1.13	0.013	0.025	1.94	0.87
Flush Group #4	16	50.20	6.2	0.20	0.0379	0.0577	1.52	0.016	0.032	1.96	0.77
	17	61.35	8.0	0.21	0.0457	0.0590	1.29	0.016	0.032	1.96	0.81
	18	73.82	10.0	0.22	0.0423	0.0499	1.18	0.016	0.032	1.96	0.84
	19	86.29	12.0	0.23	0.0430	0.0531	1.24	0.016	0.032	1.96	0.87
	20	111.22	16.0	0.23	0.0429	0.0555	1.29	0.016	0.032	1.96	0.90
Flush Group #5	21	51.77	6.2	0.19	0.0435	0.0646	1.48	0.016	0.034	2.11	0.75
	22	62.93	8.0	0.20	0.0405	0.0570	1.41	0.016	0.034	2.11	0.79
	23	75.39	10.0	0.21	0.0302	0.0519	1.72	0.016	0.034	2.11	0.83
	24	87.86	12.0	0.21	0.0350	0.0562	1.60	0.016	0.034	2.11	0.85
	25	112.80	16.0	0.22	0.0282	0.0374	1.33	0.016	0.034	2.11	0.88
Flush Group #6	26	54.07	6.2	0.17	0.0327	0.0836	2.56	0.016	0.037	2.25	0.72
	27	65.22	8.0	0.18	0.0345	0.0727	2.11	0.016	0.037	2.25	0.76
	28	77.69	10.0	0.19	0.0328	0.0639	1.95	0.016	0.037	2.25	0.80
	29	90.16	12.0	0.20	0.0274	0.0471	1.72	0.016	0.037	2.25	0.83
	30	115.09	16.0	0.21	0.0274	0.0415	1.51	0.016	0.037	2.25	0.87
Buried Group #7	31	52.49	6.2	0.10	0.0228	0.0221	0.97	0.013	0.037	2.84	0.74
	32	63.58	8.0	0.11	0.0192	0.0186	0.97	0.013	0.037	2.84	0.78
	33	76.05	10.0	0.11	0.0190	0.0167	0.88	0.013	0.037	2.84	0.82
	34	88.52	12.0	0.12	0.0219	0.0236	1.08	0.013	0.037	2.84	0.85
	35	113.45	16.0	0.12	0.0163	0.0163	1.00	0.013	0.037	2.84	0.88

1 ft = 0.305 m.
1 lbf/ft^2 = 47.88 Pa.

Figure 82 compares the bed shear stress distributions of the model with riprap with those of the model without riprap for case 11. In this case, the shear stress for the case without riprap, τ_B, was 0.029 lbf/ft^2 (1.4 Pa), while the shear stress for the case with riprap, τ_R, was 0.070 lbf/ft^2 (3.3 Pa). The shear ratio τ_R/τ_B is 2.4. Similarly, figure 83 and figure 84 provide the

comparison for increasingly lower contraction ratios. The shear ratios for these cases dropped to 1.4 and 1.1, respectively.

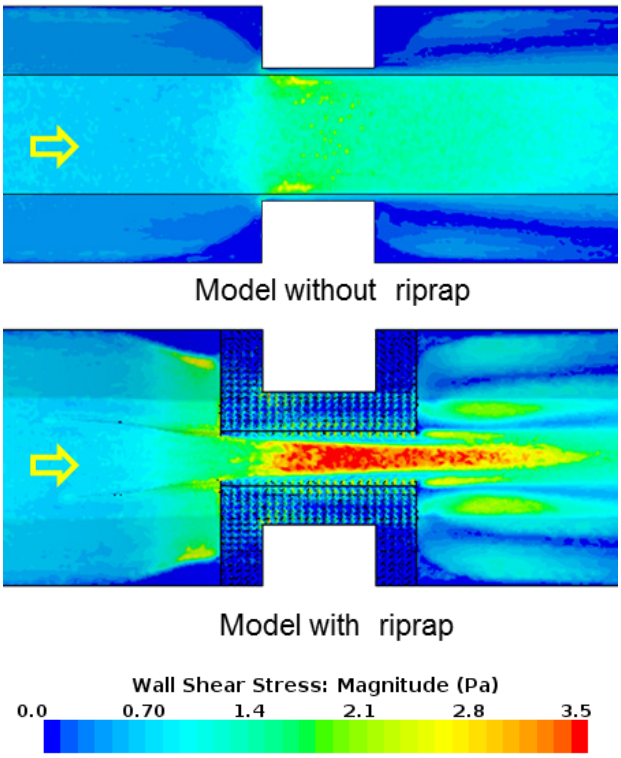

1 lbf/ft^2 = 47.88 Pa.

Figure 82. Graphics. Comparison of bottom shear stress distribution for case 11.

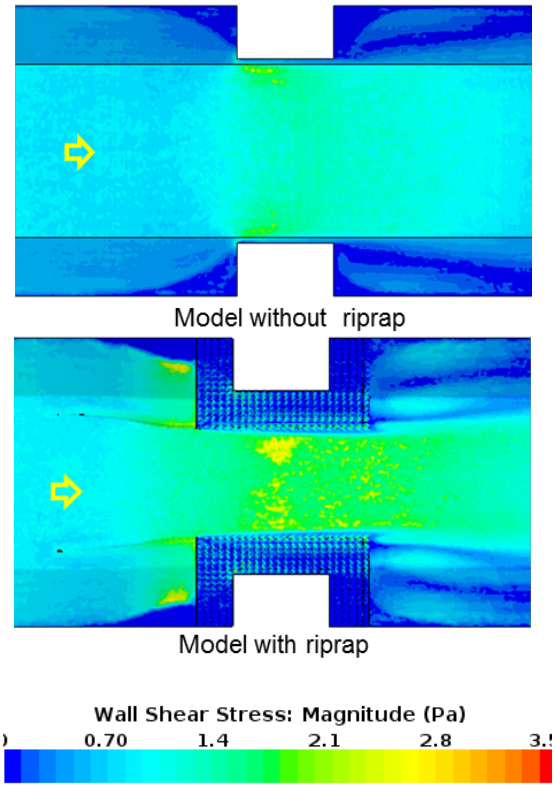

1 lbf/ft^2 = 47.88 Pa.

Figure 83. Graphics. Comparison of bottom shear stress distribution for case 13.

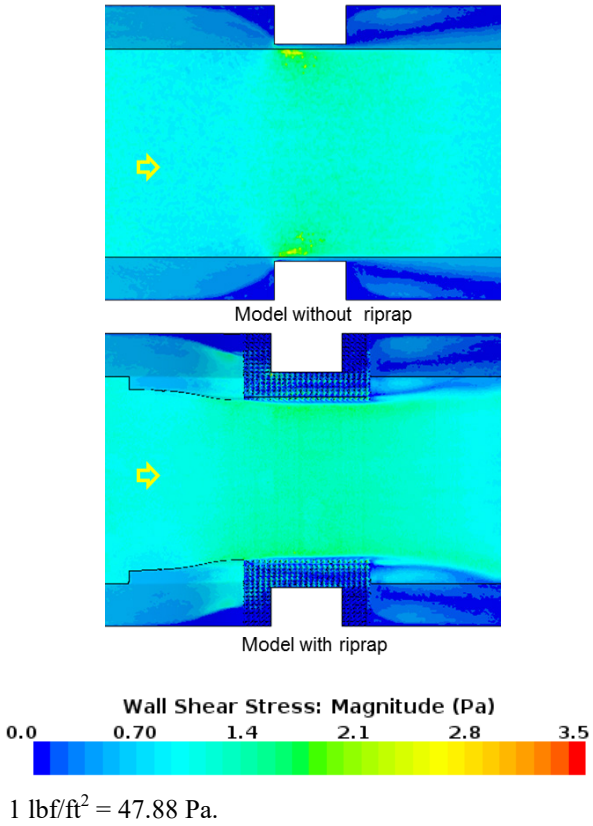

1 lbf/ft^2 = 47.88 Pa.

Figure 84. Graphics. Comparison of bottom shear stress distribution for case 15.

Figure 85 shows the velocity distribution for case 11. In this case, the apron for the model with riprap covered a significant part of the bottom, resulting in higher velocities compared with the model without riprap. As the opening became wider compared with the depth for case 13 (figure 86) and case 15 (figure 87), the difference between the model with riprap and the model without riprap diminished.

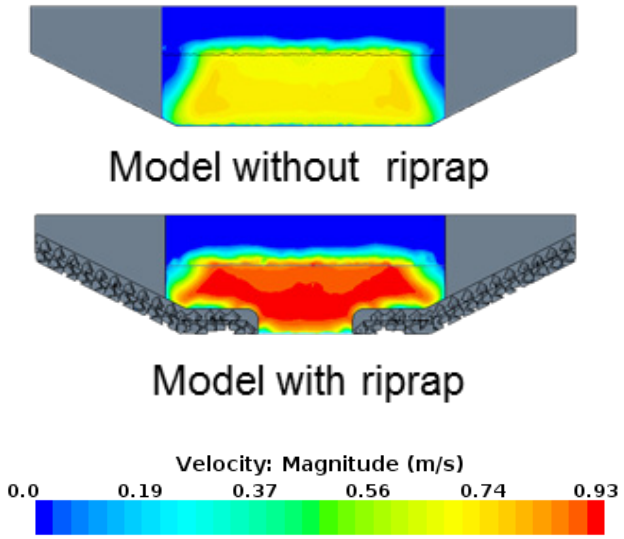

1 lbf/ft^2 = 47.88 Pa.

Figure 85. Graphics. Comparison of velocity distribution for case 11.

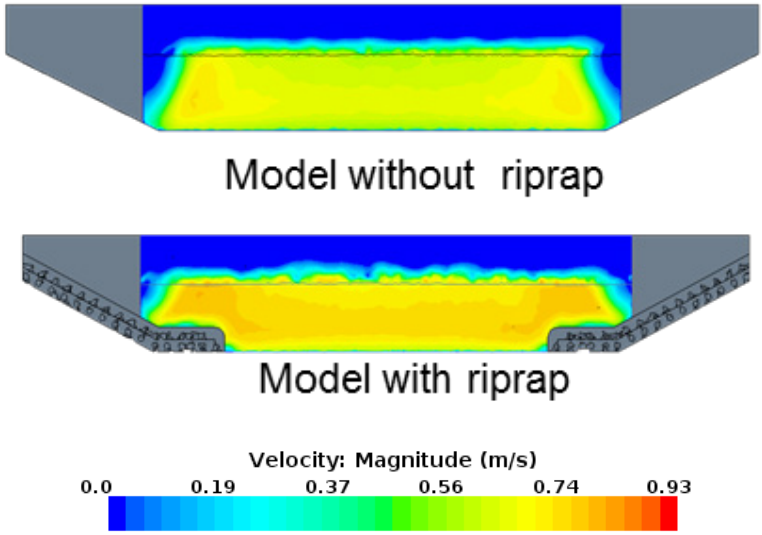

1 lbf/ft^2 = 47.88 Pa

Figure 86. Graphics. Comparison of velocity distribution for case 13.

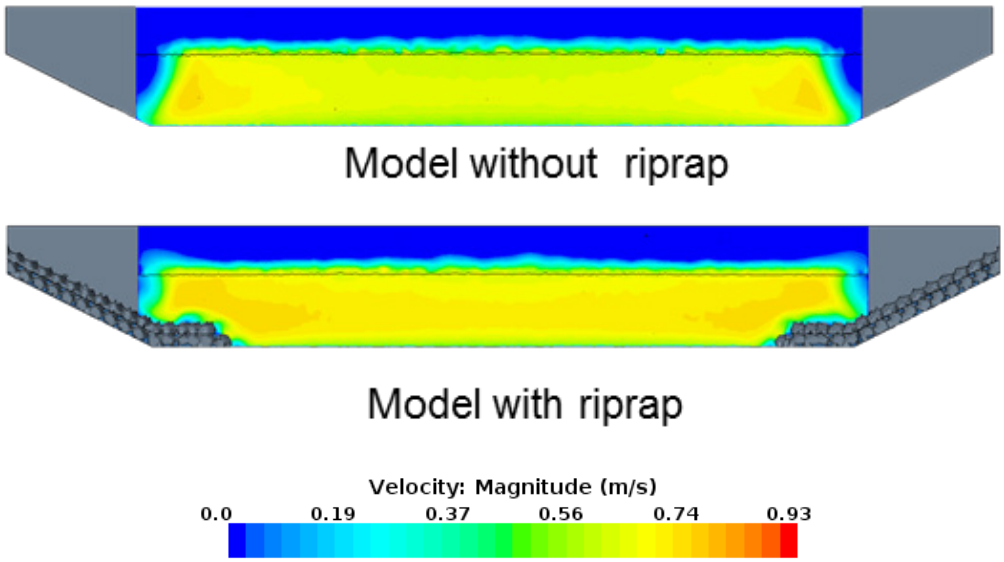

1 lbf/ft^2 = 47.88 Pa

Figure 87. Graphics. Comparison of velocity distribution for case 15.

Comparing the shear ratio of different groups in table 5, it can be seen that the shear ratio increased with the riprap size. For example, the shear ratios for three cases of the same $W_2/y_0 = 6.2$ increased from 1.27 for case 1, to 1.51 for case 6, and to 2.40 for case 11. The difference gradually decreased with increasing opening-to-width ratio, which indicated that the riprap size had a significant effect in narrower openings. The shear ratio almost doubled from case 1 to case 11, but it was only 10 percent higher comparing case 5 to case 15. This phenomenon was mainly attributed to two reasons: 1) the near-bed secondary turbulence was increased owing to the larger roughness coefficient of larger riprap, and 2) riprap of larger size occupied more cross-sectional area in the opening assuming the contraction scour depth equals to two times D_{50}. Results from full-scale CFD models showed the same trend as was observed for the laboratory-scale CFD tests.

Figure 88 summarizes the shear ratio data as a function of the ratio of W_2/y_0. As expected, the shear ratio decreased as the opening ratio increased within each group. Comparing across groups, those groups with larger riprap tended to have higher shear ratios as can be seen by comparing group 4 with group 1.

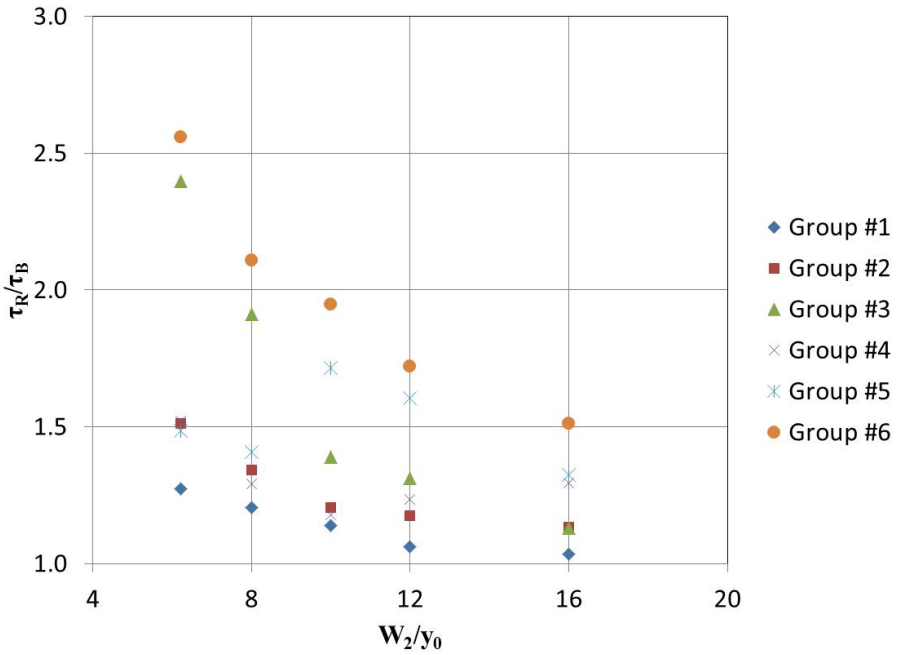

Figure 88. Graph. Relationship between the opening-to-depth ratio and shear ratio.

Returning to the conceptual equation shown in figure 55, the form of the equation appeared to validate the CFD modeling results. That equation also included a parameter, ε, which was not determined in chapter 3. However, using the CFD modeling results, a curve-fitting process was conducted based on the least squares method to determine the function ε. Values for the head loss coefficients, C_{cB} and C_{ce}, were assumed constant and equal to 0.23 for this exercise. Using these coefficients, equilibrium values of y_2 and y_{2R} were determined through iterative computations. (Alternatively, the depth values from the CFD modeling could have been used to determine the head loss coefficients, but the study did not have the resources to investigate this approach.) Figure 89 provides the resulting function.

$$\varepsilon = 1.25\frac{n_R}{n_B} - 2.55$$

Figure 89. Equation. Epsilon relation.

Figure 90 and figure 91 display the relationship between shear ratios and opening-to-depth ratios for the laboratory-scale and full-scale cases, respectively. For the laboratory-scale models, the Manning's n ratio (n_R/n_B) increases from group 1 to group 2 to group 3 with values of 1.7, 1.8, and 1.9, respectively. Similarly, for the full-scale models, the Manning's n ratio increases from group 4 to group 5 to group 6 with values of 2.0, 2.1, and 2.3, respectively. As expected, higher Manning's n ratios resulted in higher shear ratios. The approach section Froude numbers for all cases were fairly consistent, ranging from 0.25 to 0.29. The contraction ratios (W_2/W_1) ranged from 0.72 to 0.90.

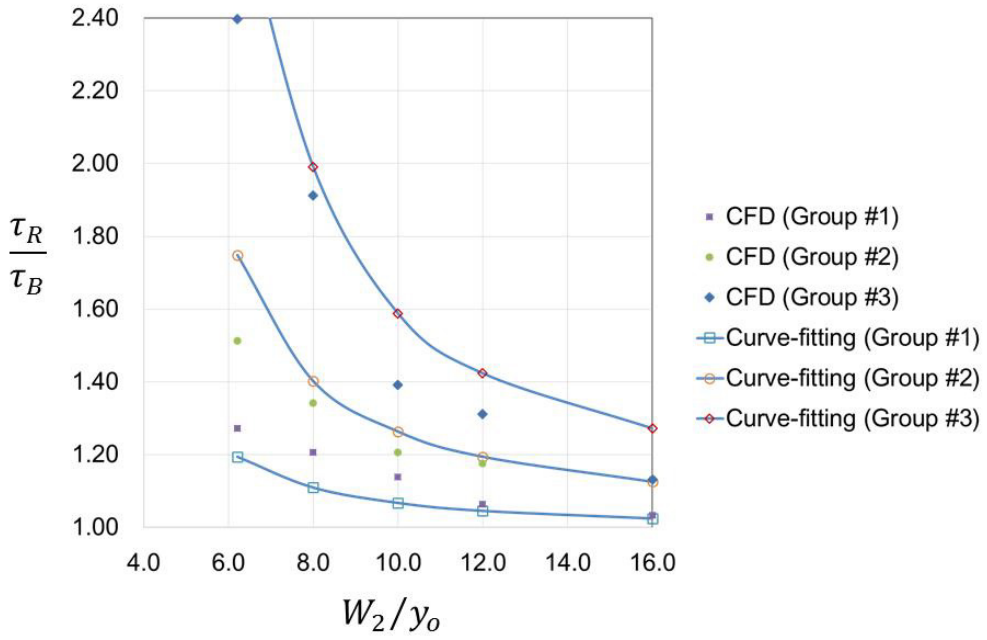

Figure 90. Graph. CFD results and curve-fitting for the laboratory-scale models.

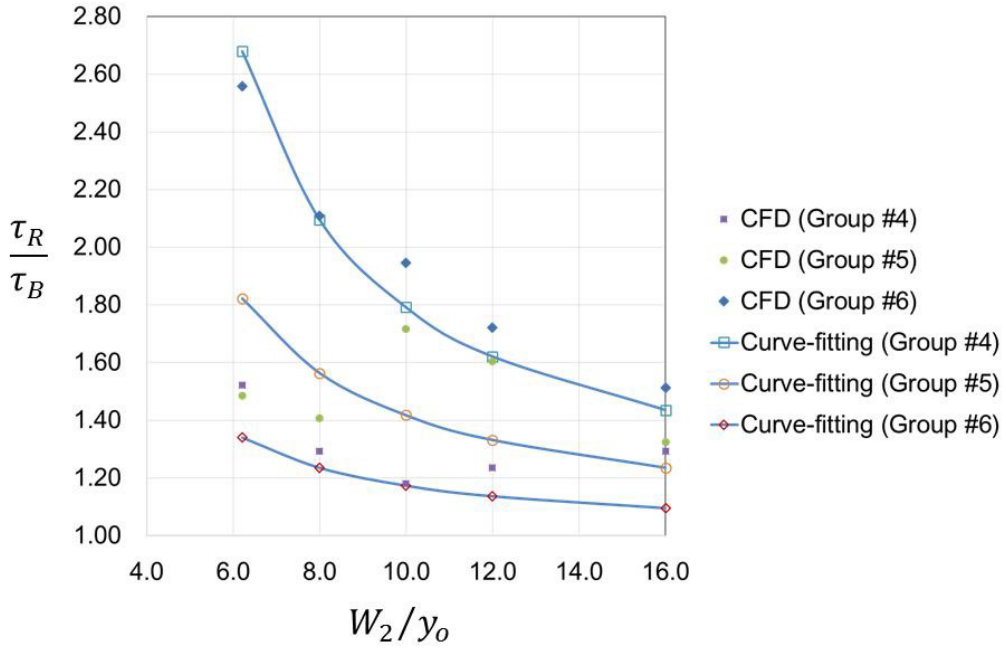

Figure 91. Graph. CFD results and curve-fitting for the full-scale models.

The estimated curves using the fitted equation in figure 55 for three groups were plotted against CFD results to verify that equation's accuracy. The curve-fitting showed reasonable agreement with the results from CFD modeling for all groups. An exception to this observation for the laboratory-scale results was that the curves significantly underestimated values for W_2/y_0 equal to 6.2 and 8.0 for group 1 while overestimating the values for groups 2 and 3. A similar pattern was seen for the full-scale results.

Buried Installation

Table 4 summarized the defining parameters for the buried installation cases in group 7 (cases 31–35) including the geometry, riprap size, bed material size, and hydraulics, and table 5 summarized the shear stress and other results for these cases. Figure 92 provides an example of the results with a comparison of the bottom shear distributions between the condition with and without the riprap apron for case 33. In this case, the shear ratio was less than 1. The other cases in this group all had low shear ratios, with the largest ratio (1.08) being for case 34. With the exception of only two cases in group 1, all of the shear ratios for the buried installation (group 7) were smaller than for the cases for a flush installation (groups 1–6).

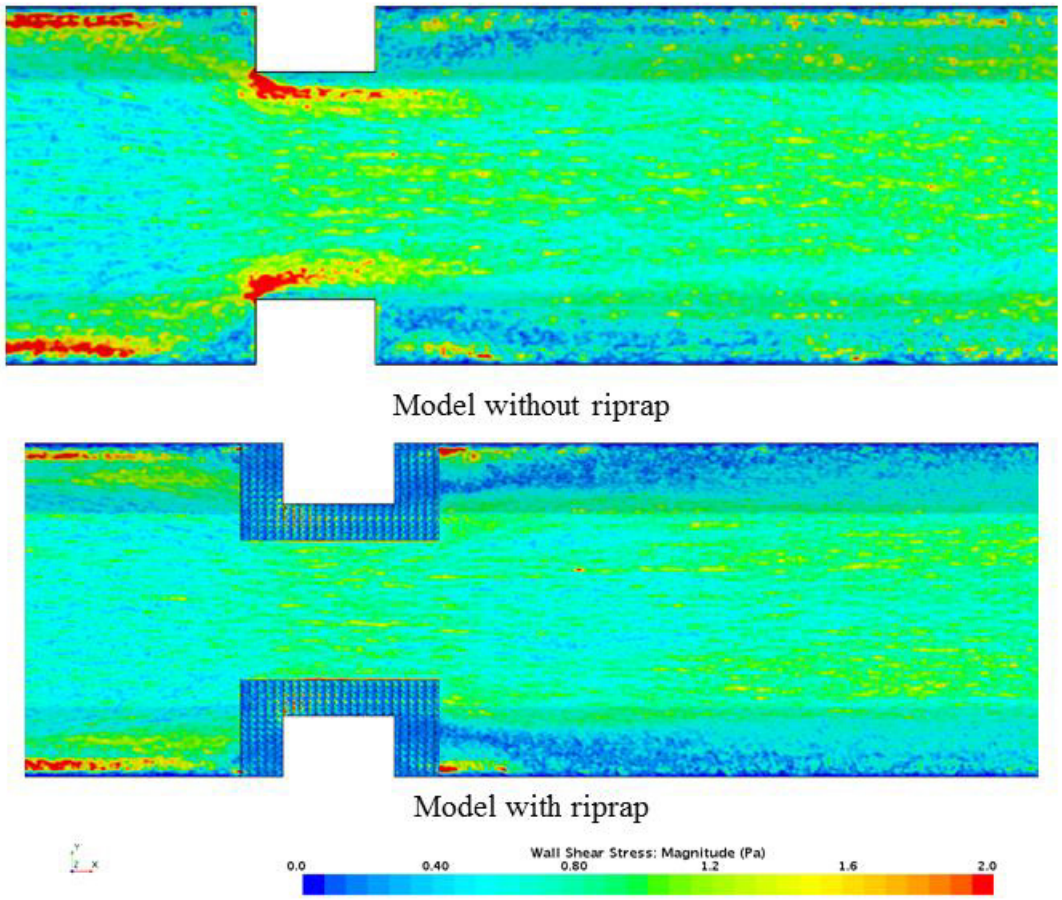

1 lbf/ft^2 = 47.88 Pa.

Figure 92. Graphics. Comparison of bottom shear stress distribution for case 33.

Burying the riprap appeared to significantly reduce or eliminate the increased shear in the unprotected channel caused by the flush installation of riprap aprons. To evaluate the possible reasons for this performance, it was useful to revisit the relation describing the shear ratio in figure 55. The variables potentially influencing the shear ratio included the roughness ratio, the width ratio, W_2/y_0, the vertical adjustment ratio, $\Delta Z/y_1$, and the approach flow Froude number. The effect of the Froude number, if any, depended on the channel shape factors.

Figure 93 displays a plot of the shear ratio for the six flush installation groups and the one buried installation group versus Manning's *n* ratio. Although group 7 had the largest Manning's *n* ratio, the data from that group did not align at all with the other groups. Similarly disjointed results were observed when examining Froude number.

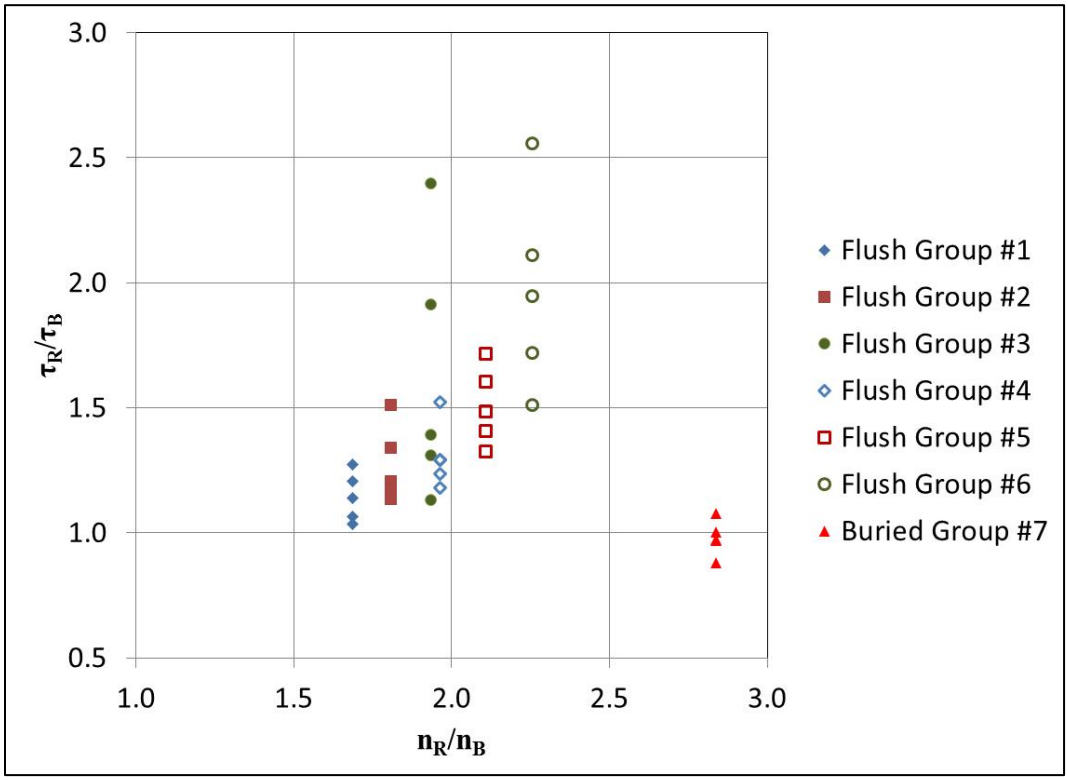

Figure 93. Graph. Shear ratio compared with Manning's *n* ratio.

Figure 94 displays a plot using the same cases of the shear stress ratio versus the vertical adjustment ratio. In this case, the group 7 data were consistent with the general trends of other groups, with the lowest set of shear ratios corresponding to the lowest set of vertical adjustment ratios. In this graph, increasing vertical adjustment ratio implies increasing shear ratio.

The vertical adjustment parameter, ΔZ, was defined in figure 44. It represented the average blocked area flush installation of riprap within the contraction scour zone. The larger this number was, the greater the blockage. If the vertical adjustment parameter was 0, as it was with the group 7 data, there was no blockage and contraction scour was unhindered. Recall that the buried riprap was intended to be located below the contraction scour zone.

The previous discussion regarding the flush installation noted the general decline in shear ratio with respect to increasing contracted width, W_2, as shown in figure 88, for example. This was true because the vertical adjustment dropped with increasing contracted width. Therefore, the primary mechanism for the shear ratio was the blockage of conveyance in the contraction scour zone by the flush installation of riprap. Buried installation below the contraction zone eliminated this problem.

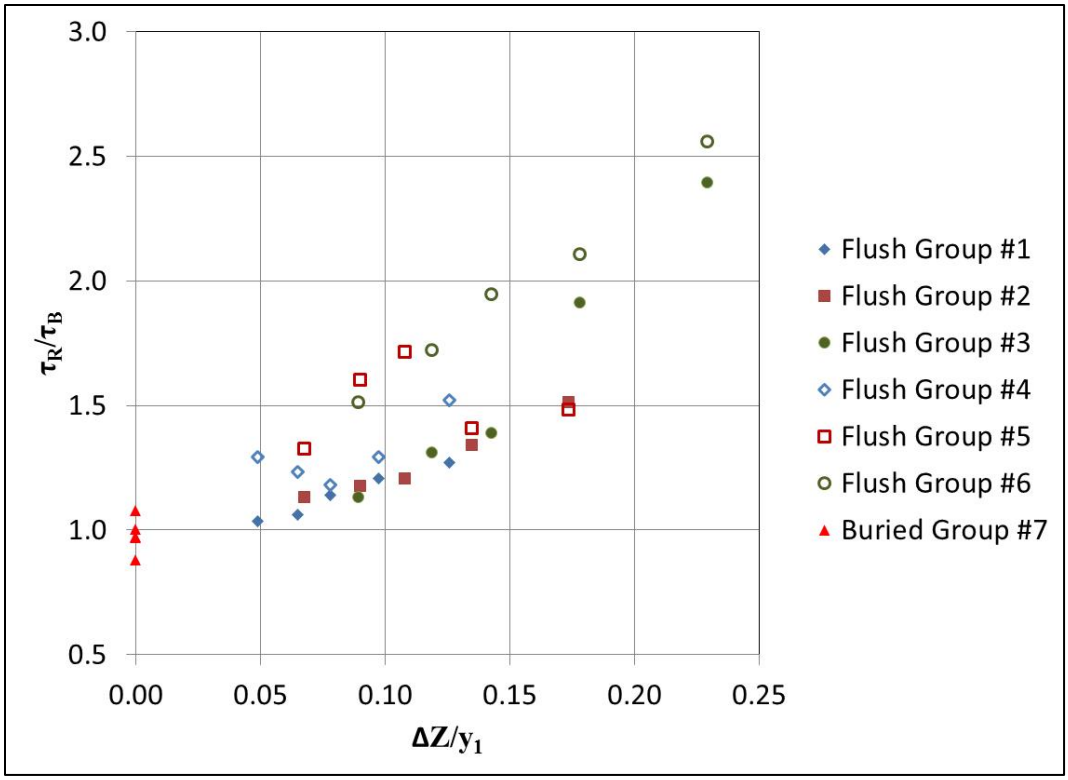

Figure 94. Graph. Shear ratio compared with vertical adjustment ratio.

Alternative Channel Setbacks

Table 6 summarizes the defining parameters for each case, including geometry, bed material size, and hydraulics for the alternative setback cases. All of these cases were without riprap. The cases with alternative setbacks can be compared with the group 7 cases 32–35.

Table 6. CFD test parameters for alternative setbacks.

Group	Case	Bed D_{50} (inches)	W_1 (ft)	y_1 (ft)	A_1 (ft^2)	V_1 (ft/s)	W_2 (ft)	y_0 (ft)	y_2 (ft)	V_2 (ft/s)
Short extension slope	36	0.04	78.35	9.68	570.9	2.02	49.87	6.23	9.68	2.46
	37	0.04	90.81	9.68	691.6	2.10	62.34	6.23	9.68	2.46
	38	0.04	103.28	9.68	812.3	2.15	74.80	6.23	9.68	2.45
	39	0.04	128.22	9.68	1053.6	2.21	99.74	6.23	9.68	2.45
Long extension slope	40	0.04	72.11	9.68	510.6	2.16	49.87	6.23	9.68	2.45
	41	0.04	84.58	9.68	631.3	2.21	62.34	6.23	9.68	2.45
	42	0.04	97.05	9.68	751.9	2.25	74.80	6.23	9.68	2.44
	43	0.04	121.98	9.68	993.3	2.29	99.74	6.23	9.68	2.44

1 inch = 25.4 mm.
1 ft = 0.305 m.
1 ft^2 = 0.093 m^2.
1 ft/s = 0.305 m/s.

Table 7 summarizes the shear stress on the bed material and other results from the runs. The effect of the channel setback on contraction shear stress may be compared for each value of

W_2/y_0. For W_2/y_0 equal to 8, cases 32, 36, and 40 were compared. For W_2/y_0 equal to 10, cases 33, 37, and 41 were compared. Similar comparisons were made for W_2/y_0 equal to 12 and 16. For each W_2/y_0, the parameters of y_2, W_2, V_2, and y_1 were held constant, while the setback was increased. Increasing the setback reduced W_1 and increased W_2/W_1, effectively reducing the contraction from the approach to the bridge opening. Because the hydraulic conditions in the contraction itself were the same, but the flow contraction from the approach was reduced, the shear stress, τ_B, generally decreased with increasing setback. This result was expected.

Table 7. CFD test results for alternative setbacks.

Group	Case	Equivalent W_1 (ft)	W_2/y_0	Fr_1	τ_B (lbf/ft^2)	n_B	W_2/W_1
Short extension slope	36	58.99	8.0	0.11	0.0203	0.013	0.85
	37	71.46	10.0	0.12	0.0144	0.013	0.87
	38	83.92	12.0	0.12	0.0175	0.013	0.89
	39	108.86	16.0	0.13	0.0138	0.013	0.92
Long extension slope	40	52.76	8.0	0.12	0.0167	0.013	0.95
	41	65.22	10.0	0.13	0.0230	0.013	0.96
	42	77.69	12.0	0.13	0.0161	0.013	0.96
	43	102.62	16.0	0.13	0.0144	0.013	0.97

1 ft = 0.305 m.
1 lbf/ft2 = 47.88 Pa

However, some shear stress values increased with increasing setback, (e.g., comparing case 41 with case 37. The approach velocity, V_1, also increased with increasing setback for a given W_2/y_0 ratio. The conflicting trends of increasing approach velocity and decreasing contraction might explain the inconsistent trend in shear stress.

Another observation pertains to the shear stress at the upstream corner of the abutment that results in abutment (local) scour. As can be seen in the shear stress figures in appendix C, increasing setback length reduced the shear stress that caused abutment scour.

This Page Is Left Blank intentionally.

CHAPTER 6. RECOMMENDED DESIGN GUIDANCE

One objective of this research study was to provide guidance for riprap apron design for vertical-wall abutments on shallow foundations. The resulting guidance covers several topics: (1) flush riprap aprons, (2) buried riprap aprons, (3) geometric parameters for irregular channel shapes, and (4) implications of contraction ratio. This guidance applies to all vertical-wall abutment designs with shallow foundations, including GRS bridge abutments.

Under existing HEC-23 DG 14 guidance, riprap aprons installed flush with the streambed to protect against abutment scour should extend out from the abutment a distance of two times the pre-scour depth of flow in the contraction or 25 ft (7.6 m), whichever is smaller.[3] This extension may leave a gap in protection across the channel that may result in contraction scour deeper than anticipated, which may ultimately increase the movement of rocks at the edges of the riprap apron (edge failure).

A buried full-width apron was proposed to address the concern regarding edge failure. Physical modeling of various apron configurations was conducted to evaluate a buried full-width apron. A buried partial-width installation was also evaluated with CFD modeling runs. In the following sections, the recommended applicability and limits for riprap aprons are provided.

FLUSH RIPRAP APRONS FOR SHALLOW FOUNDATION ABUTMENTS

Based on the conceptual analysis and experimental tests of riprap aprons installed flush with the original bed surface conducted for this study, the shear ratio, τ_R/τ_B, decreased as the relative width of the contraction increased. This conceptual relation is shown by the curve in figure 95. One would expect that in the extreme, (i.e., is when the opening is very wide), a limited width riprap apron would have little influence on the flow condition in the contraction and the shear ratio would approach 1.0. However, when the opening is narrow, the riprap would have an effect on the flow distribution and would cause the shear ratio to increase. A higher shear ratio indicated deeper contraction scour in the gap between the abutment aprons than would otherwise be expected. Therefore, as indicated by the question mark on the figure, “narrow” must be quantified for this application.

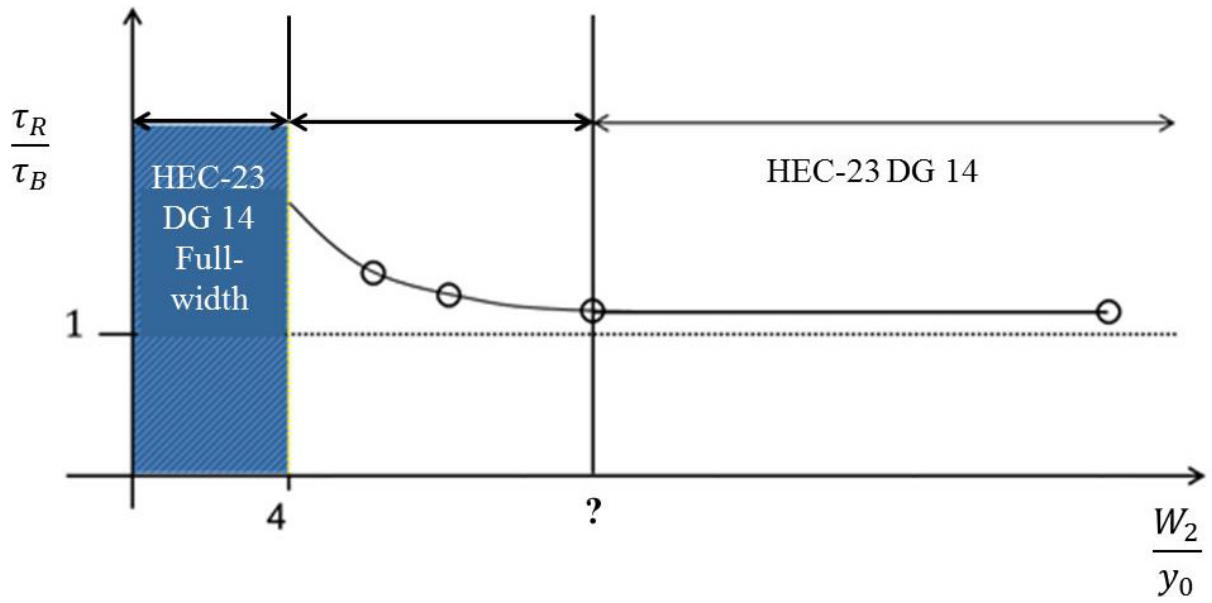

Figure 95. Graph. Conceptual definition of a narrow opening for flush apron installation.

Because HEC-23 DG 14 recommends aprons equal to two times the pre-scour flow depth, y_0, contractions with an opening ratio, W_2/y_0, less than or equal to 4 (considering the apron from both abutments) are essentially full-width aprons.[3] Above a certain opening ratio, indicated in figure 95, HEC-23 DG 14 may also be applied because the channel is sufficiently wide so that the localized effect of the riprap on the contraction scour and apron edges is negligible. This corresponds to where the shear ratio, τ_R/τ_B, is close to 1. One of the objectives of this study was to address guidance for the region between the two extremes.

As reported in the discussion of the CFD modeling results in chapter 5, shear ratios ranging from 1.03 up to 2.56 were computed over the 30 flush installation cases analyzed. These cases used different riprap and bed material sizes over a range of opening ratios from 6.2 to 16. However, it was noted that other variables also influenced the shear ratio.

A strategy for identifying an appropriate threshold was adapted from a procedure used for the seismic design of bridges. The California Department of Transportation proposed that a realistic moment-curvature curve could be approximated by considering idealized plastic behavior to estimate the plastic moment capacity of a ductile concrete structural section, as shown in figure 96.[24] The actual elastic structural behavior was approximated, identifying the intersection point between the idealized plastic behavior and a secant line representing the elastic modulus.

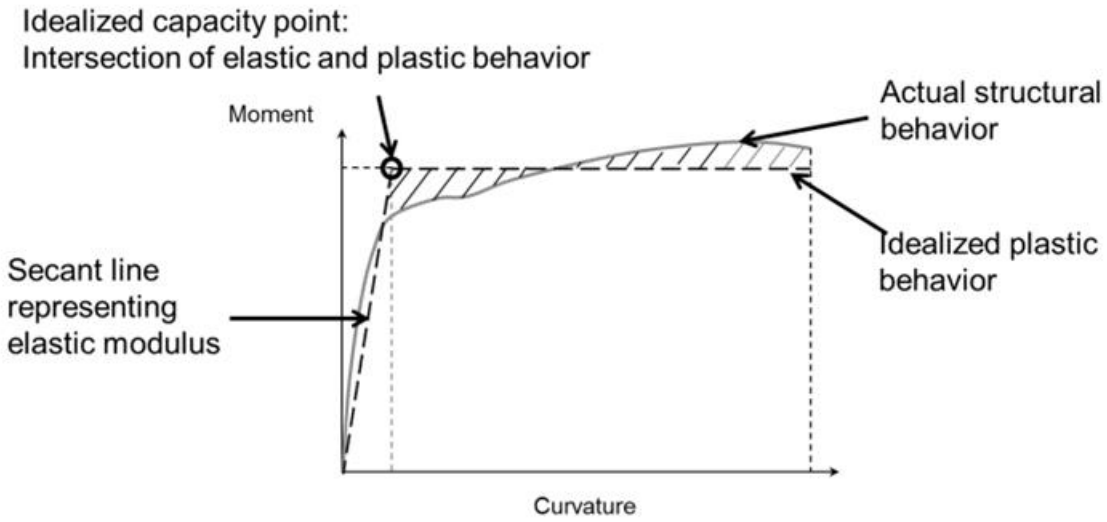

Figure 96. Graph. Idealized elastic perfectly plastic moment curvature.

Similarly, if a secant line can be identified that intersects the ideal bed shear ratio of 1.0 at a consistent ratio of W_2/y_0, this may be an appropriate technique for defining a threshold for a narrow opening. A secant line was defined by the two points at which it intersected the curve; therefore, each curve had many secant lines. For this analysis, one secant definition point was taken where W_2/y_0 was equal to 4 because this was the point at which the aprons would be full width by HEC-23 DG 14 as was shown in figure 95.[3] Ideally, the second point should be chosen so that the intersection of the secant line and the ideal shear ratio of 1.0 occurred at a consistent W_2/y_0 ratio for a family of curves. One option was to take the second point where W_2/y_0 was equal to 6 because this value would work reasonably well for the CFD data.

Figure 97 shows the result of applying secant definition points of 4 and 6 for three groups of experiments included in table 4. Using the secant method for these curves yielded a threshold value of approximately 8. However, at this opening ratio, the shear ratio ranged from 1.4 to 1.8. These shear ratios were not approaching 1.0 at this opening ratio. It should be noted that the shear ratio corresponding to an opening ratio of 4.0 was extrapolated using the fitted curves beyond the CFD experimental range, which had a lower limit of 6.2.

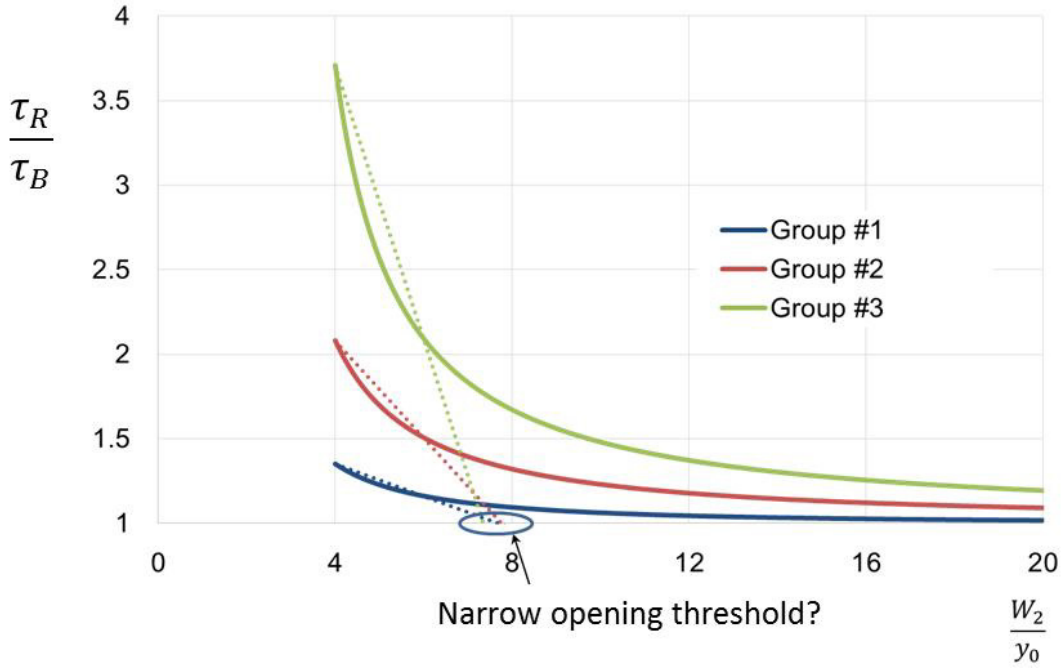

Figure 97. Graph. Secant approach applied to selected CFD modeling cases.

Data from five field sites were also examined using the secant method, as summarized in figure 98. The geometric and hydraulic characteristics of each site were entered into the equation in figure 55 to compute the shear ratio. These points are shown in the figure as the field condition. Then, the value of W_2/y_0 was varied to develop the curves for each site. The result when applying the secant approach suggests a threshold value between 7.5 and 8.0. As with the CFD results, the shear ratios for some of these sites at these opening ratios were well above 1.0.

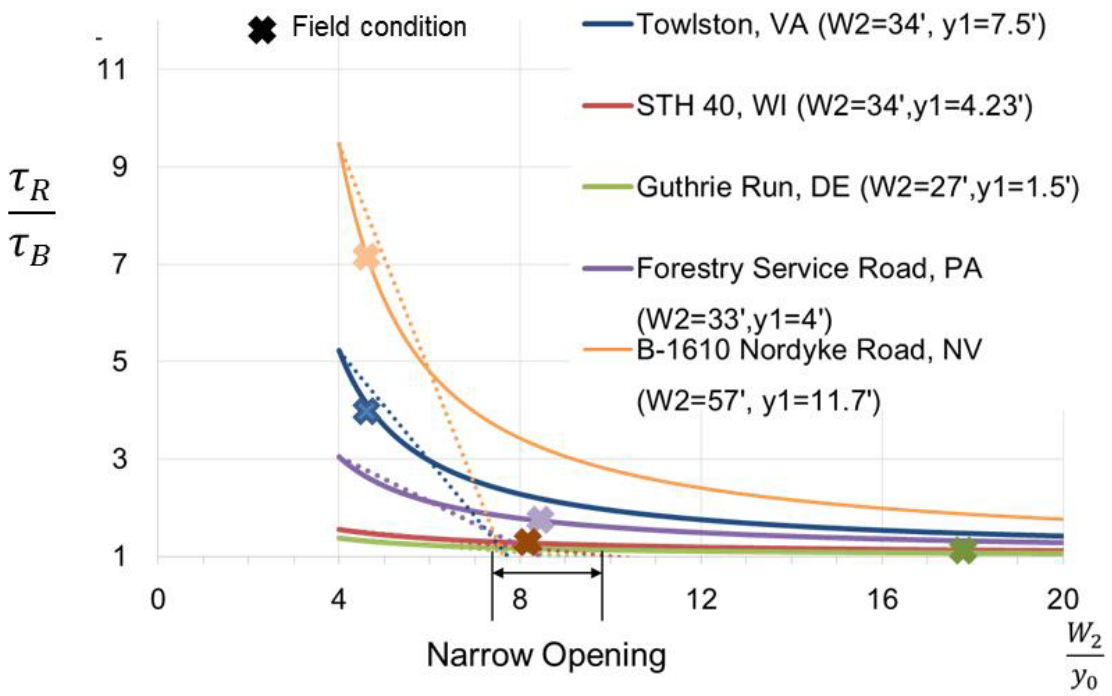

1 ft = 0.305 m.

Figure 98. Graph. Secant approach applied to field installation cases.

The results of the secant approach depended on the points used to define the secant. Selecting 4 and 6 appeared to result in a reasonably consistent intersection with the shear ratio of 1.0 at W_2/y_0 equal to approximately 8. Choosing 4 and a higher value than 6 for the second secant definition point would result in a higher, but less consistent, ratio of W_2/y_0, where the secant lines intersected the shear ratio of 1.0. However, it is important that although the intersection point was consistent with secant definition points of 4 and 6, the shear ratios where W_2/y_0 equals 8 were not close to 1.0.

Another approach for defining when full-width protection is recommended for flush installations of riprap aprons would be to use the equation in figure 55. If the result of the computation were greater than some value, say 1.3, then full-width protection would be recommended. However, this equation is not operational for design because it had not been comprehensively evaluated at the time of this study. In addition, methods for estimating some of the parameters, such as the channel shape factors, β_B and β_e, were not yet available. However, the potential for this approach is that it explicitly includes all input variables believed to be contributing to the increase in shear stress in the middle of the channel.

Based on inspection of the laboratory and field results as partially summarized in figure 97 and figure 98, respectively, partial-width riprap aprons installed flush with the bed surface would not be recommended because the shear ratio does not approach 1 except for larger ratios of W_2/y_0. Full-width installations might be acceptable from a scour perspective, but unacceptable for environmental or other reasons. If a full-width riprap apron installed flush with the bed is considered, other aspects of the apron design, including rock size, use of geotextile, and upstream and downstream extent,

should be taken from HEC-23 DG 14.[3] As much as possible, the riprap apron should conform to the stream channel and bank geometry.

BURIED RIPRAP APRONS FOR SHALLOW FOUNDATION ABUTMENTS

Physical experimental runs 6, 8, 9, and 11 described in chapter 4 explored the performance of full-width riprap aprons buried so that the top of the apron layer matched the estimated contraction scour depth for the bridge opening. In each of these runs, the rock size was selected based on HEC-23 DG 14 for abutment aprons flush with the original bed elevation.[3] In none of these runs was any failure of the buried full-width apron observed.

In all of these runs, some of the bed material above the buried apron was removed before any part of the apron was exposed to shear stresses or potential undermining at the upstream and downstream apron edges. This expansion of the bridge opening cross section increased the conveyance through the opening and decreased the shear stresses on the riprap compared with what would have been experienced if the apron had been installed at a higher elevation.

Therefore, it is anticipated that burying the apron would allow for a reduction in the apron extent and rock sizing. For example, apron extent for HEC-23 DG 14 is $2y_o$, which potentially might be reduced with a buried apron.[3]

The CFD results from group 7 (cases 31–35) suggested that burying the riprap apron reduced the shear ratio because the apron itself no longer prevented the contraction scour from occurring, which in turn allowed the conveyance to increase and the bed shear to decrease. Review of the shear summaries for these cases in figure 114 (see appendix C), shows that the shear stresses in the unprotected part of the channel in the cases with riprap were equivalent to or lower than the stresses in the same area for the cases without riprap. In addition, the riprap apron protected the areas showing elevated shear stresses that would cause the local abutment scour. These cases included evaluations for the ratio of W_2/y_0 from 6.2 to 16. Therefore, a buried installation with a riprap apron extent of at least $2y_0$ from the abutment face toward the channel thalweg could be protective of the abutment foundation for W_2/y_0 greater than 6.2. Such an installation might also be protective for narrower channel constrictions, but no data to support this conclusion was developed as part of this study.

GEOMETRIC PARAMETERS FOR IRREGULAR CHANNELS

The physical and numerical modeling for this study, as well as the conceptual framework, primarily applied to rectangular and trapezoidal channels. Because designers and engineers must apply these concepts to irregularly shaped natural channels, clarity regarding the definition of the hydraulic and channel parameters is essential.

First, all analyses assumed that all flow approaching a bridge opening passed through the opening; there was no overtopping or bypass. For situations where overtopping and bypass would occur, the upstream flow, velocity, depth, and width should be estimated considering only that portion of the flow field that was directed through the bridge opening.

In the analyses for this study, the widths of the upstream and contracted section, W_1 and W_2, respectively, were defined as the bottom width of the section. Because bottom width is difficult

to define in an irregular channel, and the bottom width and average width are were the same in the rectangular channel used in the physical experiments, the recommendation is to use average width for characterizing contraction ratio and other width-related parameters for irregular channels. Average width is defined in figure 99 for the upstream section. The analogous relation is used for the contracted section.

$$\bar{W}_1 = \frac{A_1}{y_{1M}}$$

Figure 99. Equation. Average width in the approach section.

Where:

$\bar{W}_1$ = Average width in upstream section, ft (m).
A_1 = Cross-sectional area of upstream section, ft^2 (m^2).
y_{1M} = Maximum flow depth in the upstream section, ft (m).

For depth, the average flow depths in the upstream and contracted sections (before and after contraction scour), y_1, y_0, and y_2, respectively, were defined for these analyses. For a rectangular channel, the average and maximum depths were the same. For irregular channels, it is recommended that the average depth is appropriate for estimating full-width apron design parameters. The exception is that the depth at the abutment, as defined in HEC-23 DG 14, should be used for rock sizing.(3)

Velocity and cross-sectional area parameters should be defined based on the entire upstream and contracted section. The exception would be when flow overtops or bypasses the bridge opening.

IMPLICATIONS OF CONTRACTION RATIO

Channel contraction at bridge openings may create hydraulic and scour challenges as well as environmental and ecosystem effects. With respect to the shear stress ratio described in this study, greater contraction resulted in greater flow acceleration through the bridge opening. Greater contraction (lower contraction ratio) also led to higher estimates of contraction scour and larger rock riprap sizes to protect abutments from abutment scour. For partial-width aprons, these effects would likely result in higher stresses in the gap between the aprons.

The physical modeling in this study tested two contraction ratios (W_2/W_1): 0.65 and 0.25. For the more severe 0.25 contraction ratio, the observed contraction scour depths for the two runs without riprap protection were twice the estimated values. While these estimates should not be directly compared for the reasons discussed in chapter 4, they are indicative of a severe environment.

The numerical CFD modeling tested less severe contraction ratios ranging from 0.72 to 0.90. As discussed in chapter 5, the shear ratios exceeded 2.0 in some cases depending on riprap size, opening ratio, and other factors.

The equation in figure 55 implicitly includes contraction to estimate shear ratio. Until more experience is gained with this equation and with vertical-wall abutments with shallow

foundations, it is recommended to carefully consider contraction ratio in the design. More severe contractions contribute to a more challenging hydraulic and scour environment. Lower contraction ratios (more contraction) increase contraction scour estimates, which lead to deeper riprap aprons when buried to the contraction scour depth.

CHAPTER 7. SUMMARY AND FUTURE RESEARCH

This report summarizes the results of physical and numerical modeling tests to evaluate the effects of riprap aprons on contraction scour for vertical-wall abutments with shallow foundations. The evaluations included aprons installed at the original bed surface and buried below the anticipated contraction scour depth. In both types of installations, full-width and partial-width installations were considered. Partial-width flush installations of riprap aprons introduced turbulence at the apron/bed interface and also prevented increased conveyance facilitated by contraction scour. These two effects resulted in scour observations in excess of predicted contraction scour. Potential mitigation strategies, including full channel width aprons installed flush with the streambed and buried aprons, were evaluated, and design guidance was proposed.

Recommended design guidance for riprap aprons recognizes that for these shallow foundations, the riprap apron is an integral component of the structure that must continue to perform throughout the life of the structure. As an integral component of the structure, the apron should not require maintenance as long as the design conditions are not exceeded. Detailed guidance is provided in appendix D. The following bullets summarize guidance highlights.

- For aprons installed flush with the original streambed, guidance is as follows:
  - Because the apron is installed within the contraction scour zone, partial-width flush aprons will likely experience some edge failure even when W_2/y_0 is large. Therefore, partial-width flush aprons are not recommended.
  - Full-width flush installations were not tested. In addition to unknown hydraulic performance, their use may also generate environmental criticism that exposed riprap is not conducive to supporting aquatic habitat. Therefore, they are not recommended.
- For aprons buried to the estimated elevation of contraction scour, guidance is as follows:
  - Partial-width buried riprap aprons can be effective for W_2/y_0 greater than 6.2. Concern about edge failure is significantly reduced because the apron is buried to a depth below the contraction zone. This is the basis for option 2 described in appendix D.
  - Full-width buried riprap aprons are preferred for W_2/y_0 less than or equal to 6.2 and can be considered for all openings. This is the basis for option 3 described in appendix D.
  - Riprap size, apron extent upstream and downstream, apron thickness, and other parameters may potentially be less restrictive than specified in HEC-23 DG 14, but insufficient data were available in this study to provide recommendations.[3]
- All aprons should conform to the channel bed and banks as closely as is reasonable while ensuring apron stability.

- Designers should consider the contraction ratio $\overline{W}_2/\overline{W}_1$ so that significant contractions that may contribute to severe hydraulic or scour conditions might be avoided. Insufficient data were available in this study to provide quantitative recommendations.

If riprap aprons or other scour countermeasures are not used to protect the abutments supported by shallow foundations, the foundations should be placed below the abutment (local) scour elevation as recommended in current guidance. Although this condition was not a focus of this study, the results from physical experiments 7 and 10 (with no riprap) confirmed that abutment scour might threaten shallow foundations. This condition is described as option 1 in appendix D.

This study evaluated free-surface conditions only. However, it is anticipated that pressure-flow conditions would exacerbate contraction scour compared with free-surface conditions. Because there are no experimental or field data to support the effectiveness of partial-width installations (flush or buried), it is recommended that only buried full-width installations be considered for pressure flow conditions at shallow foundations. This situation is described in appendix D.

This design guidance for free-surface conditions assumes that all approach flow passes under the bridge. If flow overtops or bypasses, the approach flow characteristics should be adjusted accordingly. The design guidance is also limited to clear-water scour conditions. The following further research is recommended to improve this guidance:

- Further developing the shear stress ratio conceptual model to a design tool that ultimately allows site-specific evaluation of stress ratios.

- Considering the aquatic organism passage and stream stability consequences of bridge abutment encroachment on the channel creating narrow (contracted) openings.

- Expanding the guidance to consider live-bed contraction scour conditions.

- Further testing pressure flow conditions.

- Considering differential guidance for rigid versus non-rigid shallow foundations if the two types of foundations might experience different failure mechanisms.

APPENDIX A. ANNOTATED LITERATURE REVIEW

The following descriptions briefly summarize relevant references.

MACKY (1986)[6]

G.H. Macky studied the effectiveness of methods of protecting bridge abutments from scour under clear-water conditions.[6] Macky undertook laboratory experiments using an idealized l:40 scale model of the Waiharakeke River Bridge on State Highway 25 near Whangamata, New Zealand. Macky attempted to model typical construction practice for scour countermeasures rather than recommended construction practice. This meant that the protection measures were extended only slightly below the existing bed level. The protection methods tested were riprap, concrete Akmon units (commonly used at coastal sites), flexible concrete mattresses, gabions laid on the embankment slope, stacked gabions staggered up the embankment slope, and boulder-filled wire mattresses laid on the bed sediment with stacked gabions on the embankment slope.

The significant findings of the study were that while the downstream side of the abutment required nominal protection only, the upstream corner of the abutment was subject to strong attack by the flow, requiring protection not only above the existing bed, but also on the slope of the developing scour hole. The high initial velocities caused damage to the abutment structure, which could possibly be avoided by preexcavating a scour hole. By using typical scour countermeasure placement practice, the abutment slopes slumped to a less steep armored slope, even though the abutment structure itself remained stable. The bridge pier adjacent to any abutment needed special protection, because it was possible that it could be sited in the abutment scour hole.

CROAD (1989)[7]

R.N. Croad studied the performance of riprap protection at abutments under clear-water conditions with preexcavated scour holes.[7] Croad also conducted some experiments with riprap placed just below the initial bed level and with riprap placed down to the initial bed level with a horizontal launching apron. The work was intended to build on that of Macky.[6]

PAGÁN-ORTIZ (1991)[8]

J.E. Pagán-Ortiz studied the stability of riprap protection placed in the apron and measured point velocities at model abutments.[8] Vertical-wall and spill-through abutment models were modeled. The riprap was placed directly on the floor of the flume, rendering the study essentially a fixed-bed investigation (i.e., scour did not occur at the abutment). Therefore, the study was useful in determining the likely position in which riprap, placed in an apron around an abutment, would first fail while the riverbed remained level. This information was useful only until a scour hole began to develop, at which time the flow regime changed, and riprap in other positions of the apron might become unstable. The tests were carried out under clear-water conditions, with V/V_{cs} values of approximately 0.9, where V is the mean approach-flow velocity and V_{cs} is the critical velocity. The abutment model was placed against the side wall of the flume and surrounded by an observation area consisting of a gravel bed placed on the floor of the flume.

The significant findings from this study were as follows:

- For a spill-through abutment, the initial failure zone began at the armored floodplain downstream of the contraction near the toe.
- For a wing-wall abutment, the initial failure zone occurred at the upstream corner of the abutment.
- The rock riprap apron should be extended along the entire length of the abutment, both upstream and downstream, and to the parallel face of the abutment to the flow.
- It would be reasonable to limit the rock riprap apron to a relatively small portion of the contraction at a bridge crossing because the velocity amplification decayed rapidly with distance from the toe of the abutment.
- Equations were recommended for sizing riprap at vertical-wall and spill-through abutments.

ATAYEE (1993) AND ATAYEE ET AL. (1993)[9,10]

A.T. Atayee studied the stability of a riprap apron using a model spill-through abutment situated on the floodplain of a compound channel. [9] The study was intended to build on that of Pagán-Ortiz by measuring the threshold of movement of the gravel material used to protect the floodplain and channel in the vicinity of the abutment.[8] The hydraulic conditions that initiate gravel movement were measured.

Failure was defined as occurring at the instant when the unprotected surface (in this case, the bed of the flume) was clearly exposed. Degradation of the gravel layer to expose the flume bed could occur very rapidly (in seconds). In all experiments, failure occurred at the toe of the embankment just downstream of the abutment centerline.

EVE (1999)[11]

N.J. Eve studied criteria for selection of riprap protection at spill-through bridge abutments with launching apron protection under clear-water and live-bed conditions.[11] The size of the riprap and the extent of the launching apron were varied systematically in the tests. The abutment embankments were constructed using the bed sediment material. The following three failure conditions were defined:

- **Total failure:** Large-scale movement of sediment and riprap occurred on the abutment slopes. The abutment fill material slumped, and large areas of sediment were exposed.
- **Partial failure:** The movement of riprap and sediment was initiated in one part of the embankment but did not result in a change of the embankment slope as a whole. Partial failure was typically observed at the water level, where a few riprap stones would be displaced and would move down the slope, and at the base of the slope if undermining of the toe occurred.

- **No failure:** No change was observed in the embankment slope, and the riprap stones did not move.

For the clear-water tests, two abutment lengths and three riprap sizes were used. Eve measured the position at which the maximum scour depth occurred in all experiments. Generally, the point of maximum scour moved away from the toe of the abutment as the size of the launching apron and riprap stone size increased, as expected. The lateral extent of the riprap-launching apron was initially set at twice the flow depth, based on the HEC-23 recommendations.(3) This criterion was found to be conservative in all cases. For subsequent experiments, the lateral extent was reduced in increments until failure occurred. An equation was proposed for the apron extent on the basis of these tests.

The live-bed experiments were conducted at 125 and 150 percent of the threshold velocity for the bed sediment. These tests were preliminary in nature, and Eve recommended further study under live-bed conditions.

In all cases, the riprap failed rapidly, apparently because of winnowing of bed sediment through voids between the riprap stones. Some of the tests were repeated with the addition of a filter fabric, which was found to improve the stability of the protection, especially at the lower flow velocity. At the higher flow velocity, the abutments failed, in spite of the presence of the geotextile, because of undermining of the abutment toe, which led to slumping of the sediment beneath the filter fabric. The following three types of failure were observed in the live-bed tests:

- **Catastrophic rapid failure:** Occurred without a geotextile where the embankment fill material was rapidly winnowed from between the riprap stones, leading to disintegration of the structure.

- **Slumping failure**: Abutment failed owing to exposure of the underlying geotextile at the abutment toe, allowing the embankment fill material to slump beneath the geotextile. Exposure of the geotextile at the toe of the embankment slope exacerbated the failure process.

- **Riprap failure**: Riprap layer failed, but the embankment remained intact at the end of the test.

HOE (2001)(12)

D.A. Hoe undertook preliminary tests to investigate the use of CTBs to protect spill-through bridge abutments from scour under clear-water conditions.(12) Hoe used the same experimental setup as that used in the clear-water experiments by Eve.(11) Ceramic tiles were used to model the CTB blocks. They were joined together by gluing them onto a flexible loose-woven fabric. The embankment slopes of the abutment were covered with the ceramic tiles, and an apron with a width equal to twice the flow depth was laid around the abutment.

The study showed that the apron protected the abutment from being undermined for approach flow conditions less than 66 percent of the threshold velocity. For higher flow velocities (resulting in deeper scour), the abutment toe was undermined causing abutment failure.

Some experiments were repeated with an increased level of protection, which was achieved by adding additional sections of the ceramic blocks to the standard apron This had the effect of deflecting the scour hole slightly away from the abutment, thereby protecting the abutment from failure at the higher approach flow velocities. Hoe observed that the additional apron was vulnerable to overturning when located in the contracted zone of the flow and recommended that further testing focus on methods to prevent overturning of CTB mats.

CHEUNG (2002)[13]

M. Cheung studied the effectiveness of CTB scour countermeasures around piers and wing wall abutments under clear-water conditions.[13] Cheung used two types of CTBs in the experimental study—ceramic tiles and truncated square pyramid blocks. The blocks were intended to be more representative of commercially available prototype CTBs. Both types of blocks were joined together to form an apron by gluing them onto a flexible loose-woven fabric.

Experiments were conducted with and without the apron attached to the abutment face and with and without geotextile filters placed underneath the aprons. At the end of each experiment, the level of protection provided by the countermeasure was assessed. Failure criteria were developed based on the ability of the foundation structure to continue to support the bridge. An abutment was considered to have failed if the CTB protection could no longer provide any protection for the abutment by allowing excessive amounts of sediment to be scoured away, which would eventually undermine the abutment foundations. The following failure conditions were defined by Cheung:

- **No failure**: Mattress stayed relatively flat around the pier.
- **Partial failure**: Mass movement of sediment occurred at a localized region of the apron only. For the case of partial failure, the apron could still fail because of undermining, but to a lesser extent than for total failure.
- **Total failure:** Scour hole formed in close proximity to the abutment and the bed material was removed from underneath the apron, as a result of undermining.

MARTINEZ (2003) AND KORKUT (2004)[14,15]

E. Martinez and R. Korkut undertook laboratory experiments to evaluate the use of geobags as a scour countermeasure to protect bridge abutment foundations from failure.[14,15] Geobags are geotextile cloth bags filled with the local sediment or concrete. The experiments focused on the performance of geobag aprons, which were placed around a pile-supported wing-wall abutment retaining an erodible embankment. Martinez focused mainly on geobag performance under clear-water conditions while Korkut studied geobag performance under live-bed conditions. The experiments were intended to investigate the possible use of geobags as a scour countermeasure.

Martinez concluded that local scour could not be eliminated by a geobag apron, but that it could shift the scour region away from the abutment. In this regard, geobag aprons could be effectively used to protect abutments from scour, so long as the shifting of the scour hole did not imperil other hydraulic structures nearby. Martinez suggested that geobags were an effective scour

countermeasure for wing-wall abutments when the width of the apron W, exceeded the length of the abutment L.[14]

Korkut used a wing-wall abutment model similar to that used by Martinez, but it was supported by piles and retained an erodible embankment. An equivalent experiment was conducted with a riprap apron. The resulting scour at the abutment was similar for the two experiments, showing that untied geobag aprons functioned in a similar manner to riprap aprons. In both cases, significant scour occurred at the abutment face, exposing the piles of the wing-wall structure.[15]

As a result, the embankment material was winnowed out from underneath the abutment causing the embankment retained by the wing-wall structure to collapse. Other experiments were run with geobags placed underneath the abutment, geobags tied together in the apron, and additional geobags placed under the apron around the perimeter of the apron.[15]

To adequately protect the abutment from scour, Korkut suggested that it was necessary to tie the geobags in the apron together and that the apron should have a toe or skirt that extended below the apron with at least two geobag thicknesses. The live-bed conditions proved to be more critical for abutment protection (compared to the clear-water experiments by Martinez), mainly due to bed-form destabilization of the geobags around the edges of the apron.[14] The passage of the troughs of the bed forms undermined the apron, dislodging the individual geobags or causing the tied geobag apron to fold down.

MELVILLE ET AL. (2006A)[17]

B.W. Melville et al. studied the performance of riprap and CTB aprons as a scour countermeasure for a spill-through abutment.[17] The abutment model was placed on the flood plain of a compound channel. The compound channel comprised a fixed-bed main channel in the approach and an erodible sand bed in the test section. The bank slope was erodible but protected with riprap in the test section and with a V:H slope of 1:2 for all tests. The scour countermeasure experiments were run in clear-water conditions. Abutment length, floodplain width, and apron extent were varied for both apron types.

The purpose of the study was to determine the minimum required apron extent to sufficiently protect the abutment from failure and to determine the scour-hole geometry under clear-water conditions due to variations in the flood plain width, abutment length, and apron extent. Uniform coarse sand was used for all experiments. The riprap protection to the abutment slopes and in the apron comprised uniform-sized gravels with a thickness of $1.5 \times D_{50}$, equivalent to two riprap layers. A filter fabric was placed over the abutment and covered with riprap or CTBs. The filter fabric was also placed beneath the CTB apron but not the riprap apron because this could induce edge failure of the riprap.

The study had the following significant findings:

- A riprap apron protection to spill-through abutment structures did not act principally to reduce the extent and depth of local scour. Rather, the apron deflected the scour development a sufficient distance away from the abutment toe that damage was prevented.

- With increasing toe protection (i.e., increasing apron extent), the scour hole at spill-through abutments sited in the flood channel typically was deflected further away from the abutment and was reduced in size. However, for abutment and compound channel configurations where the scour-hole formed close to the main channel bank, the scour hole could increase in size as the apron extent was increased.

- CTB mats allowed scour holes to form closer to the abutment, compared with scour holes at abutments protected by equivalent riprap aprons, and resulted in deeper scour holes.

- An equation that predicted the scour depth for spill-through abutment situated on the flood plain of a compound channel was given.

- An equation that predicted minimum apron width (apron extent) to prevent undermining of the toe at spill-through abutments was given.

- A design methodology was proposed for evaluation of the stability of spill-slope fill material at spill-through abutments in terms of the extent of apron protection.

MELVILLE ET AL. (2006B)[18]

B.W. Melville et al. studied the performance of riprap and CTBs as scour countermeasures for wing-wall abutments under live-bed conditions for different flow depths, flow velocities, apron extents, and apron burial depths.[18] The aim of the experiments was to investigate the minimum required apron extent to sufficiently protect abutment from scour under live-bed flow conditions.

The majority of the experiments were conducted in a compound channel with a fixed-bed floodplain and a mobile-bed main channel. The wing-wall abutment was sited at the bank of the main channel. These experiments were designed such that the scour process was dominated by bed-form trough migration. In addition, four experiments were run with a different abutment model to investigate the effects of local and contraction scour only. For these experiments, the floodplain was removed, and the abutment model was simplified to a trapezoidal-shaped structure. The two models were referred as the “compound channel model” and the “rectangular channel model.” Uniform coarse sand was used as mobile-bed material for all experiments.

For both channel configurations, the settlement of CTB and riprap aprons at the end of each experiment were measured, and it was defined as the distance from the average bed level to the top of the apron after settlement. Two cases of apron settlement were observed. For case I, apron settlement occurred at the outer edge, whereas for case II the entire apron settled (i.e., scour at the abutment face also occurred). Melville et al. observed a trend of increased apron settlement of the outer edge with increasing flow depth and flow velocity. Also, scour at the upstream corner of the abutment was deeper than at the downstream corner. For case II, scour was deepest at the outer edge of the apron. The burial depth of the apron did not affect its settlement depth at the outer edge, but it did affect the stability of the apron.

Melville et al. concluded that the scour at wing-wall abutments under live-bed conditions was directly related to the level of deepest bed-form trough that propagated past the abutment, together with any localized scour that might occur. Only a vertical settlement was observed at the

outer edge of CTB aprons, allowing the scour to occur closer to the abutment face than for an equivalent riprap apron, which tended to settle and move away from the abutment, deflecting the maximum scour depth further away from the abutment. The researchers developed an equation for prediction of the minimum width of apron that remained horizontal after erosion.

MELVILLE ET AL. (2007)[19]

B.W. Melville et al. conducted an experimental investigation to determine the stone size D_{50} of riprap aprons around a wing-wall abutment necessary to withstand shear failure induced by the approach flow.[19] The experiments were conducted in a compound channel with a fixed-bed floodplain and an erodible main channel under live-bed conditions. The experimental results were then compared with predictions of riprap stone size D_{50} given by existing equations.

The stability of the riprap stones against shear failure was observed after each run. Experiments were classified as stable (no entrainment) and shear failure (entrainment of rocks). It was observed that the dislodged rocks were transported some distance downstream. Often these rocks were entrained from the edges of the apron (i.e., edge failure was a failure mechanism linked).

PETERSEN ET AL. (2015)[5]

T.U. Petersen et al. conducted two experiments to investigate the mechanisms of edge scour in currents to better understand its causes.[5] The first type of experiment was conducted under live-bed conditions for scour testing, while the subsequent test was conducted in the clear-water regime to obtain clear particle image velocimetry (PIV) measurements.

The results were measured with a variety of devices, including a mini underwater video camera that videotaped the overall time development of the scour process, a laser rangefinder that measured the scour profiles, and a laser Doppler anemometer that measured the velocity profiles across the water depth. The miniature underwater video camera also used the movement of the sand grains in the video recordings as flow tracers. The data were then used to visualize the flow structures alongside the toe of the stone layer and individual stones. The second experiment used PIV measurements to investigate the three-dimensional flow in the cross-sectional plane at the meeting of the sand and stone layer. Objectives for the experiment included obtaining the secondary currents and estimating the turbulence intensity field over the two layers.

Based on the data that were collected, the secondary flow very close to the bed in the sand section was directed away from the stone layer toe, and that over the stones was directed into the stone layer. This pattern resulted in a pattern of deposition occurring inside the toe of the stone layer, scour occurring at the edge of the stone layer, and finally a slight deposition of sediment. These secondary currents originated from either transition in surface roughness between the sand and stone layer or from corner effects.

The mechanisms governing the edge scour was the turbulence in the primary flow as it neared the intersection between the stone layer and sand bed and the secondary flow. The sediment was brought into suspension by the turbulence and was subsequently carried away by the secondary flow. Two types of turbulence together caused the sediment to be brought into suspension: turbulence in the primary flow generated in the fully developed boundary layer over the sand bed and stone layer, and the turbulence generated locally around individual stones at the toe, which

formed horseshoe-vortices and lee-wake flow. As the scour around the stones occurred, the process removed sand below the stones and subsequently caused the stones to slump into the scour hole. Shear failure of the sand also contributed to the movement of the stones and might have caused some stones to sink into the sediment bed. As the lower rocks slumped, the upper rocks also moved toward the edge. Horseshoe vortex and vortex shedding occurred and was revealed by sediment, which was used as flow tracers. These mechanisms increased the turbulence intensity and when paired with contraction of streamlines at the side edge of the stone caused scour holes around the toe stones. In addition, sand infiltrated into the cover stone layer, and a substantial quantity of deposition took place within the stone layer. Consequently, the combination of primary and secondary flow caused deposition to occur both in the stone layer and elsewhere. The governing parameters in controlling the three-dimensional flow field, including the secondary currents and turbulence adjacent to cover-stone layer, were the size of the roughness elements and, to some degree, the side slope.

JESSON ET AL. (2013)[20]

M. Jesson et al. conducted and reported the first attempt to use the Shiono-Knight method to model velocity and boundary stress distributions in an open channel.[20] An attempt to compare physical and numerical simulations of the open channel flow was made. It had been shown in many experiments that secondary flows not only form in homogeneously rough rectangular and trapezoidal channels but also in heterogeneous channels where the secondary flows were caused by changes in roughness. These secondary flows along with general boundary shear stress conditions affected the flow structures, conveyance capacity, and transport of sediment in the channel.

Smooth and rough sections were placed at intervals based on the idea that biotope changes could occur between three and four times in the stream-wise direction of a length equivalent to 10 channel widths. In accordance with this concept, the length of the patches used in the experiment was set at three channel widths. It was observed that the flow field adjusted quickly to changes in boundary roughness.

Jesson noted that the Reynolds stresses were complex, which indicated that higher order velocities unlike stream-wise velocities took longer to adjust. In addition, cross sections upstream and downstream of a change in roughness configuration showed very little observable variation in boundary shear stress profiles. This indicated that boundary shear stress adjusted relatively quickly to local changes in surface roughness. These results were promising and indicated that robust modeling could assist environmental regulators and river managers to assess and manage river stability and sediment transport.

APPENDIX B. EQUILIBRIUM SCOUR MAPS FROM THE PHYSICAL EXPERIMENTS

This appendix contains graphical representations of scour depth maps from the physical experiments.

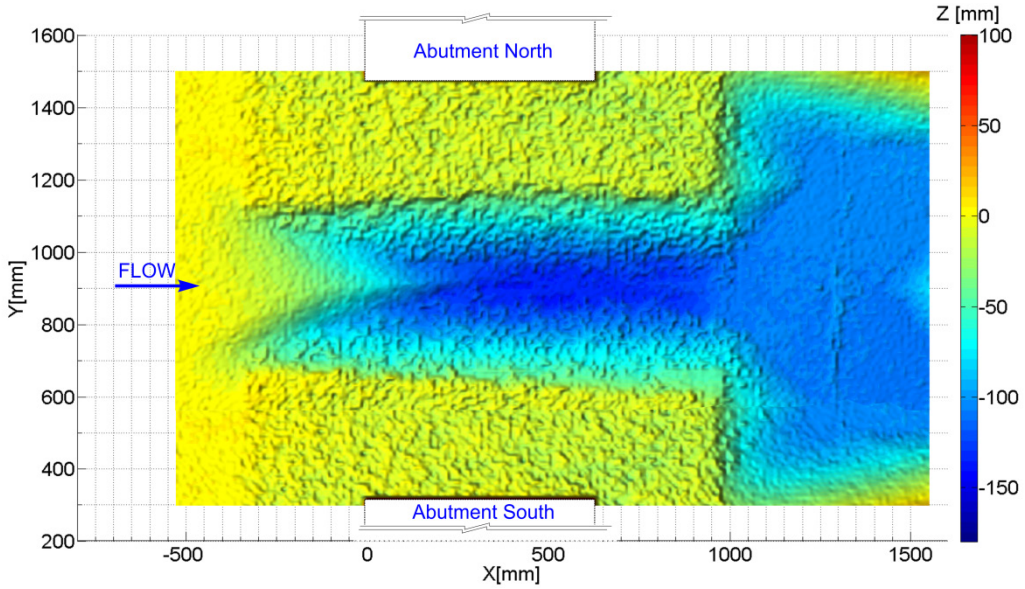

1 inch = 2.54 mm.

Figure 100. Graphic. Run 1—HEC-23 DG 14 for bridge abutments.

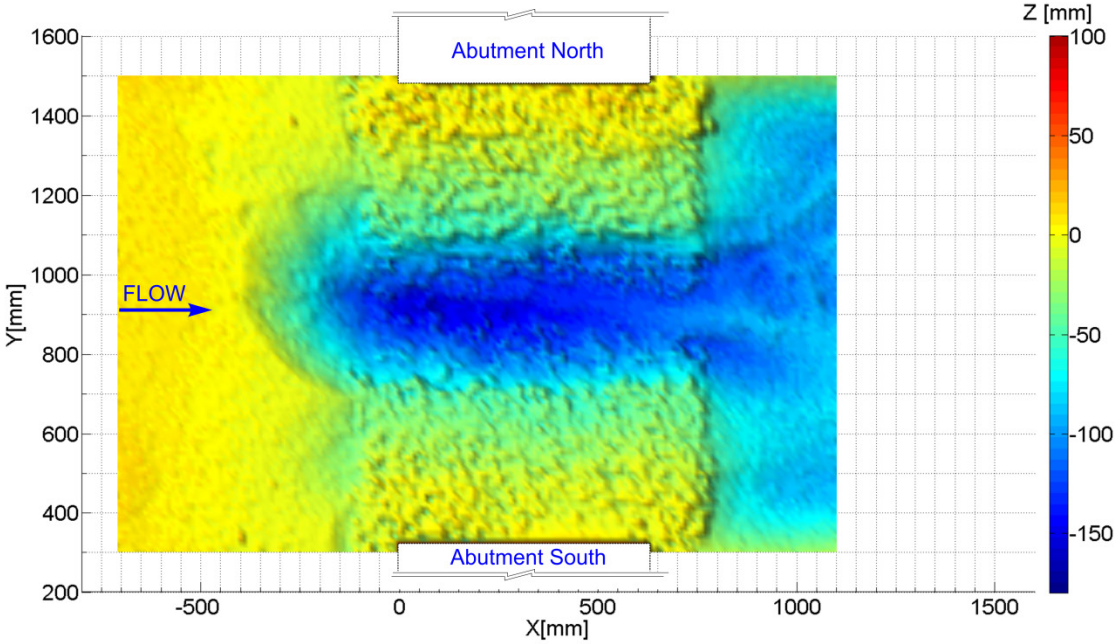

1 inch = 2.54 mm.

Figure 101. Graphic. Run 2—HEC-23 DG 18 for bottomless culverts.

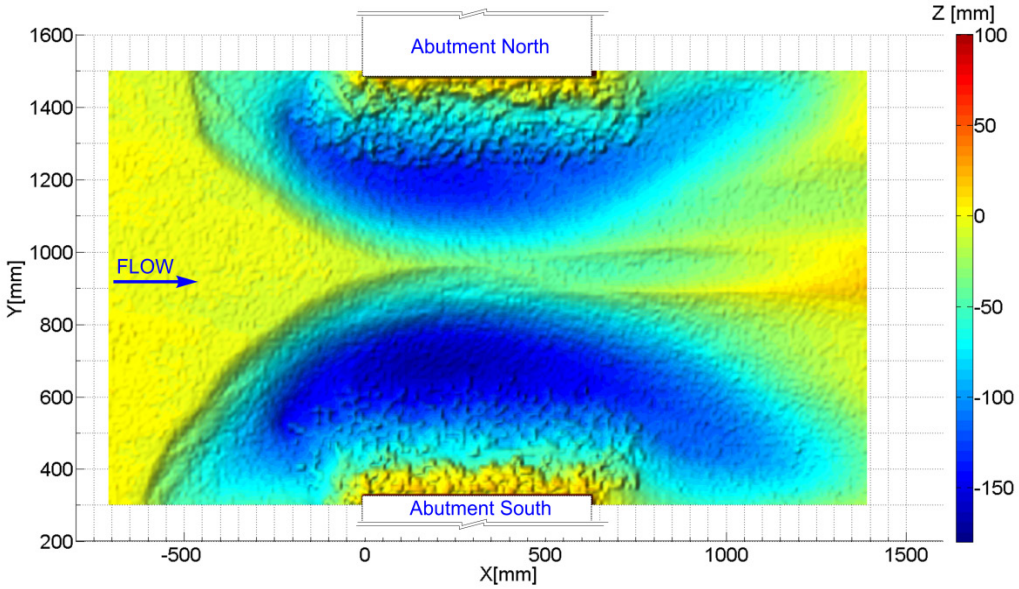

1 inch = 2.54 mm.

Figure 102. Graphic. Run 3—Field installation with riprap side sloped against abutment wall.

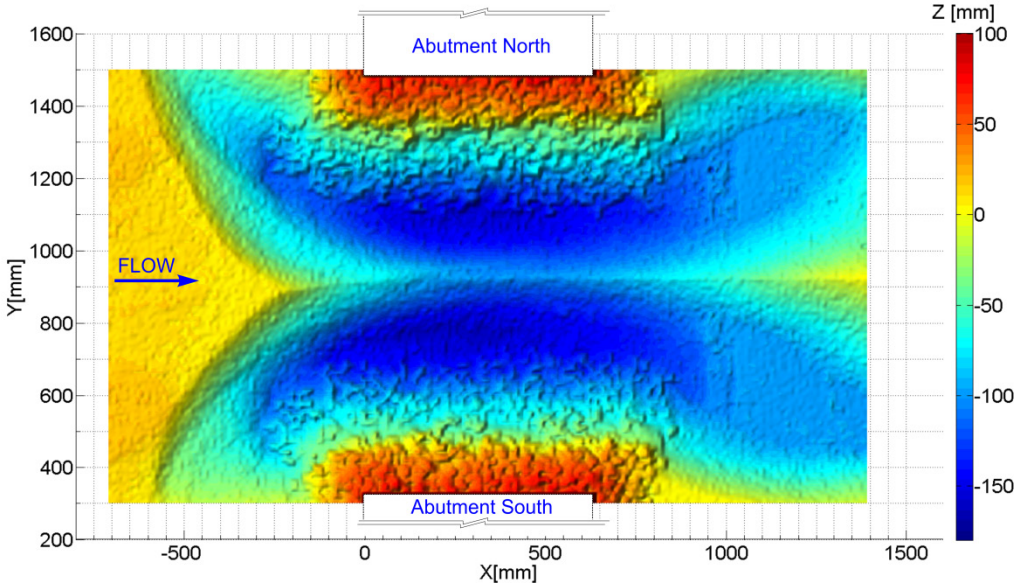

1 inch = 2.54 mm.

Figure 103. Graphic. Run 4—Riprap side sloped against abutment wall with $W_R = y_0$.

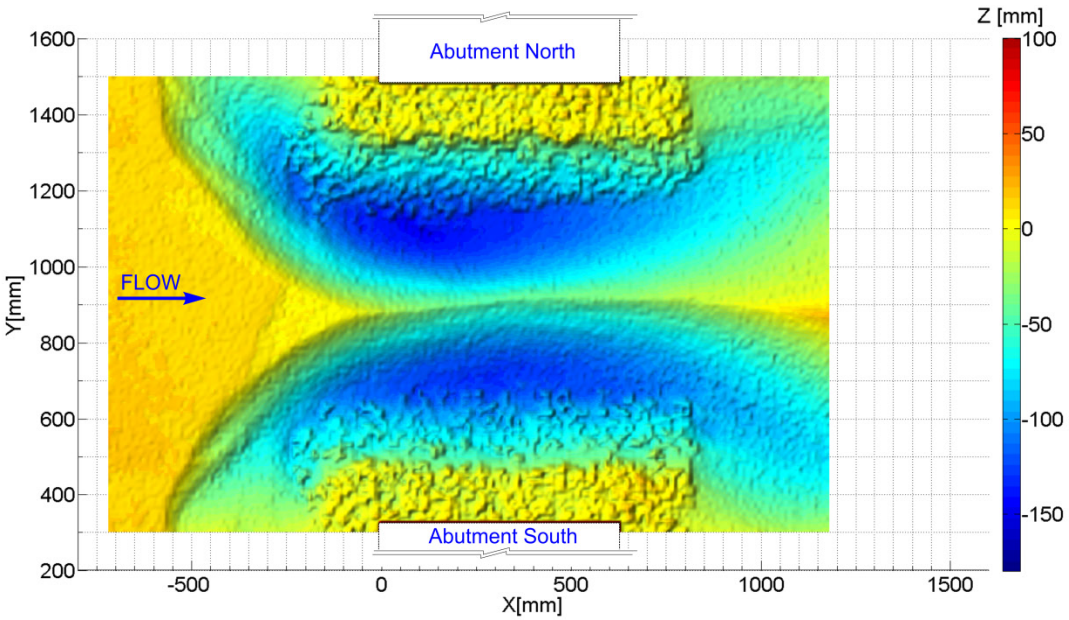

1 inch = 2.54 mm.

Figure 104. Graphic. Run 5—Flush apron level with channel bed with $W_R = y_0$.

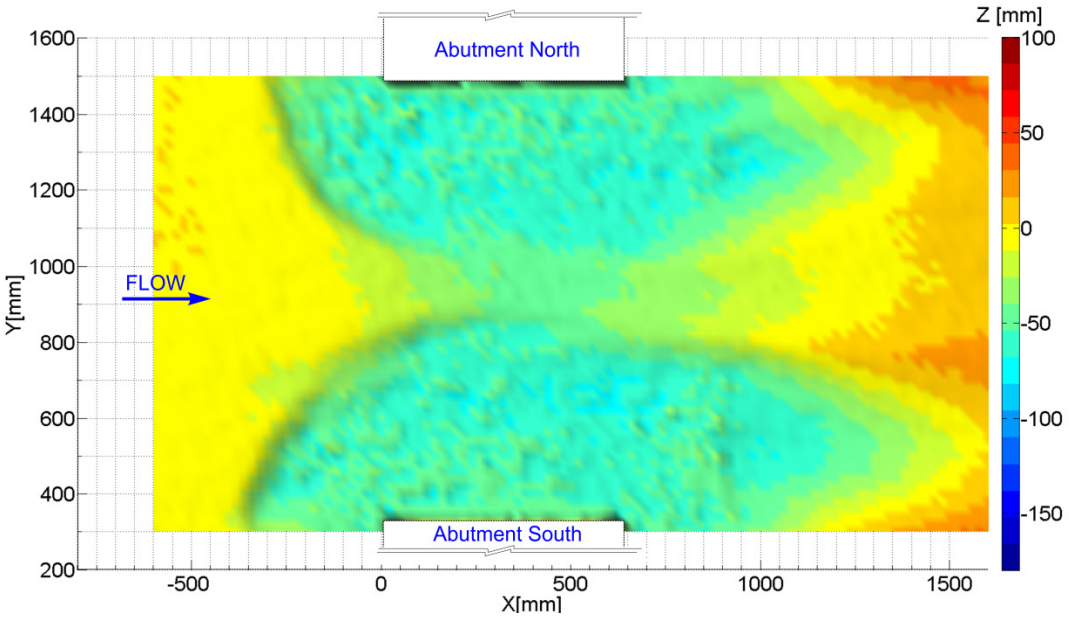

1 inch = 2.54 mm.

Figure 105. Graphic. Run 6—Proposed buried full bridge opening width with $W_1/W_2 = 1.55$.

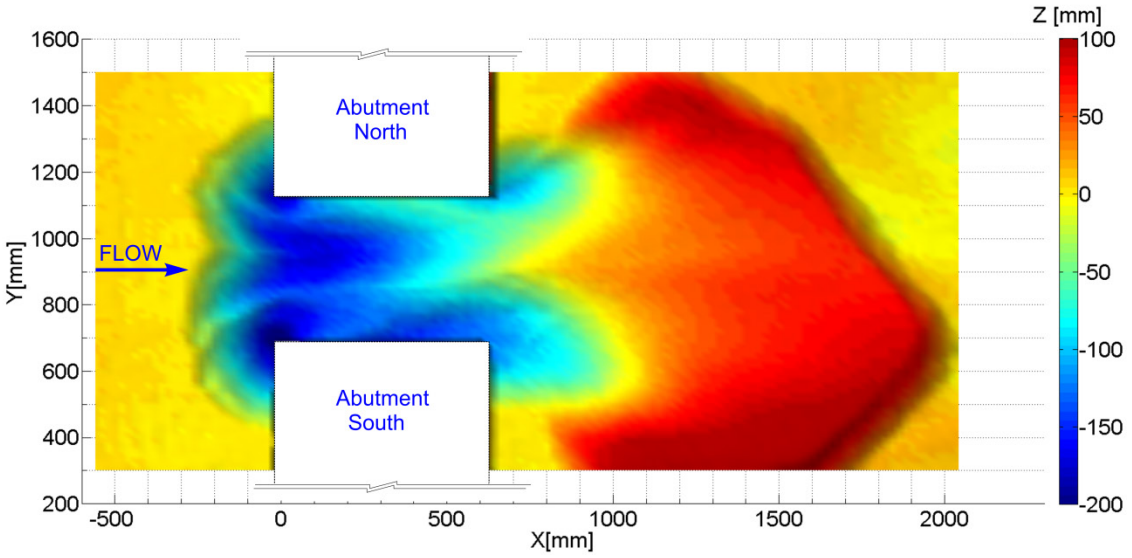

1 inch = 2.54 mm.

Figure 106. Graphic. Run 7—No riprap apron with $W_1/W_2 = 4.1$.

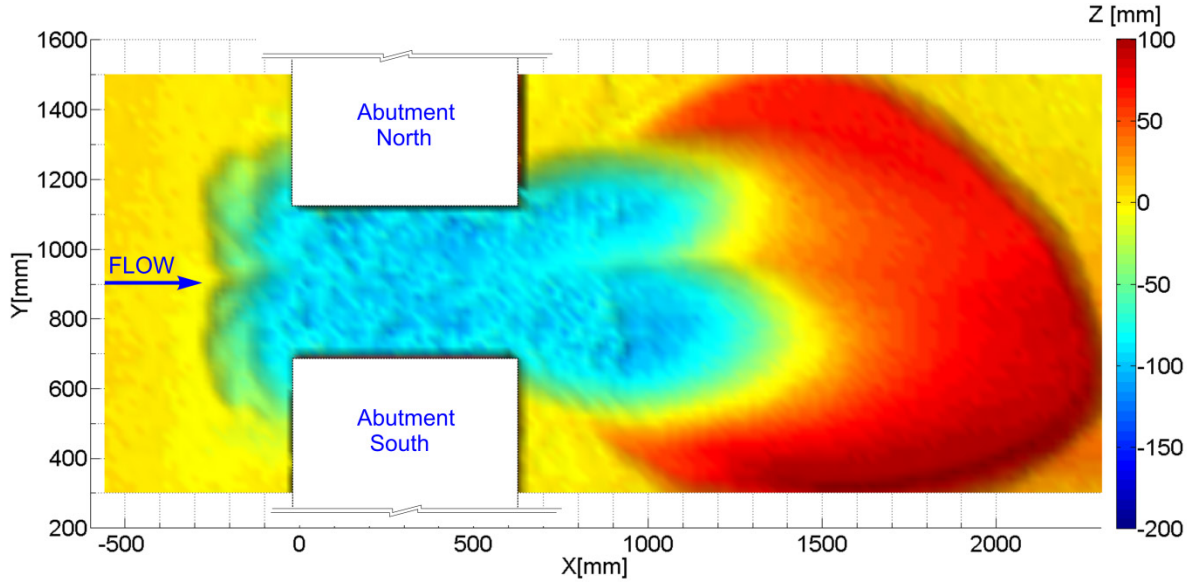

1 inch = 2.54 mm.

Figure 107. Graphic. Run 8—Proposed buried full bridge opening width with $W_1/W_2 = 4.1$.

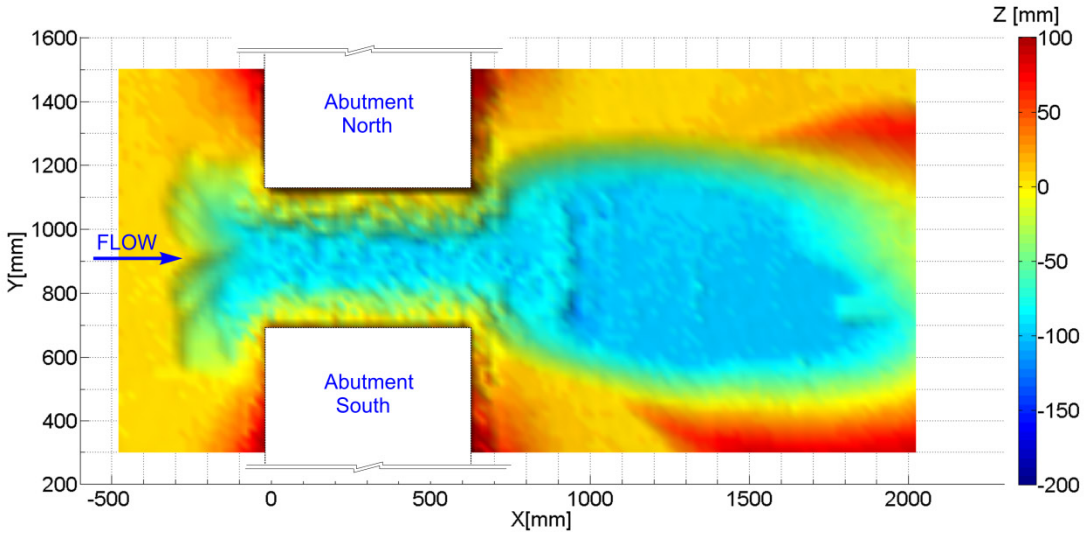

1 inch = 2.54 mm.

Figure 108. Graphic. Run 9—Proposed buried full bridge opening width with W_1/W_2 = 4.1.

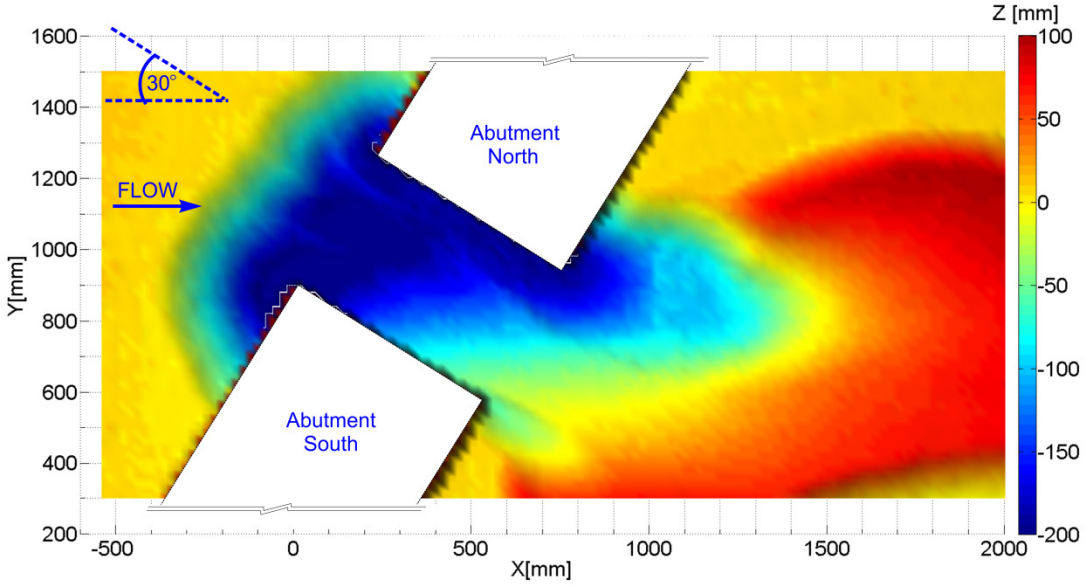

1 inch = 2.54 mm.

Figure 109. Graphic. Run 10—No riprap apron with W_1/W_2 = 4 and a 30-degree skew angle.

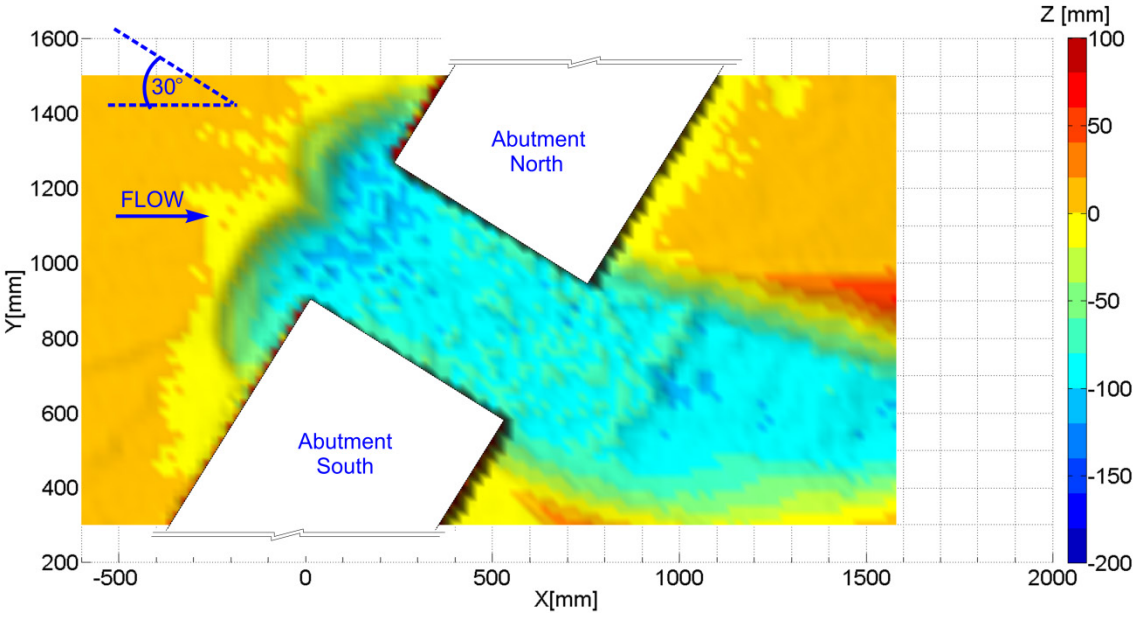

1 inch = 2.54 mm.

Figure 110. Graphic. Run 11—Proposed buried full bridge opening width with W_1/W_2 = 4.1 and a 30-degree skew angle.

APPENDIX C. CFD SHEAR STRESS AND VELOCITY DISTRIBUTIONS

This appendix contains graphical representations of the shear stress and velocity distributions for each CFD case, comparing the models with and without riprap.

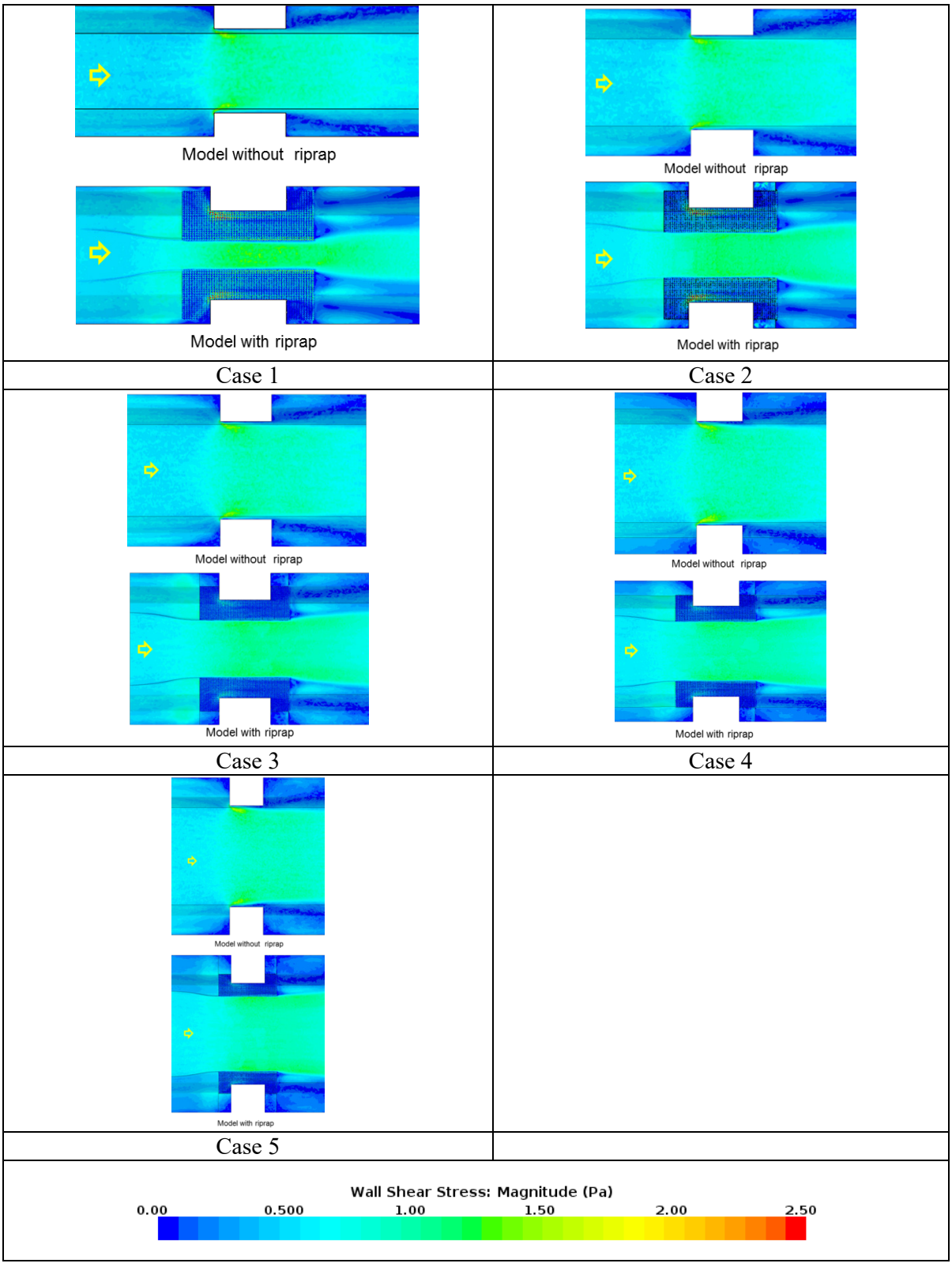

1 lbf/ft^2 = 47.88 Pa.

Figure 111. Graphics. Comparison of results of bed shear distribution for group 1.

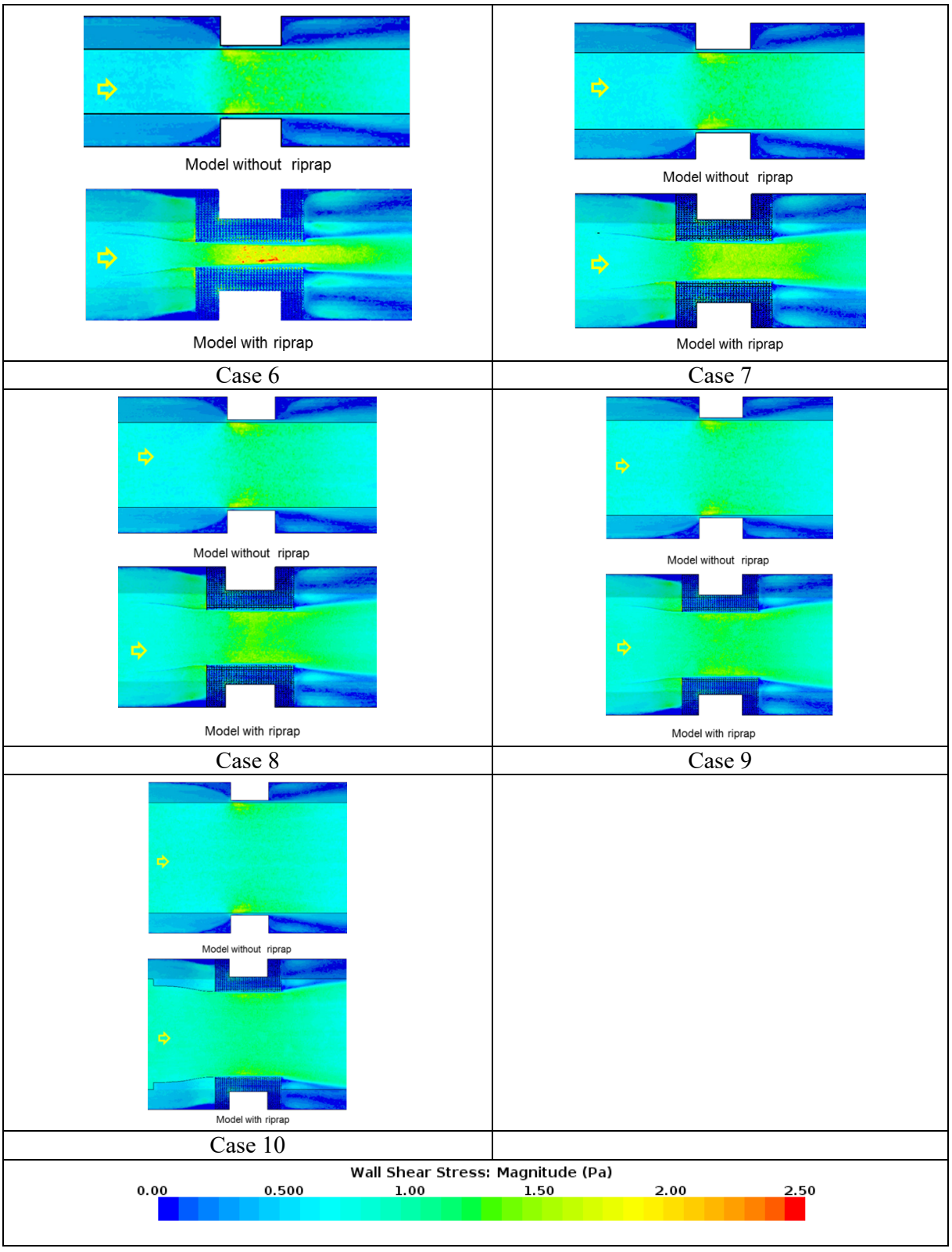

1 lbf/ft^2 = 47.88 Pa.

Figure 112. Graphics. Comparison of bed shear distribution for group 2.

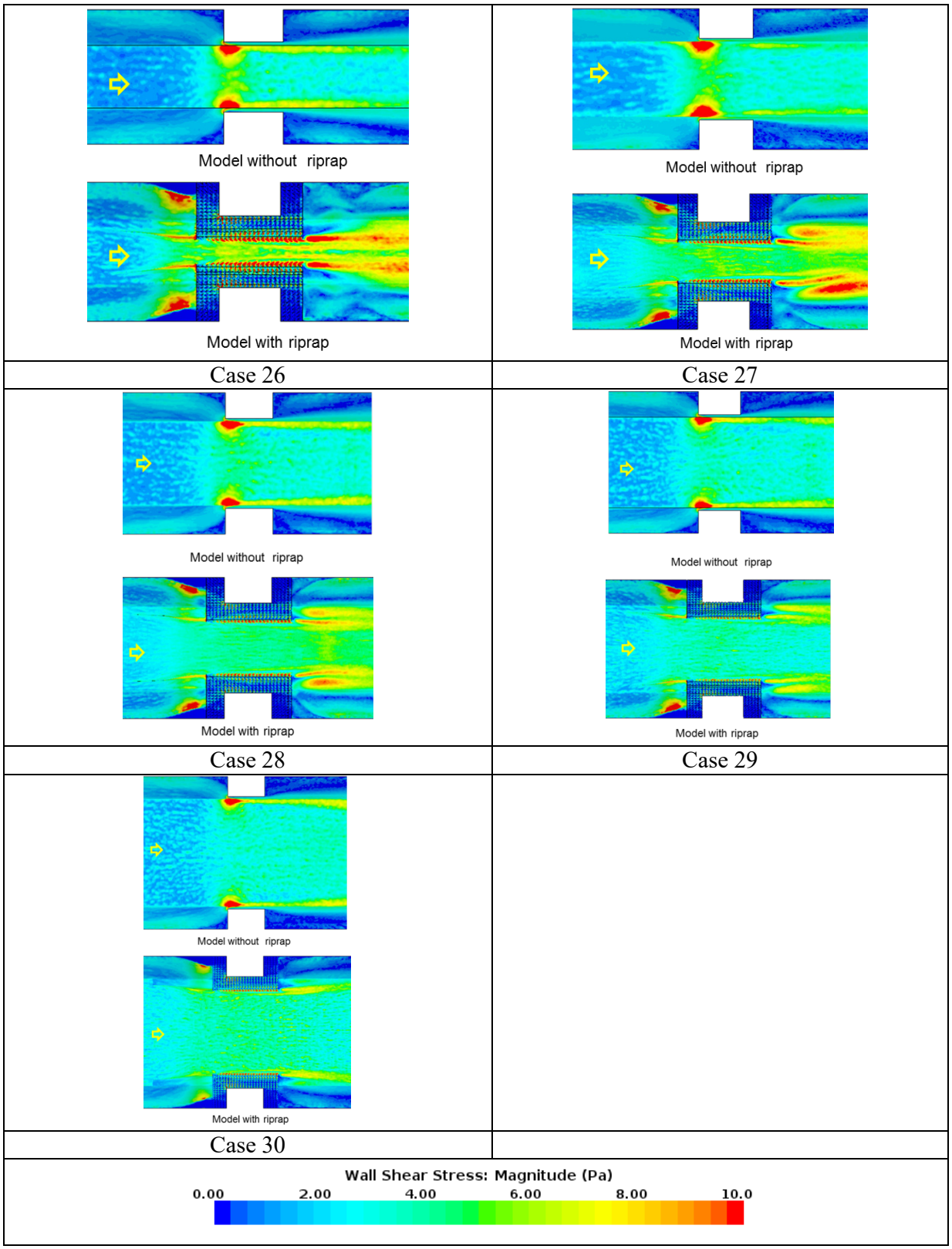

1 lbf/ft^2 = 47.88 Pa.

Figure 113. Graphics. Comparison of bed shear distribution for group 6.

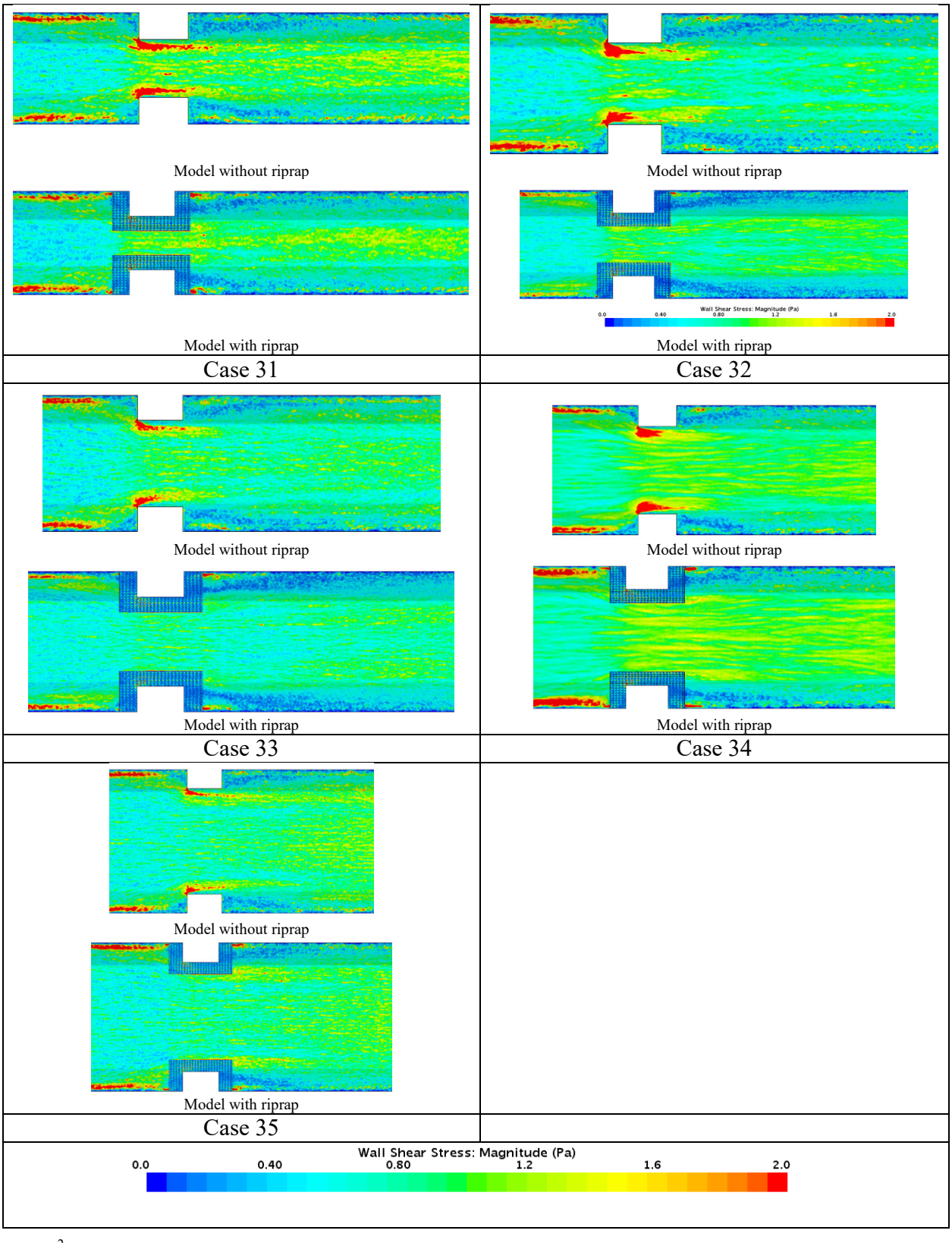

1 lbf/ft^2 = 47.88 Pa.

Figure 114. Graphics. Comparison of bed shear distribution for group 7.

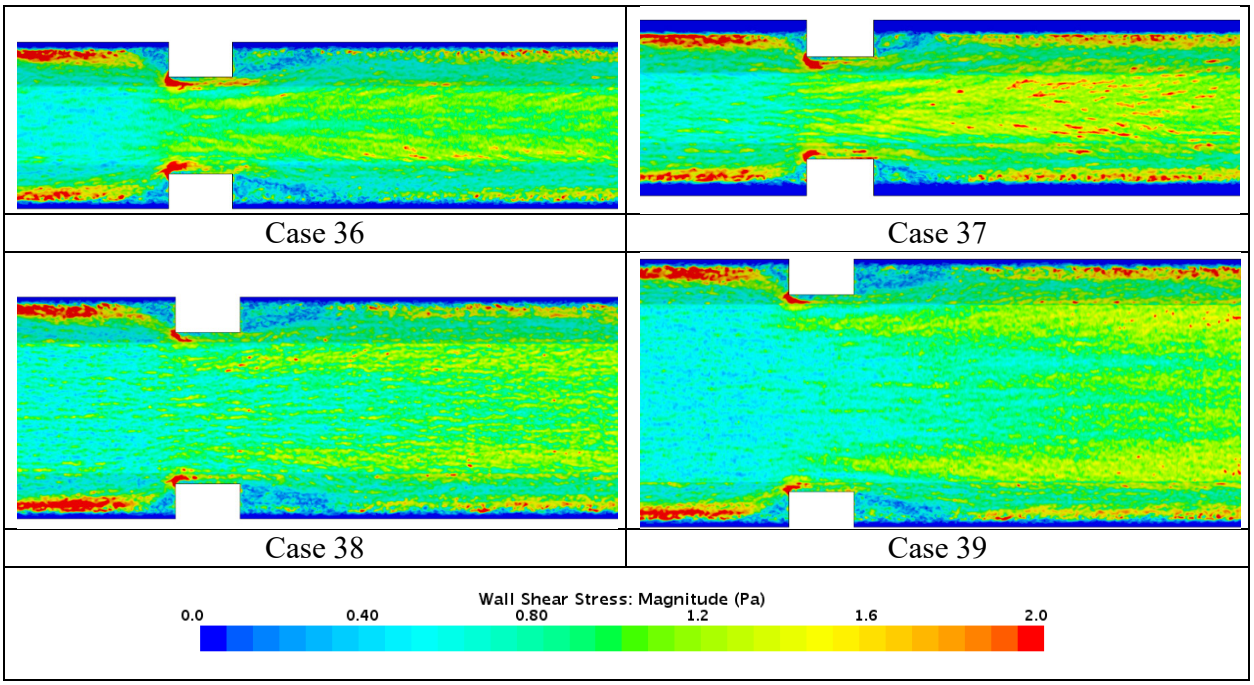

1 lbf/ft^2 = 47.88 Pa.

Figure 115. Graphics. Comparison of bed shear distribution for the short extension slope.

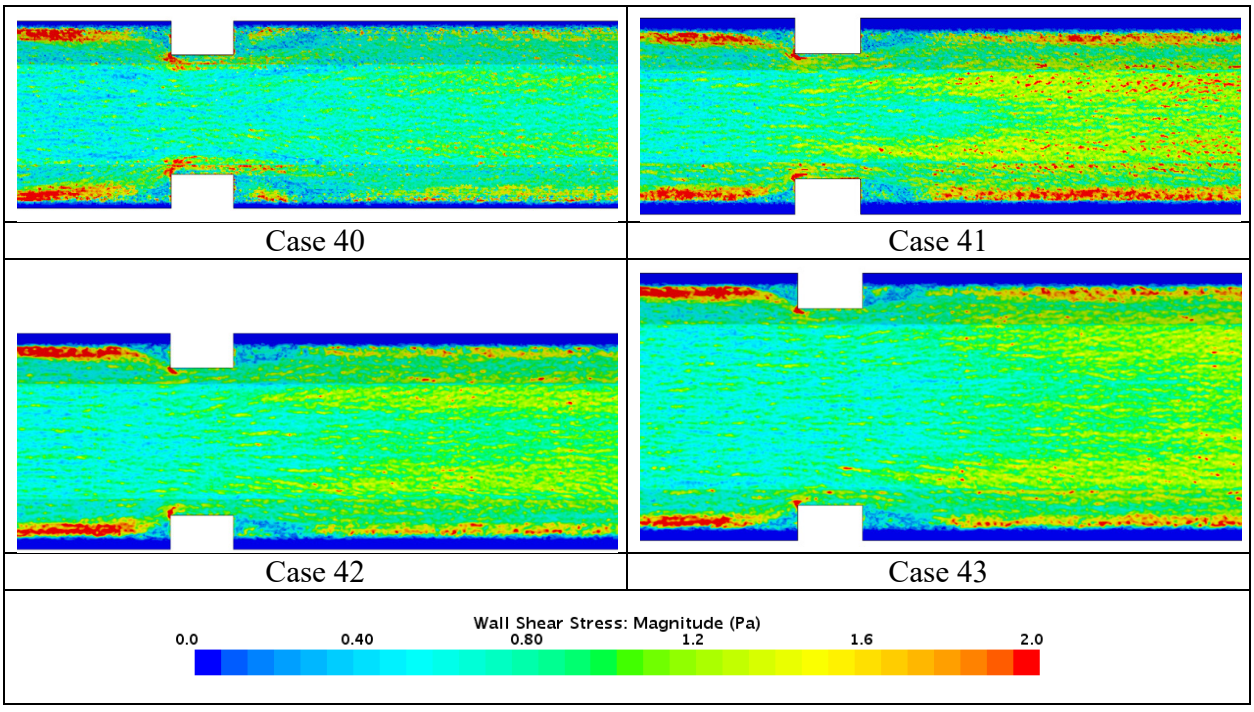

1 lbf/ft^2 = 47.88 Pa.

Figure 116. Graphics. Comparison of bed shear distribution for the long extension slope.

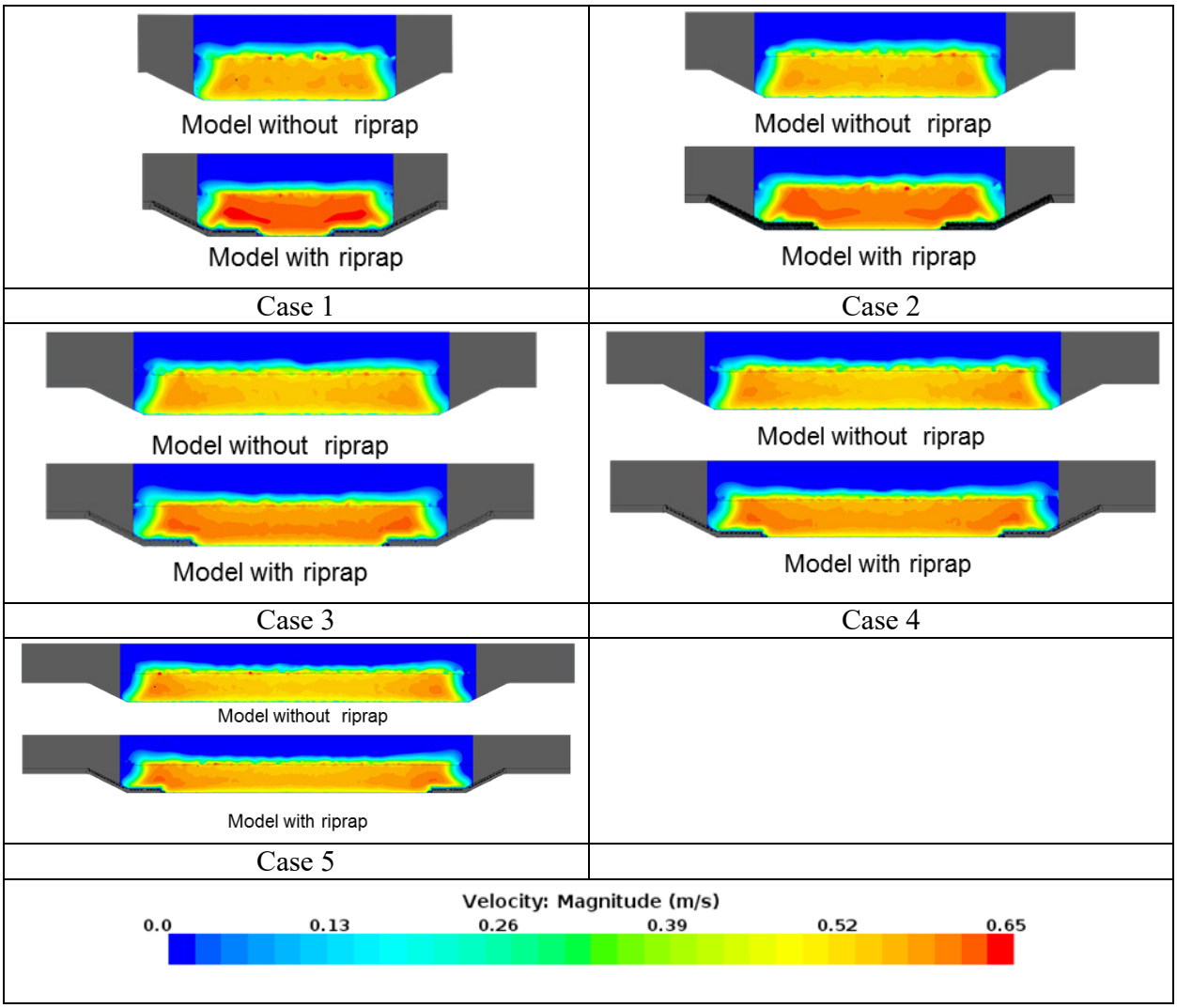

1 lbf/ft^2 = 47.88 Pa.

Figure 117. Graphics. Comparison of velocity distribution at central cross section for group 1.

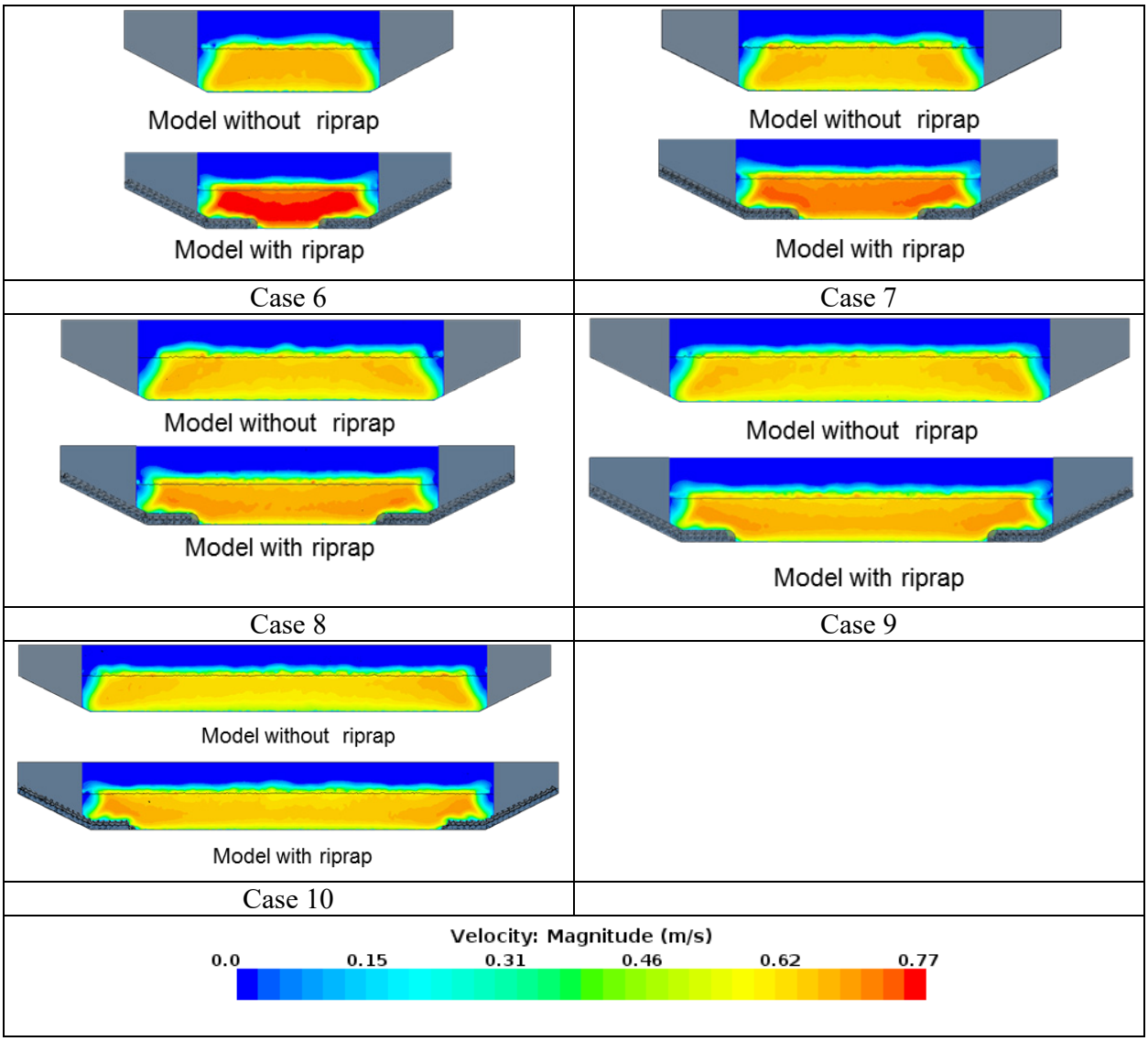

1 lbf/ft^2 = 47.88 Pa.

Figure 118. Graphics. Comparison of velocity distribution at central cross section for group 2.

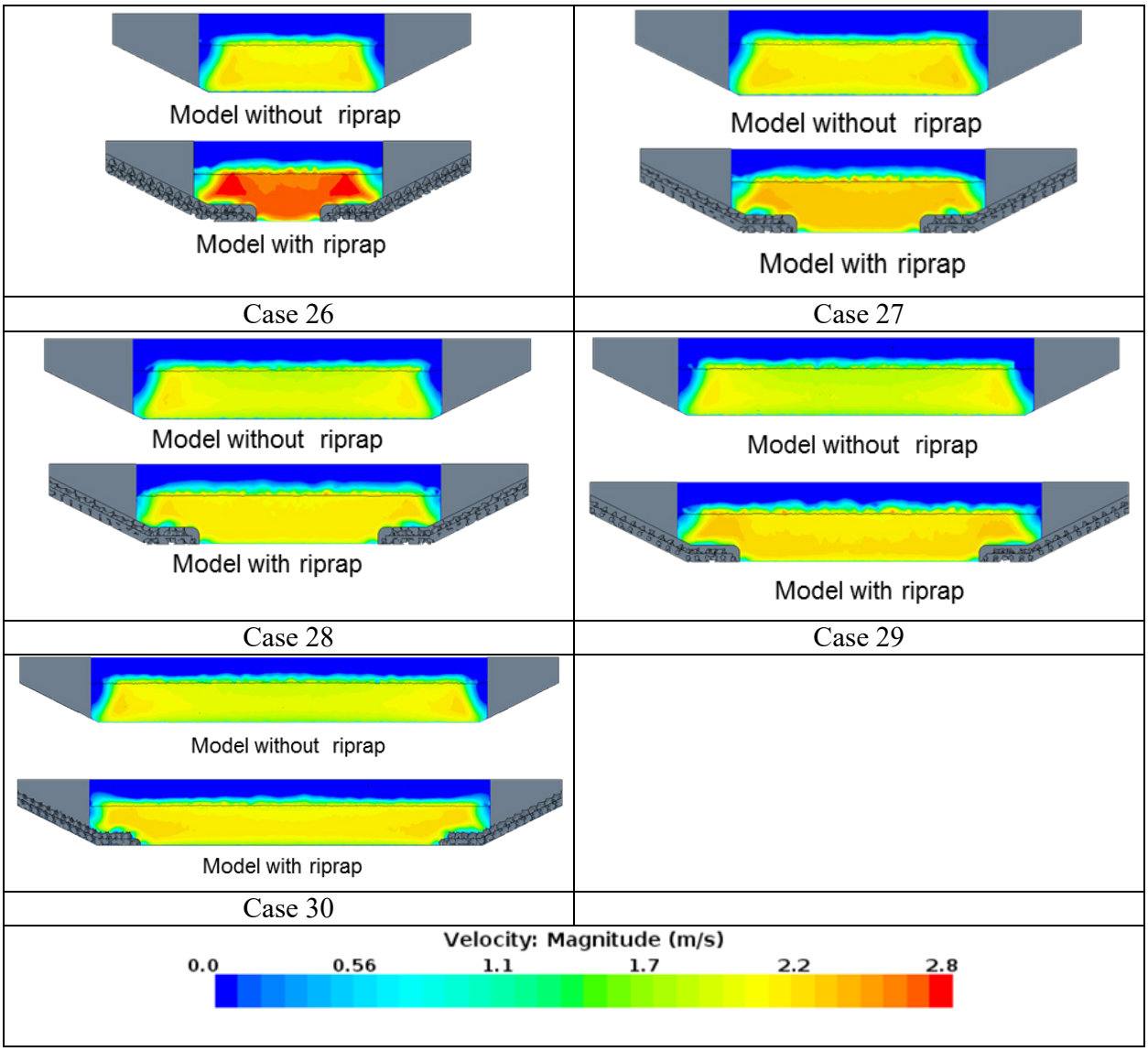

1 lbf/ft^2 = 47.88 Pa.

Figure 119. Graphics. Comparison of velocity distribution at central cross section for group 6.

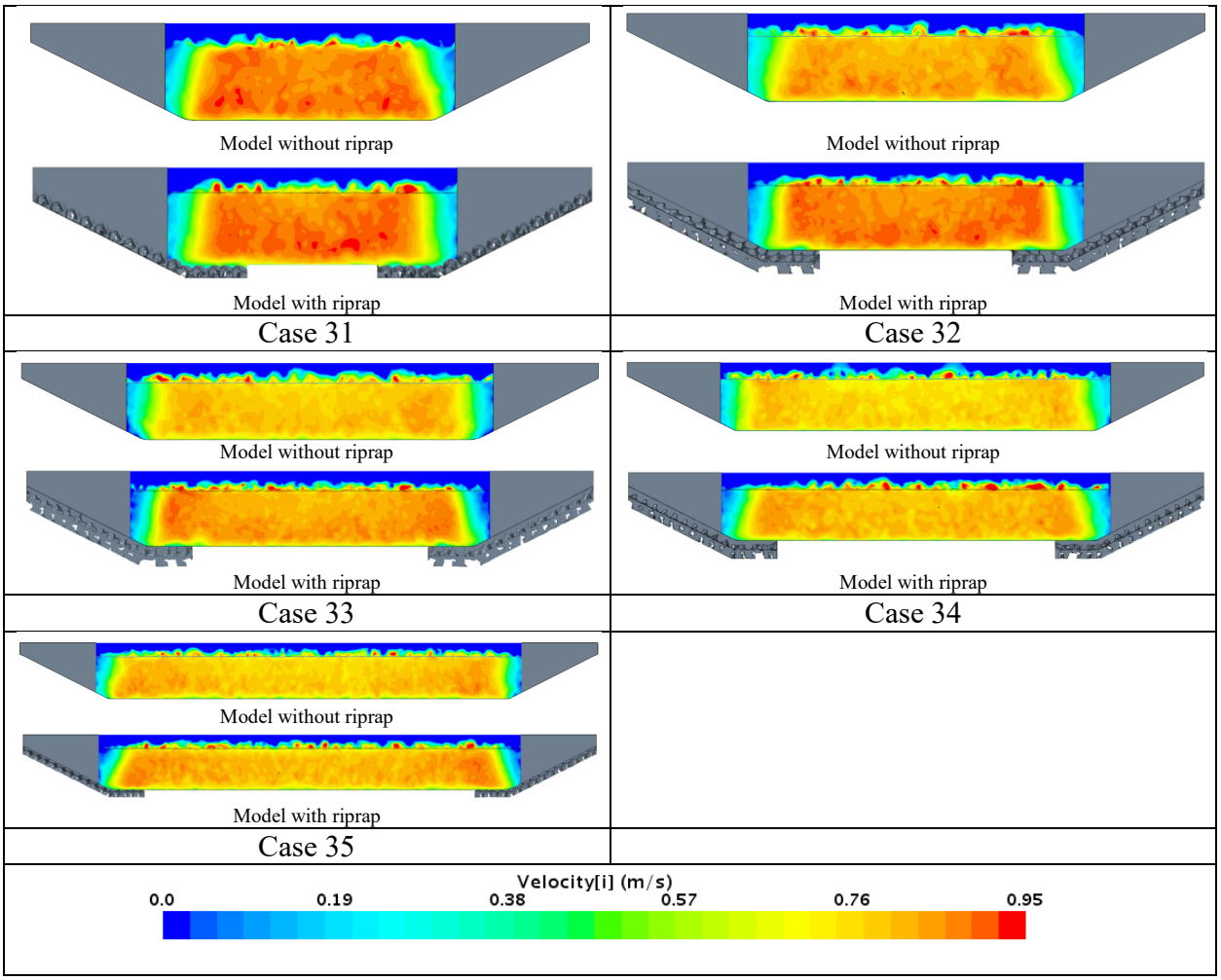

1 lbf/ft^2 = 47.88 Pa.

Figure 120. Graphics. Comparison of velocity distribution at central cross section for group 7.

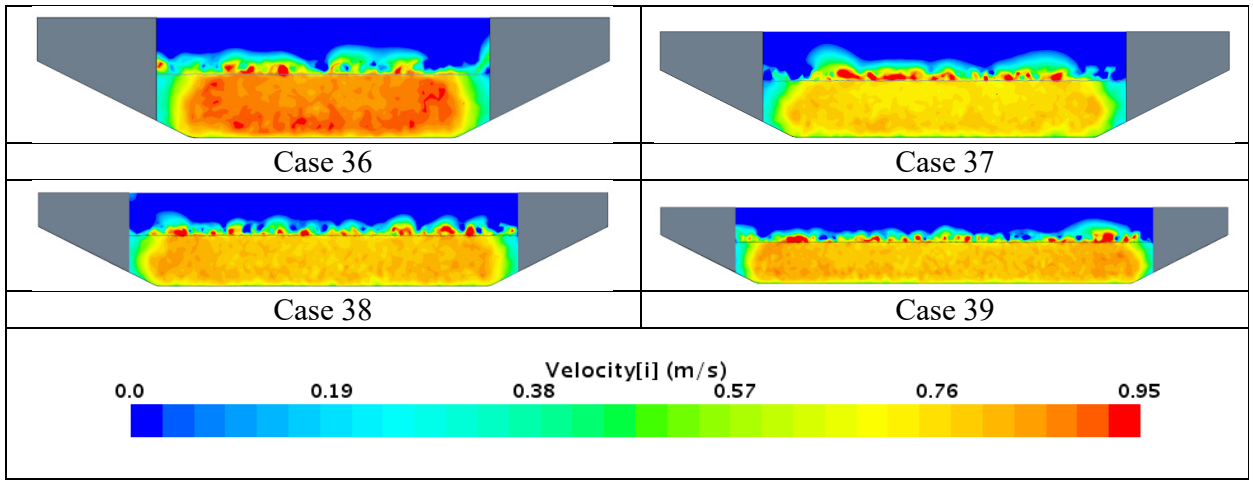

1 lbf/ft^2 = 47.88 Pa.

Figure 121. Graphics. Comparison of velocity distribution at central cross section for short extension slope.

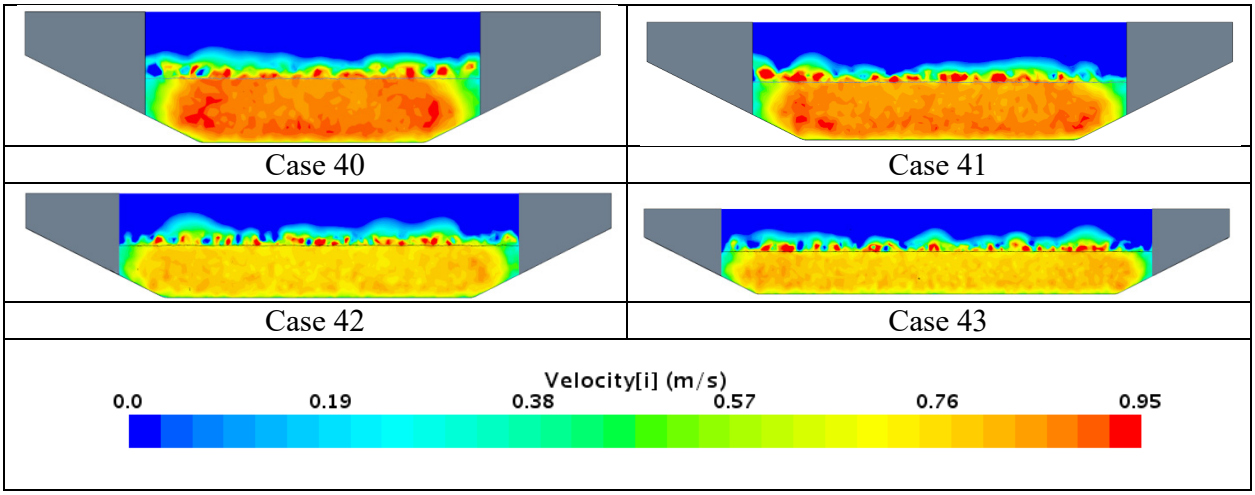

1 lbf/ft^2 = 47.88 Pa.

Figure 122. Graphics. Comparison of velocity distribution at central cross section for long extension slope.

This Page Is Left Blank intentionally.

APPENDIX D. HYDRAULIC REQUIREMENTS FOR SHALLOW ABUTMENT FOUNDATIONS

Shallow foundations (e.g., spread footings) have been successfully used for bridge abutments at river and stream crossings. However, when a shallow abutment foundation is being considered for use in a river or stream environment, it is vitally important to fully understand the hydraulic design requirements. The guidance provided in this appendix identifies the major hydraulic requirements that, if followed, provide greater assurance that the shallow foundation will perform as intended. This guidance supersedes that currently provided in HEC-18, fifth edition, and HEC-23, third edition.[2,3]

The design of bridges in a river environment is a very complex endeavor because of the complex interactions among the structural components, the soils in which they are founded, and the moving water that imparts hydraulic loading to both. For this reason, an interdisciplinary team of structural, geotechnical, and hydraulic engineers should always be fully engaged in the bridge scoping, design, and construction processes. From a strictly hydraulics perspective, it is of utmost importance that a qualified hydraulics engineer, experienced in river mechanics, sediment transport, and bridge hydraulics be part of the interdisciplinary team.

When bridges are constructed over a waterway, their foundations must be designed, detailed, and constructed in compliance with section 2.6 (Hydrology and Hydraulics) of the American Association of State Highway and Transportation Officials *Load Resistance Factor Design Bridge Design Specifications* or an FHWA division office-approved drainage or bridge manual.[25] In addition, the bridge impact on the numerous floodplain values that may be present must be evaluated in accordance with the U.S. Code of Federal Regulations (23 CFR Part 650 Subpart A).[26] These compliances are required for the project to be eligible for Federal assistance.

HYDRAULIC DESIGN CONSIDERATIONS

The minimum hydraulic design considerations that should be evaluated when deciding whether a shallow abutment foundation is appropriate for a waterway bridge follow:

- **Site selection:** The optimum stream-crossing site has a fully stable channel, which is characterized by banks and bed that are not prone to change. Detailed information on what constitutes a stable channel is contained in FHWA publication, HEC-20, *Stream Stability at Highway Structures*.[27]

- **Abutment location:** Bridge abutments are typically set back from stream channel banks to minimize potential stability problems, scour, and impact loads. Impact loads can be expected on streams that transport ice, large cobbles, boulders, or large woody debris such as tree trunks. It is recommended that abutments be set back from the channel banks a minimum distance of twice the design flow depth in the channel or 25 ft (7.6 m), whichever is less. Flow depth should be established by water surface modeling**.**

- **Adverse flow conditions:** Adverse flow conditions generate complex hydraulics and increase the potential scour and stream instability at a bridge site. Adverse flow

conditions result from bridges that have the following characteristics: (1) are highly skewed to the flow, (2) severely constrict the flow, (3) encroach on flows in steep channels, and (4) produce overtopping of the bridge or an approach roadway. Crossings with one or more of these adverse conditions must be evaluated with advanced hydraulic modeling techniques (two-dimensional modeling) to identify accurate flow depths and velocities at the necessary locations.

- **Risk-based standards:** Risk-based standards have been adopted so bridge owners can better balance the flood frequencies used for bridge design with the risks associated with the crossing (e.g., cost of the bridge, importance of bridge, traffic characteristics). Once the owner has identified the appropriate risk-based flood frequency standard for hydraulic design (i.e., bridge waterway capacity), FHWA has linked that flood frequency to recommended frequencies for the scour design and scour check floods. Reference chapter 2 of HEC-18 (i.e., *Evaluating Scour at Bridges)* for a discussion of risk-based standards and the recommended relationship between the hydraulic design and the scour floods.[(2)]

- **Local drainage:** The potential for unbalanced water pressure exists when an abutment wall can become partially submerged by a flood or when surface drainage is not controlled. All vertical-wall abutments should include provisions to accommodate surface and subsurface drainage. The following critical areas should be considered: behind the wall, at the base of the wall, and any location where a fill slope meets the wall face. For example, the design needs to include provisions for surface drainage along the fill slope adjacent to wing walls.

The listed descriptions of hydraulic design considerations reflect preferred conditions for shallow foundation abutments. The greater the departure from these preferred conditions, the more likely that alternative abutment types or drainage structure types (e.g., reinforced concrete box culverts or pipe culverts) should be considered. Under these circumstances, it is recommended that economic analyses be used to identify the preferred alternative.

HYDRAULIC DESIGN PROCESS

The bridge hydraulic design process applicable to shallow foundation abutments is illustrated in figure 123.

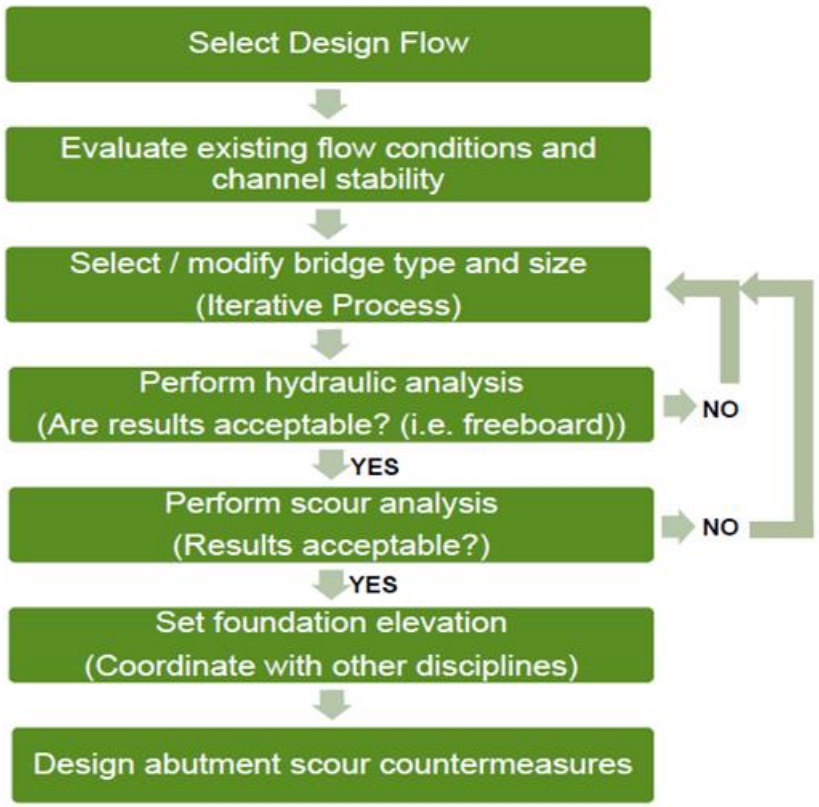

Figure 123. Flowchart. Bridge hydraulic design process.

The steps in this multidisciplinary process are described as follows:

- **Select design flow:** A minimum of three flood frequencies must be evaluated for shallow foundation design: (1) hydraulic design flood, (2) scour design flood, and (3) scour check flood. The hydraulic design flood is used to identify the necessary size (i.e., length and elevation) and orientation of the bridge opening. The scour design and check floods, which are typically larger than the hydraulic design flood, are used to design scour countermeasures and determine the minimum depth of the spread footing foundation. The appropriate frequency for these floods is typically defined by the hydraulic standards established by the bridge owner. If such standards do not exist, the appropriated flood frequencies can be identified by conducting a risk assessment or analysis for the stream crossing. Reference chapter 2 of HEC-18 for detailed discussions of risk-based standards and the recommended relationship between the hydraulic design flood and the scour floods.[(2)]

- **Evaluate existing flow conditions and channel stability:** Existing flow conditions and patterns should always be evaluated to establish a hydraulic baseline for the new or replacement bridge design. Also, stream channels should be stable, both horizontally and vertically, in the vicinity of the bridge to provide a suitable crossing environment for the life of the bridge. Details on the evaluation of channel stability are contained in HEC-20.[(27)] Details on stream instability countermeasure design can be found in HEC-23 (*Bridge Scour and Stream Instability Countermeasures)*.[(3)]

- **Select/modify bridge type and size:** As indicated in figure 123, this step is the beginning of an iterative process that evaluates the hydraulics and potential scour resulting from the alignment and grade of the approach roadways, as well as the size and orientation of the bridge. Proposed layouts of these elements must be hydraulically modeled for a range of discharges that includes the hydraulic design flood and the scour floods to accurately estimate the hydraulic parameters (e.g., depths and velocities) affecting the bridge, the approach roadways, and the floodplain.

- **Perform hydraulic analysis:** The hydraulic model used must be capable of developing water-surface profiles upstream, downstream, and through the bridge to identify reasonable estimates of the key hydraulic parameters. This requires that a one-dimensional water-surface profile model, such as HEC River Analysis System (i.e., HEC-RAS), be used at minimum. If adverse flow conditions exist, or are created at the crossing, a two-dimensional model, such as the Sedimentation and River Hydraulics—Two-Dimensional (i.e., SRH-2D), should be used. Also, if channel geometry can change over time, multiple hydraulic models may be needed to identify worst-case hydraulics and scour. The possible alignments, grades, and bridge geometries are evaluated with the hydraulic model(s) until an acceptable crossing configuration is found for the design floods. Refer to FHWA publication *Hydraulic Design of Safe Bridges* for detailed guidance on one- and two-dimensional hydraulic modeling.[(28)]

- **Perform scour analysis:** The hydraulics for floods up to and including the scour check flood standard are used to identify the worst-case scour depths for the applicable scour components and the total scour that can be generated at each bridge foundation. If a computed worst-case scour depth is not acceptable (i.e., too deep for the abutment to be economically built and/or protected), adjustments to the bridge type, size, or even location need to be made until an acceptable total scour value results. Such adjustments should be made only after in-depth consultations with the project geotechnical and structural engineers. Reference HEC-18 for detailed guidance on conducting scour evaluations and analyses.[(2)]

- **Set foundation elevation:** There are two basic options for establishing the spread footing elevation: 1) the top of the footing may be set below the total scour depth for the scour check flood at the abutment, without the need for an abutment scour countermeasure, or 2) the top of the footing may be set at or below the contraction scour elevation for the scour design flood (includes any LTD), with a properly designed and constructed abutment scour countermeasure. As indicated in figure 123, the task of setting the final spread footing elevation can only be done effectively through in-depth consultation and coordination with the project geotechnical and structural engineers.

- **Design abutment scour countermeasures:** When it is not practical to set the abutment foundation below the total scour depth, a designed abutment scour countermeasure is required to ensure stability during the scour check flood. See the sections entitled Scour Design and Scour Countermeasure Design later in this appendix for more information on the design of scour countermeasures for shallow abutment foundations.

APPLICABLE SCOUR COMPONENTS

For shallow abutment foundation design, the following primary scour components must be computed and evaluated: (1) LTD, (2) contraction scour, and (3) abutment scour. Both the contraction scour and abutment scour components are sensitive to what sediment transport regime exists upstream of the bridge (i.e., live-bed versus clear-water) and whether the scour floods are under free-surface flow or pressure flow conditions (e.g., bridge girders are in the flow) at the bridge. Because of the dramatic increase in potential scour depth, pressure scour should be avoided, if at all possible. In addition, the abutment scour component is sensitive to the location of the abutment relative to the main channel. When the abutment is located close to the channel, the scour is computed differently than when it is some distance away (i.e. more than twice the main channel flow depth for the scour check flood).

The manner in which these individual scour components are evaluated for floods up to and including the scour check flood standard is summarized as follows by flow condition.

Free-Surface Flow

- LTD = Greater of the following two evaluations:
    - Computed depth from equilibrium slope or armoring analyses, based on HEC-20 guidance.[27]
    - A specified depth for other degradation phenomenon, such as head cut depth, or historical observation.
- Contraction scour (horizontal):
    - For clear-water conditions = Clear-water contraction scour estimate.
    - For live-bed conditions = Lesser of the following:
        - Live-bed contraction scour estimate.
        - Clear-water contraction scour estimate.
- Abutment scour:
    - Amplification factor, based on abutment location, multiplied by one of the following, as appropriate:
        - Clear-water contraction scour estimate.
        - Live-bed contraction scour estimate.

Pressure Flow

- LTD (same as for free-surface flow).
- Contraction scour (vertical) = Pressure scour.

- Abutment scour (component presently undefined for pressure flow; research in progress).

As indicated, the conditions and interaction of the scour components can be complicated and must be identified and analyzed by a qualified hydraulics engineer. Refer to HEC-18 for detailed definitions of the individual scour components and conditions that apply to abutment analysis and design, and for the various methods available to compute the scour magnitude for each component.(2)

SCOUR DESIGN

The scour used to establish the spread footing foundation elevation is the worst-case combination of applicable scour components estimated for floods up to and including the appropriate scour flood standard (e.g., Q500 for scour check flood), and depends on the flow condition (i.e., whether free-surface or pressure flow exists at the bridge). The manner in which the individual scour components are combined for scour design is summarized below for each flow condition and illustrated in figure 124 through figure 127. The combinations listed are for abutments located close to the channel bank. Note that the underlining is a reminder to the user that measurements for scour check flood should be used and not those for scour design flood.

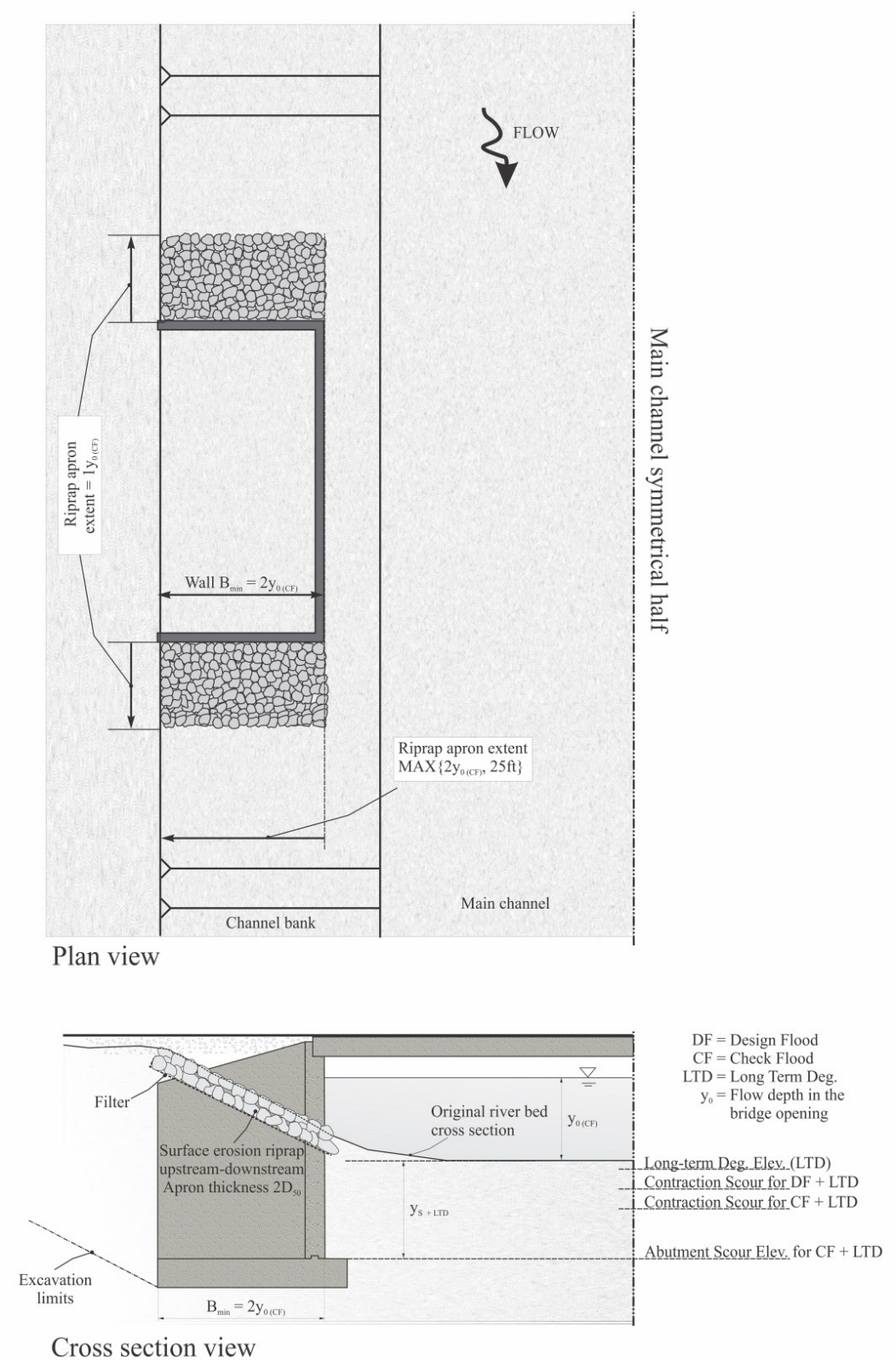

1 ft = 0.305 m.

Figure 124. Drawing. Free-surface flow with no scour countermeasure (option 1).

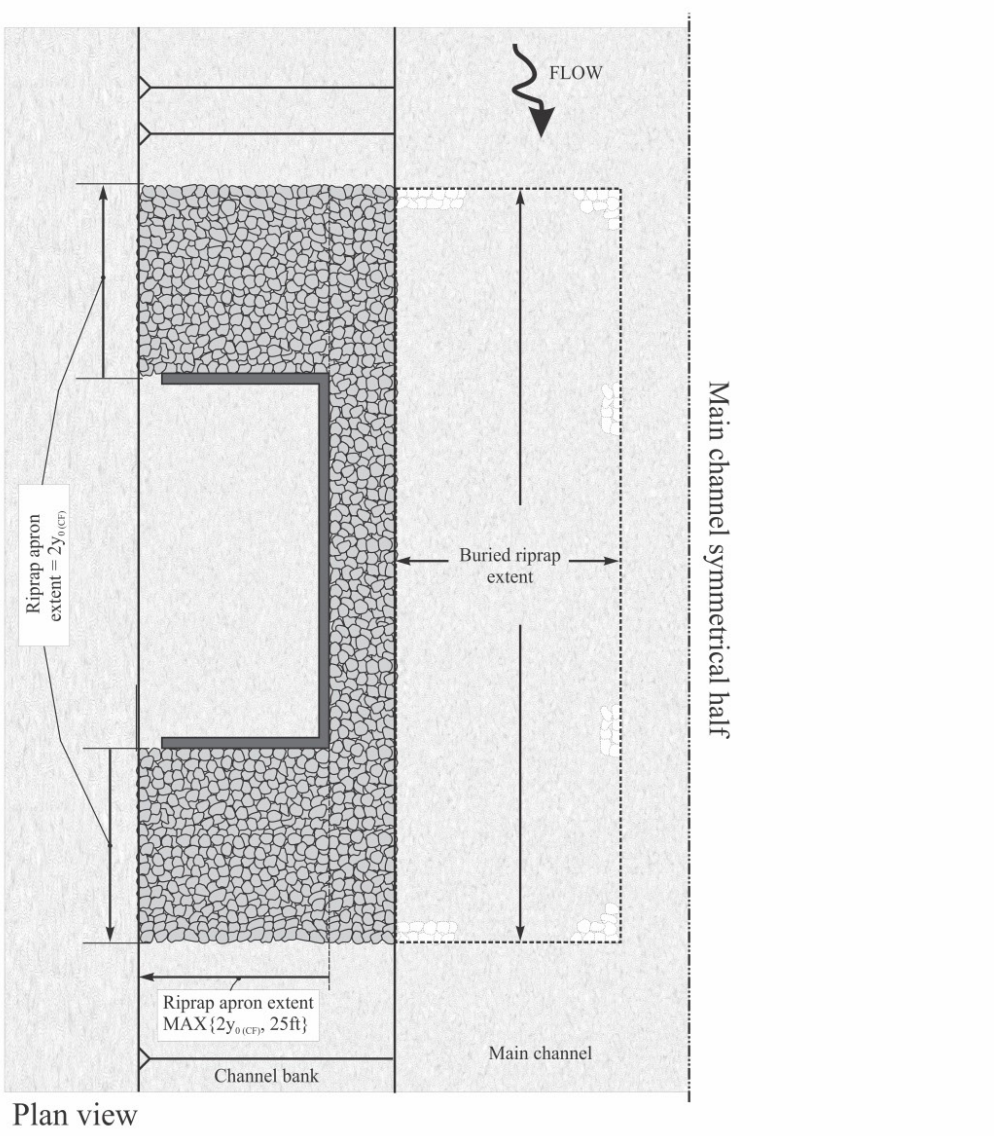

1 ft = 0.305 m.

Figure 125. Drawing. Free-surface flow with narrow-opening scour countermeasure (option 2).

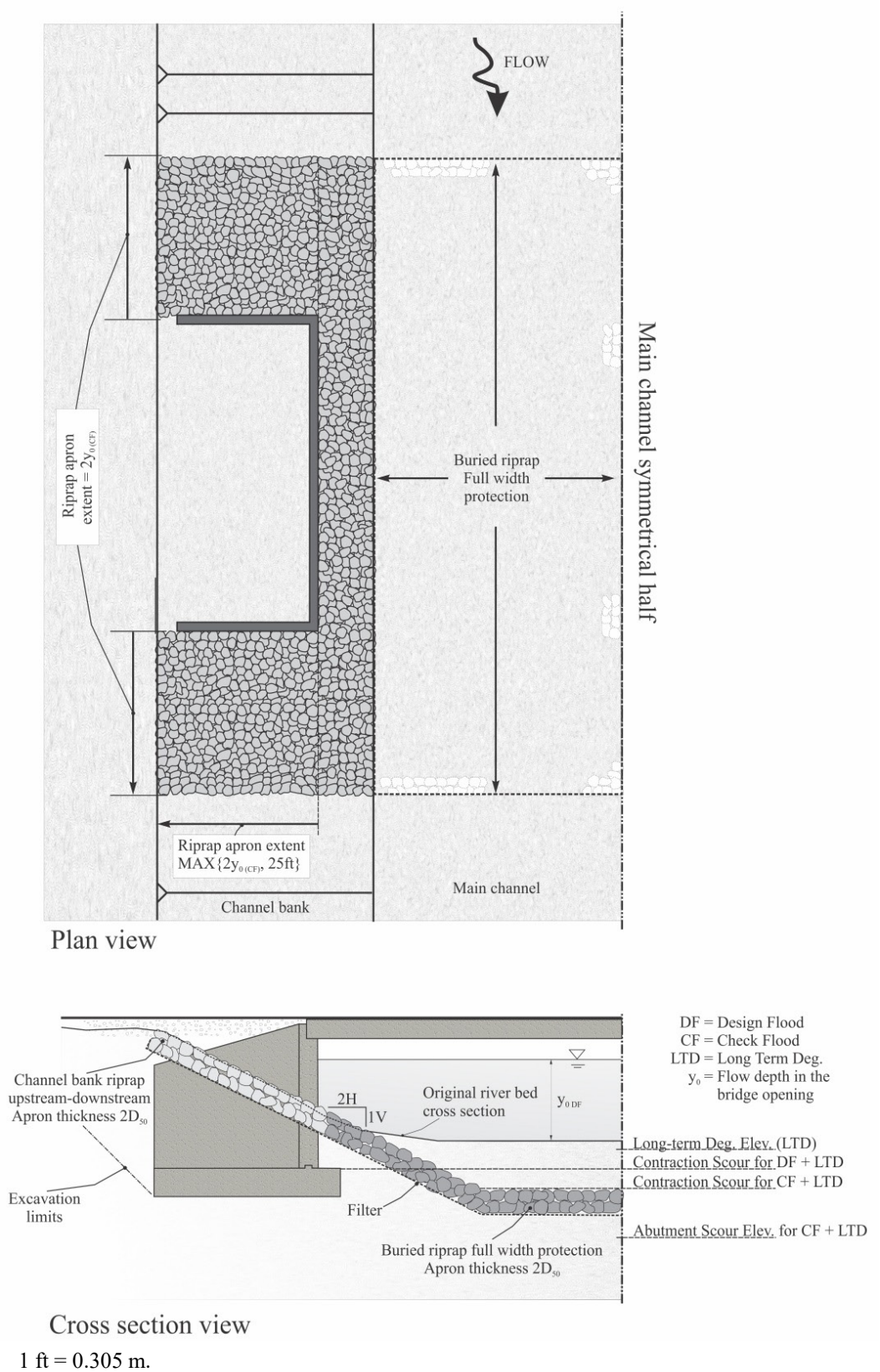

1 ft = 0.305 m.

Figure 126. Drawing. Free-surface flow with full-width scour countermeasure (option 3).

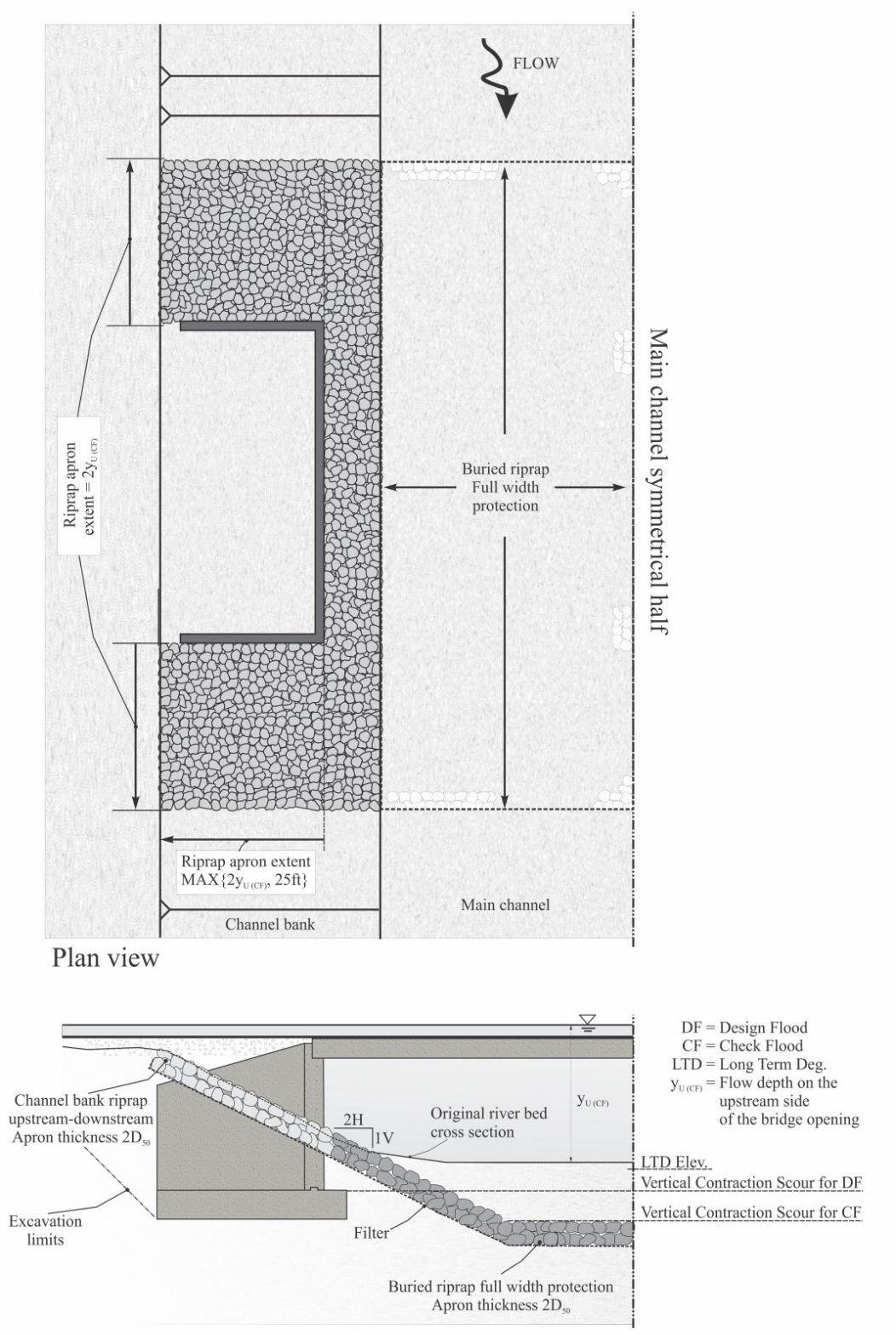

1 ft = 0.305 m.

Figure 127. Drawing. Pressure flow scour countermeasure.

Free-Surface Flow

- **Option 1 (no countermeasure)**: Minimum depth to top of footing = Total scour at abutment = LTD + abutment scour for the scour check flood (see figure 124).

- **Option 2 (wide-opening countermeasure; for $W_2/y_0 > 6.2$ only)**: Minimum depth to top of footing = LTD + contraction scour depth for the scour design flood; minimum depth to top of abutment countermeasure apron = LTD + contraction scour for scour check flood (see figure 125).

- **Option 3 (narrow-opening countermeasure)**: Minimum depth to top of footing = LTD + contraction scour depth for the scour design flood; full-width countermeasure protection required from abutment to abutment; top of full-width countermeasure below LTD + contraction scour depth for scour check flood (figure 126).

Pressure Flow

- **Pressure flow countermeasure:** Minimum depth to top of footing = greater of LTD or pressure scour depth for the scour design flood; full-width countermeasure protection required from abutment to abutment; top of full-width countermeasure below greater of LTD or pressure scour depth for scour check flood (figure 127).

It is important to note that scour depths must be tied to an appropriate reference elevation. The channel thalweg elevation should be used as the reference elevation for abutments located near the main channel.

SCOUR COUNTERMEASURE DESIGN

When a shallow abutment foundation requires installation of a scour countermeasure, the countermeasure must include a horizontal apron designed to be stable for the scour check flood. The apron should surround the entire abutment face and extend upstream and downstream of the abutment. For free-surface flow options 2 and 3, the extensions should be a distance equal to twice the main channel flow depth through the bridge, $2y_0$. For pressure flow, the extensions should be a distance equal to twice the main channel flow depth upstream of the bridge, $2y_u$. In addition, the same designed countermeasure should run up the channel bank and protect the abutment embankment. To do this effectively, the countermeasure should be configured to cover the embankment to an appropriate height (including freeboard) and for a distance of 2 times the main channel flow depth or 25 ft (7.6 m), whichever is greater, behind the abutment and parallel to the roadway.

Figure 124 through figure 127 illustrate the appropriate scour and countermeasure design configurations for the described flow conditions and options. Note that, although the countermeasure configurations are all similar, there are dimensional differences that make each case unique. Also note that the figures reflect the use of rock riprap as the countermeasure type. When riprap is used as the designed countermeasure, an appropriate filter must be placed under the riprap to prevent the underlying soils from being winnowed out through the interstitial openings between rocks.

There is one additional scour countermeasure design consideration for shallow foundations that support GRS and similar abutments. When the scour check flood overtops an approach roadway, a potential exists for the GRS abutment to be attacked from the back side. The likelihood depends on the depth of the overtopping flow, its duration, and the erosion resistance of the embankment. Research that defines the potential failure mechanism and most appropriate countermeasure configuration has yet to be conducted. However, the following additional countermeasure treatment is recommended when abutment embankment overtopping occurs for the worst-case scour condition:

- Wrap the geotextile layers on back side of abutment full height to enable the abutment to stand unsupported should the embankment fail.

- Extend the abutment embankment protection to the top of the embankment.

There is also one hydraulic/structural design consideration for GRS type abutments. When a scour flood inundates an abutment, either by free-surface overtopping flow or pressure flow conditions, the top of the GRS mass is subject to unknown hydrodynamic forces that may scour GRS material from around the beam seat. Should either of these flow conditions be present, it is recommended that the GRS abutment be constructed wide enough to accommodate placement of the scour countermeasure on top of the GRS mass.

Designing countermeasures for shallow foundation abutments in a river environment can also be a very complicated endeavor because of the complex interaction between the hydraulics, the multiple scouring mechanisms that are typically present, and the structural components. For these reasons, it is again of utmost importance that a qualified hydraulics engineer, experienced in river mechanics, sediment transport, and bridge hydraulics, perform the analyses required for countermeasure design.

At the time of this report, the complete details of scour countermeasure design specifically for shallow foundation abutments, which are too extensive to include herein, were being compiled and summarized for inclusion in the next edition of FHWA publication HEC-23.[3]

RIPRAP COUNTERMEASURE SPECIFICATIONS

As indicated in the preceding discussions, engineers must rely on countermeasures to ensure embankment, and at times, foundation stability during the scour check flood. Because of its flexibility, availability, and relative cost, the countermeasure of choice is often rock riprap. Accordingly, engineers must be aware that there are many sources of uncertainty associated with the design, manufacture, installation, performance, and maintenance of a riprap mass. Among the causes of premature riprap failure related to design and construction are the following:

- Inadequate rock quality, size, and/or gradation.
- Inadequate embedment and/or toe-down depths.
- Inadequate thickness.
- Segregation of rock sizes.
- No or improperly installed filter.
- Damaged filter material.

A designed granular or geotextile filter must be installed under all riprap installations to prevent finer-grained base soils from being winnowed out through the passages between individual rocks, causing premature failure.

Without comprehensive construction acceptance testing, there is little assurance that the riprap mass will perform as intended. Consequently, when a riprap countermeasure is used, rock quality, acceptance criteria, and testing frequency requirements must be developed and included in the construction contract specifications to properly control the manufacture, placement, and acceptance of the riprap. In addition, the size and gradation test methods to be used for accepting the riprap mass must be included in, or referenced by, the contract. Including such provisions in the contract will reduce the chances of premature riprap failure. The FHWA Office of Federal Lands Highways' *Standard Specifications for Construction of Roads and Bridges on Federal Highway Projects*, FP-14, Sections 251 and 705, provide sampling, testing, and acceptance requirements; and material requirements, respectively, for rock riprap.[(29)]

After construction, riprap countermeasure condition and channel instability should be assessed during each regular bridge inspection and after large flood events. Any countermeasure failure or significant change in channel stability should be noted and scheduled for repair or stabilization. Without proper inspection and maintenance, a scour countermeasure may fail or a channel may become unstable, which can lead to bridge abutment failure.

This Page Is Left Blank intentionally.

REFERENCES

1. Adams, M.T., Schlatter, W., and Stabile, T. (2007) "Geosynthetic Reinforced Soil Integrated Abutments at the Bowman Road Bridge in Defiance County, Ohio." *Proceedings of Geo-Denver 2007: Geosynthetics in Reinforcement and Hydraulic Applications*, p. 1–10. American Society of Civil Engineers, Reston, VA.

2. Arneson, L.A., Zevenbergen, L.W., Lagasse, P.F., and Clopper, P.E. (2012) *Evaluating Scour at Bridges,* Hydraulic Engineering Circular No. 18. Fifth Edition. Report No. FHWA-HIF-12-003. Federal Highway Administration, Washington, DC.

3. Lagasse, P.F., Clopper, P.E., Pagán-Ortiz, J.E., Zevenbergen, L.W., Arneson, L.A., Schall, J.D., and Girard, L.G. (2009) *Bridge Scour and Stream Instability Countermeasures,* Hydraulic Engineering Circular No. 23. Report No. FHWA-NHI-09-111. Federal Highway Administration, Washington DC.

4. Laursen, E.M. (1963) "An Analysis of Relief Bridge Scour," *Journal of the Hydraulic Division, 89*(3), p. 93–118.

5. Petersen, T.U., Sumer, M.B., Boegelund, J., Yazici, A., Fredsoee, J., and Meyer, K.E. (2015) "Flow and Edge Scour in Current Adjacent to Stone Covers," *Journal of Waterway, Port, Coastal, and Ocean Engineering, 141*(4).

6. Macky, G.H. (1986) *Model Testing of Bridge Abutment Protection.* Report 3-86/12, Central Laboratories, Ministry of Works and Development, Lower Hutt, New Zealand.

7. Croad, R.N. (1989) *Investigation of the Pre-Excavation of the Abutment Scour Hole at Bridge Abutments*. Report 89-A9303, Central Laboratories, Works and Development Services Corporation (NZ) Ltd, Lower Hutt, New Zealand.

8. Pagán-Ortiz, J.E. (1991) *Stability of Rock Riprap for Protection at the Toe of Abutments Located at the Flood Plain*. Report No. FHWA-RD-91-057. Federal Highway Administration, Washington, DC.

9. Atayee, A.T. (1993) "Study of Riprap as a Scour Protection for Spill-Through Abutments." *Transportation Research Record 1420*: *Hydrology, Hydraulics, and Water Quality*, p. 40–48.

10. Atayee, A., Pagán-Ortiz, J., Jones, J.S., and Kilgore, R. (1993) "Study of Riprap as Scour Protection for Bridge Abutments." *Proceedings of Conference on Hydraulic Engineering, Part 1,* p. 973–978.

11. Eve, N.J. (1999) *Riprap Protection of Bridge Abutments.* Master of Engineering Thesis, Department of Civil and Resource Engineering, University of Auckland, Auckland, New Zealand.

12. Hoe, D.A. (2001) *Cable-Tied Block Protection of Bridge Abutments.* Project Report No. PCRE 01:08. Department of Civil and Resource Engineering, University of Auckland, Auckland, New Zealand.

13. Cheung, M. (2002) *Cable-Tied Blocks as a Countermeasure.* Master of Engineering Thesis, Department of Civil and Environmental Engineering, University of Auckland, Auckland, New Zealand.

14. Martinez, E. (2003) *An Assessment of Two Countermeasures to Reduce Abutment Scour*. Master of Science Thesis, Civil and Environmental Engineering Department, University of Iowa, Iowa City, IA.

15. Korkut, R. (2004) *Geobags as Abutment Scour Countermeasure*. Master of Science Thesis, Civil and Environmental Engineering Department, University of Iowa, Iowa City, IA.

16. Barkdoll, B., Ettema, R., and Melville, B. (2007) *Countermeasures to Protect Bridge Abutments from Scour*. Report No. NCHRP-587. National Cooperative Highway Research Program, Transportation Research Board, Washington, DC.

17. Melville, B.W., van Ballegooy, S., Coleman, S.E., and Barkdoll, B. (2006) "Scour Countermeasures for Wing-Wall Abutments," *Journal of Hydraulic Engineering, 132*(6), p. 563–574.

18. Melville, B.W., van Ballegooy, S., Coleman, S.E., and Barkdoll, B. (2006) "Countermeasure Toe Protection at Spill-Through Abutments," *Journal of Hydraulic Engineering, 132*(3), p. 235–245.

19. Melville, B.W., van Ballegooy, S., Coleman, S.E., and Barkdoll, B. (2007) "Riprap Size Selection at Wing-Wall Abutments," *Journal of Hydraulic Engineering, 133*(11), p. 1,265–1,269.

20. Jesson, M., Sterling, M., and Bridgeman, J. (2013) "Modeling Flow in an Open Channel with Heterogeneous Bed Roughness," *Journal of Hydraulic Engineering, 139*(2), p. 195–204.

21. Horton, R.E. (1933) "Separate Roughness Coefficients for Channel Bottoms and Sides," *Engineering News-Record 111*(22), p. 652–653.

22. Einstein, H.A. (1934) "Der Hydraulische Oder ProfilRadius," *Schweizerische Bauzeitung Zurich, 103*(8), p. 89–91.

23. Strickler, A. (1923) *Mitteilungen des Eidgenossischen Amtes fur Wasserwirtschaft*. Swiss Department of the Interior Report of the Bureau of Water Affairs, Bern, Switzerland. Translated as *Contributions to the Question of a Velocity Formula and Roughness Data for Streams, Channels and Closed Pipelines* by T. Roesgan and W.R. Brownie, Translation T-10, W. M. Keck Laboratory of Hydraulics and Water Resources (1981), California Institute of Technology, Pasadena, CA.

24. California Department of Transportation. (2013) "Seismic Design Criteria," chapter 3 of *Capacities of Structure Components*. Version 1.7. California Department of Transportation, Sacramento, CA.

25. American Association of State Highway Transportation Officials (2010) *Load Resistance Factor Design Bridge Design Specifications*. Fifth Edition. American Association of State Highway Transportation Officials, Washington, DC.

26. Code of Federal Regulations, *Title 23, Part 650, Subpart A*. U.S. Government Printing Office, Washington, DC. Available online at http://www.ecfr.gov/cgi-bin/text-idx?rgn=div5&node=23:1.0.1.7.28#sp23.1.650.a. Last accessed December 12, 2016.

27. Lagasse, P.F., Schall, J.D., and Richardson, E.V. (2001) *Stream Stability at Highway Structures,* Hydraulic Engineering Circular No. 20. Third Edition. Report No. FHWA-NHI-01-002. Federal Highway Administration, Washington, DC.

28. Zevenbergen, L.W., Arneson, L.A., Hunt, J.H., and Miller, A.C. (2012) *Hydraulic Design of Safe Bridges*. Report No. FHWA-HIF-12-018. Federal Highway Administration, Washington, DC.

29. Federal Highway Administration. (2014) *Standard Specifications for the Construction of Roads and Bridges on Federal Highway Projects* (FP-14). U.S. Department of Transportation, Washington, DC.